



TECHNISCHE UNIVERSITÄT MÜNCHEN

Lehrstuhl für Ernährung und Immunologie

Impact of unfolded protein responses on intestinal epithelial homeostasis in genetically modified mouse models

Emanuel Clemens Berger

Vollständiger Abdruck der von der Fakultät Wissenschaftszentrum Weihenstephan für Ernährung, Landnutzung und Umwelt der Technischen Universität München zur Erlangung des akademischen Grades eines

Doktors der Naturwissenschaften

genehmigten Dissertation.

Vorsitzende: Univ.-Prof. Dr. H. Daniel

Prüfer der Dissertation:

1. Univ.-Prof. Dr. D. Haller
2. Univ.-Prof. Dr. M. Heikenwälder
3. Univ.-Prof. Dr. B. Stecher
(Ludwig-Maximilians-Universität München)

Die Dissertation wurde am 05.02.2014 bei der Technischen Universität München eingereicht und durch die Fakultät Wissenschaftszentrum Weihenstephan für Ernährung, Landnutzung und Umwelt am 21.03.2014 angenommen.

Felix, qui potuit rerum cognoscere causas (Vergil, *Georgica* 2, 490)

PUBLICATIONS AND PRESENTATIONS

Peer-reviewed manuscripts

Berger E, Yuan D, Waldschmitt N, Rath E, Allgäuer M, Staszewski O, Boekschoten M, Müller M, Prinz M, Weber A, Gerhard M, Janssen KP, Heikenwälder M, Haller D.

Mitochondrial Unfolded Protein Responses Control Epithelial Stem Cell Proliferation in the Intestine. (manuscript in preparation).

Waldschmitt N, **Berger E**, Rath E, Sartor BR, Weigmann B, Heikenwalder M, Gerhard M, Janssen KP, Haller D.

C/EBP homologous protein inhibits tissue repair in response to gut injury and is inversely regulated with chronic inflammation. *Mucosal immunology*. 2014. Epub 2014/05/23.

Chang JS, Ocvirk S, **Berger E**, Kisling S, Binder U, Skerra A, Lee AS, Haller D.

Endoplasmic reticulum stress response promotes cytotoxic phenotype of CD8 $\alpha\beta$ ⁺ intraepithelial lymphocytes in a mouse model for Crohn's disease-like ileitis. *J Immunol*. **2012**. 189(3):1510-20.

*Rath E, ***Berger E**, Messlik A, Nunes T, Liu B, Kim SC, Hoggenraad N, Sans M, Sartor RB, Haller D. dsRNA-activated protein kinase links mitochondrial unfolded protein response to intestinal inflammation in humans and mice. *Gut*. **2011**. 61(9):1269-78.

(*E.R. and E.B. are joint first authors)

Berger E, Haller D.

Structure-function analysis of the tertiary bile acid TUDCA for the resolution of endoplasmic reticulum stress in intestinal epithelial cells. *Biochem Biophys Res Commun*. **2011**, 409: 610-615.

Published abstracts

Waldschmitt N, Rath E, **Berger E**, *et al.*

Expression of C/EBP Homologous Protein in intestinal epithelial cells is not associated with the development of chronic inflammation: A transgenic approach. *Gastroenterology*. **2012**. 142(5): S-124.

Berger E, Kisling S, Pitariu S, Schümann K, Haller D.

Chemical Chaperones Modulate Endoplasmic Reticulum Stress Pathways in Intestinal Epithelial Cells. *Gastroenterology*. **2010**. 138(5): S-427.

Rath E, **Berger E**, Messlik A, *et al.*

Mitochondrial Stress Induction in the Epithelium Fuels Endoplasmic Reticulum Unfolded Protein Responses via Double-Stranded RNA-Activated Protein Kinase (PKR) Under Conditions of Chronic Intestinal Inflammation. *Gastroenterology*. **2010**. 138(5): S-50.

Chang JS, **Berger E**, Kisling S, *et al.*

Endoplasmic Reticulum Stress Responses Contribute to the Cytotoxic Phenotype of CD8αβ Intraepithelial Lymphocytes Through the Regulation Granzyme B Activity in Crohn's Disease-Like TNFΔ are Mice. *Gastroenterology*. **2010**. 138(5): S-104 – 105.

Messlik A, Rath E, **Berger E**, *et al.*

Signal integration of endoplasmic reticulum and mitochondrial unfolded protein stress responses in intestinal epithelial cells of patients with ulcerative colitis and murine models of immune- mediated colitis: Inhibitory mechanisms of Interleukin 10. *Gastroenterology*. **2009**. 136(5): A-700.

Oral presentations

- Digestive Disease Week (DDW) 2014 in Chicago, USA
- United European Gastroenterology Week (UEGW) 2013 in Berlin, Germany
- Annual meeting of German Nutrition Society (DGE) 2012 in Freising, Germany
- Annual meeting of German Nutrition Society (DGE) 2011 in Potsdam, Germany
- European Mucosal Immunology Group (EMIG) meeting 2010 in Amsterdam, Netherlands
- Annual meeting of German Nutrition Society (DGE) 2010 in Jena, Germany
- Annual meeting of German Nutrition Society (DGE) 2009 in Gießen, Germany

Poster presentations

- International Congress of Mucosal Immunology 2013 in Vancouver, Canada
- Cell Symposia: Mitochondria – From Signaling to Disease 2013 in Lisbon, Portugal
- Annual meeting of German Nutrition Society (DGE) 2013 in Bonn, Germany
- European molecular biology organization conference series “The Biology of Molecular Chaperones” 2011 in Grundlsee, Austria
- Annual meeting of German Society of Hygiene and Microbiology (DGHM) section “Microbiota, Probiota and Host” 2011 in Seeon, Germany
- Digestive Disease Week (DDW) 2010 in New Orleans, USA

Grants

- Travel grant of the United European Gastroenterology Week (2013)
- Travel grant of GlaxoSmithKline Foundation (2011)
- Travel award for the European Mucosal Immunology Group meeting (2010)
- Travel grant of Danone Institute (2010)

Memberships

- TUM Graduate School since 2010
- Associated fellowship of the DFG-Graduiertenkolleg 1482 “Interface functions of the intestine between luminal factors and host signals” since 2008

ZUSAMMENFASSUNG

Das Darmepithel ist die Schnittstelle zwischen dem Darmlumen und dem mukosalen Immunsystem des Wirts, wobei es Signalen von beiden Seiten ausgesetzt ist. Ein Set von Programmen zur Signalverarbeitung, die für die Aufrechterhaltung der Epithelhomöostase unverzichtbar sind, stellen die „unfolded protein responses“ (UPR) des Endoplasmatischen Retikulums (ER) und der Mitochondrien (MT) dar. Eine dysregulierte UPR in Darmepithelzellen (DEZ) wurden mit der Pathogenese von chronisch entzündlichen Darmerkrankungen (CED) in Zusammenhang gebracht. Die vorliegende Arbeit untersucht die Verschränkung von ER und MT UPR in DEZ und den Einfluss einer Chaperon-Defizienz auf die epitheliale Homöostase.

In der vorliegenden Arbeit wurden neue DEZ-spezifische transgene Mausmodelle generiert, die die UPR-relevanten Transkriptionsfaktoren *Chop* und *nATF6* exprimieren. Darüber hinaus ein Mausmodell, dem das MT UPR assoziierte Chaperon „heat shock protein 60“ (HSP60) fehlt. Die Charakterisierung der transgenen Mausmodelle findet gegenwärtig in enger Verbindung zur vorliegenden Arbeit statt. Im Folgenden liegt der Schwerpunkt auf der Charakterisierung des HSP60 defizienten Mausmodells. Die Züchtung epithelspezifischer HSP60 defizienter Mäuse zeigte eine beeinträchtigte Embryonalentwicklung ab dem Stadium E11,5 und führte letztlich zur Embryoletalität. Eine Induktion der *Hsp60*-Deletion im adulten Darmepithel verursachte massive Veränderungen der Villus-Krypt Architektur des Dünndarms begleitet von Symptomen einer akuten Nährstoffmangelversorgung. Das sporadische Misslingen der Cre-Rekombinase vermittelten *Hsp60*-Deletion resultierte in der Ausbildung hochgradig proliferativer HSP60-positiver „escaper“-Zellen, die den Stammzellmarker Olfactomedin 4 (OLFM4) exprimieren. Im Gegensatz zum Dünndarm, zeigte das Kolon - makroskopisch gesehen - keine Anzeichen von Pathologie trotz geringfügiger Infiltration von Makrophagen. Unabhängig von hyper-proliferativen Krypt-Herden zeigten HSP60 defiziente Krypten im Dün- und Dickdarm eine ausgeprägte MT UPR, die mit einer verringerten Expression von *Ki67*, *Lgr5* und *Olfm4* einherging – Ein deutliches Zeichen für den Verlust von Stammzellen. Eine Microarray-Analyse des HSP60 defizienten Epithels wies 2.512 differentiell regulierte Gene aus ($q < 0,01$), darunter ein Set von spezifisch „C/EBP-homologous protein“ (CHOP) regulierten Zielgenen. Die Mitochondrien im HSP60 defizienten Epithel zeigten Veränderungen in der Morphologie und eine verringerte Expression von Funktionalitätsmarkern wie die MT kodierte Cytochrom C Oxidase I (*mtCoxI*) – eine Untereinheit des Atmungskettenkomplexes IV. Um mögliche zelluläre Kompensationsmechanismen der reduzierten HSP60 Spiegel zu untersuchen, untersuchten wir haplodefiziente *Hsp60*^{+/-} Mäuse. Diese Reduktion verursachte keine Pathologie unter Normalbedingungen. Darüber hinaus zeigten *Hsp60*^{+/-} Mäuse keine deutliche Verstärkung der Darmgewebepathologie, die durch entzündliche Stimulationen

hervorgerufen wurden. Dies deutet auf eine beträchtliche Anpassungsfähigkeit des mitochondrialen Chaperon-Systems in Darmepithelzellen hin.

Zusammenfassend konnte gezeigt werden, dass eine gewebespezifische Deletion des MT Chaperons HSP60 die Epithelhomöostase sowohl in der vorgeburtlichen Entwicklung als auch im adulten Darm beeinträchtigt unabhängig von einem akut entzündlichen Geschehen. Eine *Hsp60*-Deletion in DEZ stimuliert die MT UPR und geht mit einer gestörten Proliferation und einem Verlust von Stammzellen einher.

ABSTRACT

The intestinal epithelium is the key interface between luminal factors of the gut and the mucosal immune system of the host receiving manifold signals from both sides. One set of signal processing programs are the unfolded protein responses (UPR) of the endoplasmic reticulum (ER) and the mitochondria (MT) crucial for maintaining epithelial homeostasis. De-regulated UPR in intestinal epithelial cells (IEC) have been implicated in the pathogenesis of inflammatory bowel diseases (IBD). This study investigates the impact of persistently activated ER and MT UPR pathways in IEC on the epithelial homeostasis by the use of genetically modified mouse models.

In the present study we generated novel IEC-specific transgenic mouse models expressing the key UPR-related transcription factors *Chop* and *nATF6* as well as a model deficient for the MT UPR associated chaperone heat shock protein 60 (HSP60). The characterization of the transgenic mouse models is currently running in two PhD projects closely related to the present work. Here we focus on the characterization of the HSP60 deficient mouse model. Generation of IEC-specific *Hsp60* knockout mice (*Hsp60^{flox/flox}X VillinCre*) antagonized embryonic development at E11.5 and induced embryonic lethality. Postnatal induction of HSP60 deficiency (*Hsp60^{flox/flox}X VillinCreER^{T2}*) caused massive aberrations in the villus-crypt architecture of the small intestine associated with symptoms of severe wasting within one week. Sporadic failure of Cre-mediated *Hsp60* deletion resulted in the formation of highly proliferative HSP60-positive escaper cells expressing the stem cell marker olfactomedin 4 (OLFM4). At the macroscopic level, the colonic tissue was free of any pathology, despite an increased infiltration of macrophages. Independent of hyperproliferative crypt foci, HSP60-deficient crypts in colon and small intestine revealed hallmarks of MT UPR, associated with an abrogated expression of *Ki67*, *Lgr5* and *Olfm4*, indicating a significant loss of epithelial stemness. Microarray analysis of HSP60-deficient colonic epithelium identified 2,512 differentially expressed genes ($q < 0.01$), including a set of distinct C/EBP-homologous protein (CHOP) target genes. Mitochondria in the HSP60-deficient epithelium showed altered morphology, as well as decreased expression of functional markers like the MT encoded cytochrome c oxidase I (*mtCoxI*) subunit located in the respiratory chain. To address compensatory mechanisms upon reduced levels of HSP60, we investigated haplodeficient *Hsp60^{+/-}* mice. This reduction did not cause any pathology under steady-state conditions. Moreover, *Hsp60^{+/-}* mice showed no marked increase of intestinal tissue pathology triggered by inflammatory stimuli pointing to a distinct resilience of the MT chaperone system in IEC.

In summary, a tissue-specific deletion of the MT chaperone *Hsp60* disrupts epithelial cell homeostasis in both the pre- and postnatal gut, independent of an inflammation-associated pathology. *Hsp60* deletion in the intestinal epithelium triggers mtUPR and alterations in mitochondrial function, leading to an impaired proliferative response and a loss of stemness.

TABLE OF CONTENTS

Publications and presentations.....	5
Zusammenfassung - Abstract.....	7
Table of contents	11
1 Introduction	15
1.1 IBD – a prototypic multifactorial chronic degenerative lifestyle disease.....	15
1.2 Multi-functional role of the epithelium in mucosal homeostasis	17
1.3 Mouse models for the impact of epithelial integrity on IBD	19
1.4 Unfolded protein responses for homeostasis and in disease.....	20
1.4.1 The ER unfolded protein response.....	20
1.4.2 Involvement of ER UPR mechanisms in disease pathogeneses	23
1.4.3 The mitochondrial unfolded protein response	25
1.4.4 The ER - mitochondrial signaling network.....	27
1.5 HSP60 – chaperone and danger signal	29
2 Aim of the work	35
3 Material and Methods	37
3.1 Supplier of experimental material	37
3.2 Animal models	38
3.2.1 Ethics statement and animal housing.....	38
3.2.2 Purchase of established mouse models.....	38
3.2.3 Generation of new mouse models.....	39
3.2.4 Embryo preparation and genotyping	40
3.2.5 Induction of postnatal genomic recombination and monitoring of animals.....	40
3.2.6 Nutrient uptakes in small intestinal everted gut rings	41
3.2.7 Calorimetry of fecal samples	41
3.2.8 Ussing chamber measurements.....	41
3.2.9 Tissue processing, H&E-, alcian blue-, IHC- and IF staining, ISH	42
3.2.10 Isolation of total primary IEC and jejunal villus tip and crypt bottom epithelium	44
3.3 Cell lines and bacteria	45
3.3.1 Mode K	45
3.3.2 Competent <i>E. coli</i>	46
3.4 Plasmids	47
3.5 Molecular cloning.....	48
3.6 Transfection of adherent cell lines.....	54
3.7 Chromatin Immunoprecipitation for analysis of DNA-protein-interaction	55
3.8 Quantitative real time PCR	56
3.9 Discontinuous denaturing polyacrylamid gel electrophoresis	58
3.10 Western blot.....	59
3.11 Electron microscopy	61
3.12 RNA Microarray	61
3.13 Statistical analysis	62

TABLE OF CONTENTS

4	Results	63
4.1	Interrelation of ER- and MT UPR signaling	63
4.1.1	Promoter analysis of ER- and MT UPR responsive genes	63
4.1.2	Construction and <i>in vitro</i> validation of <i>Chop</i> and <i>nAtf6</i> overexpressing vectors	64
4.2	Generation of the <i>nAtf6-HA</i> and <i>Chop-HA</i> conditional transgenic mouse models	67
4.3	Generation of the constitutive and conditional <i>Hsp60</i> knockout mouse model.....	67
4.4	Characterization of the constitutive <i>Hsp60</i> ^{+/-} mouse model	67
4.4.1	Genotyping	67
4.4.2	Embryolethality of <i>Hsp60</i> ^{+/-} mice.....	68
4.4.3	Phenotypic screening of selected organs of <i>Hsp60</i> ^{+/-} mice.....	68
4.4.4	Basic characterization of the intestine of <i>Hsp60</i> ^{+/-} mice.....	69
4.4.5	<i>Hsp60</i> ^{+/-} mice in an acute and a chronic model of intestinal inflammation.....	72
4.5	Characterization of the <i>Hsp60</i> ^{Δ/ΔIEC} mouse.....	76
4.5.1	Genotyping of the conditional knock out allele	76
4.5.2	Embryolethality of the <i>Hsp60</i> ^{Δ/ΔIEC} mouse	76
4.6	Characterization of the tamoxifen inducible <i>Hsp60</i> ^{Δ/ΔIEC} mouse.....	78
4.6.1	Phenotypic, metabolic and intestinal characterization of the <i>Hsp60</i> ^{Δ/ΔIEC} mouse.....	78
4.6.2	Functional characterization of the epithelium in <i>Hsp60</i> ^{Δ/ΔIEC} mice.....	82
4.6.3	Characterization of the epithelial stress responses in <i>Hsp60</i> ^{Δ/ΔIEC}	84
4.6.4	Characterization of the mitochondrial appearance in IEC of <i>Hsp60</i> ^{Δ/ΔIEC} mice.....	88
4.6.5	Effects of HSP60 depletion on epithelial proliferation	90
4.7	Characterization of a stem cell specific Hsp60 depletion in <i>Hsp60</i> ^{Δ/ΔISC} mice	94
5	Discussion	97
5.1	<i>Hsp60</i> ^{Δ/ΔIEC} mice – the paradox of embryolethality.....	97
5.2	<i>Hsp60</i> ^{Δ/ΔIEC} mice – the complexity of a fatal phenotype	98
5.3	The impact of HSP60 deficiency on mitochondria in IEC.....	100
5.4	<i>Hsp60</i> ^{Δ/ΔIEC} mice – a model for activated MT UPR and oxidative stress in IEC	101
5.5	<i>Hsp60</i> ^{Δ/ΔIEC} mice – a model for stem cell loss and epithelial regeneration?.....	102
5.6	The compensatory potential of HSP60 in haplodeficient <i>Hsp60</i> ^{+/-} mice.....	105
6	Conclusion and perspective	109
7	Appendix.....	111
7.1	Sequence of HA-nATF6 and nAFT6-HA	111
7.2	Generation of the <i>nAtf6-HA</i> conditional transgenic mouse	113
7.3	Sequence of HA-CHOP and CHOP-HA	115
7.4	Generation of the <i>Chop-HA</i> conditional transgenic mouse	116
7.5	Sequence of HSP60 and truncated HSP60	118
7.6	Generation of the <i>Hsp60</i> constitutive and conditional knock out mouse model.....	119

List of Figures	123
List of Tables	125
List of Abbreviations	127
List of References.....	129
Acknowledgements	141
Curriculum Vitae	143
Erklärung	145

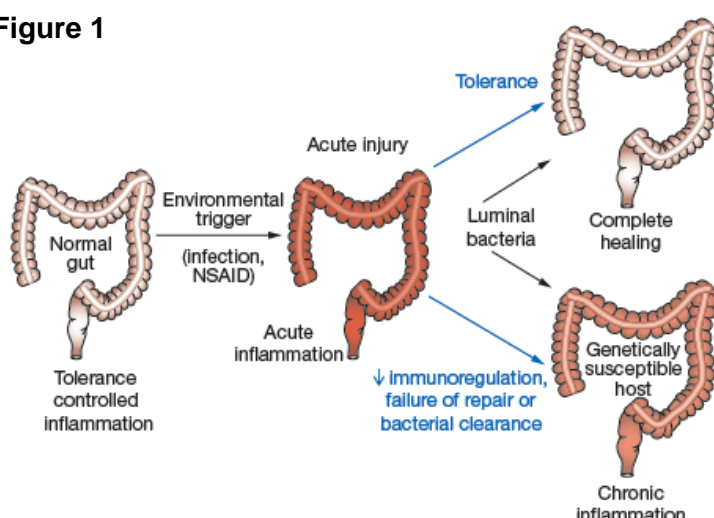
1 INTRODUCTION

1.1 IBD – a prototypic multifactorial chronic degenerative lifestyle disease

During the second half of the twentieth century, lifestyle changed dramatically in the western industrialized countries accompanied by an excessive supply of food and high medical (and hygienic) standard. While the number of infective diseases declined rapidly, the incidence of chronic degenerative lifestyle diseases rose erratically. These diseases comprise obesity, metabolic syndrome, diabetes, cardiovascular-, autoimmune- and neurodegenerative disorders as well as cancer and inflammatory bowel diseases (IBD). All of these show a multifactorial etiology meaning that their onset and perpetuation is a consequence of a complex interplay between genetic predispositions and diverse environmental triggers.

The prevalence of IBD rapidly increased in Europe and North America during the last decades and is becoming more common in the rest of the world as different countries adopt a Western lifestyle. IBD comprise mainly Crohn's disease (CD) and ulcerative colitis (UC) and are characterized by a chronically relapsing inflammation of the intestinal mucosa with still unknown etiology. UC is a continuous mucosal disease with high epithelial involvement that always affects the rectum and extends proximally to involve a variable length of the colon and is characterized by the infiltration of majorly polymorphic nuclear leucocytes and the appearance of crypt abscesses. CD can affect any part of the gastrointestinal (GI) tract, preferentially ileum and colon. The inflammation is discontinuous, transmural and characterized by lymphocyte infiltration, granulomas and the risk of stenosis formation [1].

IBD reflect the concept of a multifactorial etiology, since both disease phenotypes comprise a genetic susceptibility, environmental triggers, luminal microbial antigens (and adjuvants) and dysregulated immune responses acting in concert both for their pathogenesis and the chronic relapsing course [2, 3]. In the current model of the disease pathology, a genetically predisposed host with mutations in genes of the innate immune response, mucosal barrier function and bacterial defense is exposed to an environmental trigger. These comprise e.g. smoking, the use of antibiotics and nonsteroidal anti-inflammatory drugs, stress or infection, which alter mucosal barrier integrity, immune responses or the luminal microenvironment and cause an acute but transient inflammatory response [2]. In contrast to a normal host which quickly clears infections of invasive enteric bacteria, downregulates innate immune responses and heals the injured mucosa without stimulating effector T-cell responses, the host with a disease-susceptible genotype is unable to compartmentalize the intestinal microbiota in appropriate distance to the epithelium and cannot generate tolerogenic immune responses to commensal microbial antigens. This is due to the disability to mount appropriate immunity, to downregulate immune responses and to heal the mucosal barrier resulting in continuously activated T-cell responses to commensal bacteria and proceeding to chronic, relapsing intestinal inflammation [2] (Fig. 1).

Figure 1**Fig. 1 Current model for the pathogenesis of IBD**

In a genetically susceptible host, an acute mucosal defect caused by environmental triggers cannot be healed due to a lack of immunoregulation and the failure to repair the epithelium and clear bacteria. This leads to a chronic inflammation mediated by a persistent T-cell response towards the continuously aggravating microbiota meaning the loss of oral tolerance [2].

The importance of genetics on the etiology of IBD is still a matter of debate, since the concordance rate in identical twins is relatively low (~50% for Crohn's disease, and ~10% for ulcerative colitis), but an increased incidence of IBD in first-degree relatives of patients with either disease cannot be neglected [4]. In addition, genome wide association studies (GWAS) on over 25 000 IBD patients identified in total 163 genomic loci associated with IBD. These analyses highlight 110 shared loci for both disease subtypes, while 30 are classified as specific for CD and 23 for UC [5]. So far, only few genes out of the 163 loci have been identified, repeatedly associated with IBD and systematically investigated in mouse models of intestinal inflammation. Notably, many of the so far investigated genes affect explicitly the functions of the intestinal epithelium attributing a key role to this tissue for the etiology of IBD. Tab. 1 gives examples of such genes.

Gene	Function	Assos.	Ref.
NOD2/CARD15	NF- κ B activation and/or regulation, killing of intracellular pathogens, Paneth cell function (α -defensin production)	CD	[6, 7]
SLC22A4 & SLC22A5	Organic cation, carnitine transporters, possibly transport xenobiotic substances	CD	[8]
DLG5	Epithelial scaffolding protein	CD	[9]
PPAR γ	Intracellular inhibitor of NF- κ B and cellular activation	CD	[10]
ATG16L1	Autophagy as part of innate immunity (clearance of intracellular pathogens) and Paneth cell function (granules, lysozyme production)	CD	[11, 12]
XBP-1	Unfolded protein response; Adaptation to high demands of secreted proteins in goblet and Paneth cells	CD/UC	[13]
MDR1	Efflux transporter for drugs and, possibly, xenobiotic compounds	UC	[14, 15]
MUC3(A), MUC19	Components of mucus layer (microbial exclusion) and IEC signaling (EGF like motif of Muc3A).	CD/UC	[16-18]

Tab. 1 Examples for IBD susceptibility genes with verified impact on epithelial function in human IBD and experimental intestinal inflammation (adapted from [2])

1.2 Multi-functional role of the epithelium in mucosal homeostasis

The gastrointestinal tract provides the nutrient supply enabling all metabolic processes executed in every body cell, a prerequisite for the life of a complex organism. The uptake of nutrients in the gastrointestinal tract is accompanied by chronic exposure to a huge burden of various microorganisms (commensal and pathogenic), non-digestible substrates, dietary antigens as well as toxic molecules [3, 19]. Therefore, the gut has to organize the water and nutrient uptake in a highly selective way. At the same time, the gut acts as a barrier against potentially harmful molecules and defends against invasion of the intestinal microbiota in parallel. This dual function of selective absorption and defense is mainly accomplished by the intestinal epithelial cells (IEC) forming a rapidly self-renewing tissue in close contact with the enteral environment. The epithelial mucosa comprising the IEC monolayer, circum- and underlying cells like fibroblasts and immune cells is carefully folded, producing crypts and villous protrusions. The crypts are the site, where the five IEC types differentiate from pluripotent stem cells [20]. Absorptive enterocytes, mucus producing goblet cells, opioid secreting Tuft and hormone releasing enteroendocrine cells migrate to the tip of the villus, where they undergo spontaneous apoptosis several days after terminal differentiation [21]. On the contrary, Paneth cells producing anti-microbial peptides remain within the crypt to execute their role in antimicrobial defense [22]. Approx. 80% of IEC belong to the absorptive lineage, whereas the secretory lineage (goblet, Paneth, Tuft and enteroendocrine cells) represents a minority among the IEC [23].

Despite its non-hematopoietic derivation and its lack of professional immune cell competence, the intestinal epithelium represents a core element of innate immunity, since it assists the underlying mucosa-associated lymphoid tissue (MALT) in various ways. First, the intestinal epithelium represents a pure physical barrier between the luminal microenvironment and the host. Its permeability is regulated by the presence of tight junctions, which together with adherence junctions and desmosomes link IEC to each other and seal the intracellular spaces on the luminal surface, regulating the passage through the paracellular spaces and enabling a directed and selective transepithelial uptake and release of water, electrolytes, lipids and proteins via transport channels [19].

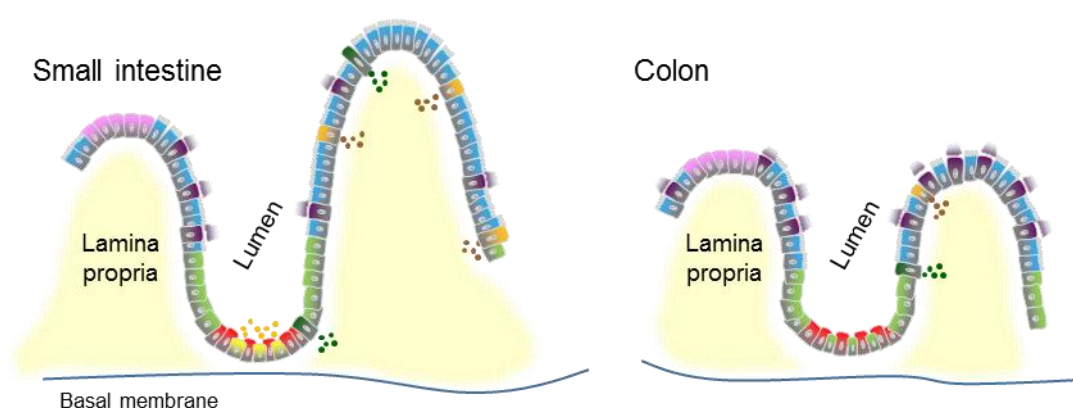
Second, specialized enterocytes, the M cells, which overlay organized lymphoid structures (Solitary lymphoid follicles, Payer's patches *et al.*; Fig. 2), play an important role in the controlled transepithelial uptake and delivery of luminal antigens to professional antigen presenting cells (APC) like dendritic cells or macrophages ensuring quiescence towards harmless and induction of defense towards pathogenic organisms [3].

Third, the epithelium exerts its immune function by secreting a large repertoire of antimicrobial proteins in order to prevent microbial invasion of the intestinal tissue. Majorly Paneth cells produce enzymatically active proteins (e.g. lysozyme and secretory

phospholipid A2), defensins, cathelicidins, RNases and C-type lectins. Goblet cells produce the mucus layer covering the entire length of the GI tract to further protect the mucosal surface from harmful molecules and bacteria and reinforce the overall intestinal barrier [19] (Fig. 2). A further element of the IEC barrier function is the transport of dimeric immunoglobulin (Ig) A to the intestinal lumen by enterocytes to prevent microbial invasion. IgA dimers produced by plasma cells of the lamina propria bind the polymeric IgA receptor at the basolateral side of the IEC, are transcytosed to the apical surface and released to the lumen where they capture antigens of the intestinal microbiota as a non-inflammatory exclusion strategy of defense [24, 25].

Finally, IEC are producers of and responders to various cytokines and chemokines that link innate and adaptive immune responses [19]. IEC produce the immune-activating cytokines TNF, IL1 β , IL6, IL-15, IL-18 and chemokines like IL-8, RANTES, IP-10, MIP2 and MCP-1. On the other hand, IEC produce the anti-inflammatory cytokines TGF β and IL-10 which are important for mucosal healing [26]. In addition, IEC express receptors for pro- (TNF, IFN γ , IL-1b, IL-6, [27], IL-17, IL-22, [28]) as well as anti-inflammatory cytokines (TGF β and IL-10 [29]). The complexity of factors interacting with IEC is still increasing reflecting the interface function of the epithelium between luminal factors and host derived signals, but also implicates that a defect in this tissue can severely compromise intestinal homeostasis.

Figure 2



Symbol	Cell type	Function
	Intestinal stem cells	Epithelial regeneration
	Enterocytes	Absorption of nutrients, Antigen uptake and presentation
	Paneth cells	Release of antimicrobial substances; support of stem cells
	Transit amplifying cells	Renewal of all types of epithelial cells
	Goblet cells	Mucus production (bacterial exclusion)
	Enteroendocrine cells	Gut hormone production (e.g. GLP-1)
	Tuft cells	Opioids release, prostanoids production
	M cells on Peyer's patch	Sampling of luminal antigens and delivery to APC

Fig. 2 Graphical overview of the different types of IEC in the intestinal mucosa

1.3 Mouse models for the impact of epithelial integrity on IBD

It seems obvious that a compromised epithelial cell function impacting barrier permeability and IEC-immune cell interaction plays a key role in the disease process of IBD [3]. Therefore, various mouse models have been designed to mimic this disease process or to understand the role of certain genes in this context. Besides models, that shed light on the deregulated immune response (*Tnf*^{ARE/WT}, *Il-10*^{-/-}, transfer of colitogenic T-cells into *Rag*^{-/-} recipients) and on the concept of IBD as a dysbiosis of the intestinal microbiota (colonization of germ-free genetically susceptible mice with pathobionts), approx. 20 mouse models exist that focus on primary defects of IEC function. Tab. 2 gives examples of different types of such models.

Model	Phenotype	Epithelial dysfunction	Ref
A) Chemically induced model			
DSS-induced colitis	Superficial colitis with ulcerations, infiltration of acute infl. cells, crypt distortion and goblet cell loss	Chemical destruction of mucosal barrier with consequent increase in luminal bacterial translocation	[30]
B) Genetic model affecting epithelial barrier integrity			
Dominant negative N-cadherin transgenic	Patchy foci of ileal inflammation with crypt abscesses, epithelial hyperplasia and lymphoid aggregates	Breakdown of intestinal epithelial apical junctional complexes; aberrant cell migration, proliferation and apoptosis in small intestinal crypts	[31]
C) Genetic model affecting epithelial innate responses			
<i>Nemo</i> ^{IEC-KO}	Pancolitis with mucosal thickening, enlarged crypts loss of goblet cells, extensive epithelial destruction marked infiltration of mononuclear cells	Colonic epithelial cell apoptosis (via increased sensitivity to TNF) due to IEC specific inhibition of NF-κB; Impaired expression of anti-microbial peptides; Deregulated epithelial barrier integrity	[32]
D) Genetic model affecting epithelial cell integrity and mucus production			
<i>Xbp-1</i> ^{IEC-KO}	Focal non-granulomatous enteritis with absence of Paneth cells, loss of goblet cells, lamina propria mononuclear infiltrates, crypt abscesses, mucosal ulcerations, villus shortening	Impaired innate immune response due to Paneth cell loss by apoptosis; ER stress; Increased pro-inflammatory signaling due to increased SAPK/JNK activation secondary to the lack of XBP1	[13]
<i>Muc2</i> mutant (Winnie/Eeyone strain)	Superficial colitis; more severe in the distal colon. Focal epithelial erosions, crypt elongation, neutrophilic infiltrate, crypt abscesses and goblet cell loss	Altered bacterial stimulation of IEC due to a diminished mucus layer. Increased ER stress due to mutated MUC2 protein misfolding and accumulation in ER	[33]
E) Spontaneous model			
C3H/HeJBir (Multigenic etiology)	Colitis; Primary localization in the caecum with acute and chronic inflammatory infiltrate, crypt abscesses Ulcerations and regenerative hyperplasia	Deregulated epithelial innate responses; Ineffective bacterial clearance; Hyper-responsiveness to flagellin stimulation	[34]

Tab. 2 Examples for mouse models of intestinal inflammation with primary defects of the epithelium function (adapted from [19])

1.4 Unfolded protein responses for homeostasis and in disease

Besides others, the *Xbp-1*^{IEC-KO} mouse model sheds light on the contribution of epithelial unfolded protein responses (UPR) for the pathogenesis of IBD. In the following, the UPR mechanisms and pathways shall be introduced. In general, specialized eukaryotic cells like IEC organize their cellular processes in specialized organelles like the ER which is responsible for the correct assembly of secretory proteins and the mitochondria which supply the cell with energy. To fulfill their tasks properly, the abundance and capacity of each organelle has to be tightly regulated to meet fluctuating cellular demands. One critical process that limits organelle and cellular function is the availability of correctly folded proteins. Therefore, autoregulatory mechanisms, the so called unfolded protein responses (UPR), have evolved in the cytoplasm, the ER and the mitochondria to ensure adaptation to peaking demands of functional proteins upon environmental triggers and/or host derived signals (Fig. 3) [35]. Generally, triggers affecting protein homeostasis comprise infections, oxidative stress and metabolic alterations [36, 37] – situation that especially IEC face frequently. If the demand of functional proteins exceeds the capacity, sensor molecules at the respective organelle detect the accumulation of un- or misfolded proteins tending to aggregate and elicit a retrograde signaling to the nucleus leading to a translational stop, to the expression of additional chaperones promoting folding and preventing aggregation, and to the expression of proteases which reduce the load of unfolded proteins to restore protein homeostasis (Fig. 3) [38, 39].

Figure 3

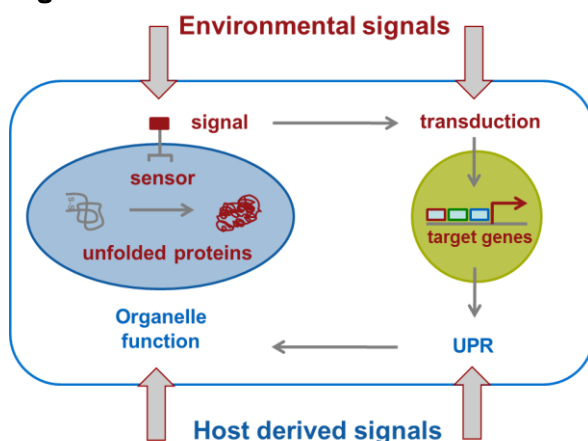


Fig. 3 Principle scheme of UPR

Exogenous or endogenous triggers evoke elevated protein synthesis in different organelles. Un-/or misfolded proteins tend to aggregate which is sensed at the organelle and transduced to the nucleus. The transcriptional response enhances folding capacity and restores protein/organelle homeostasis. (adapted from [35])

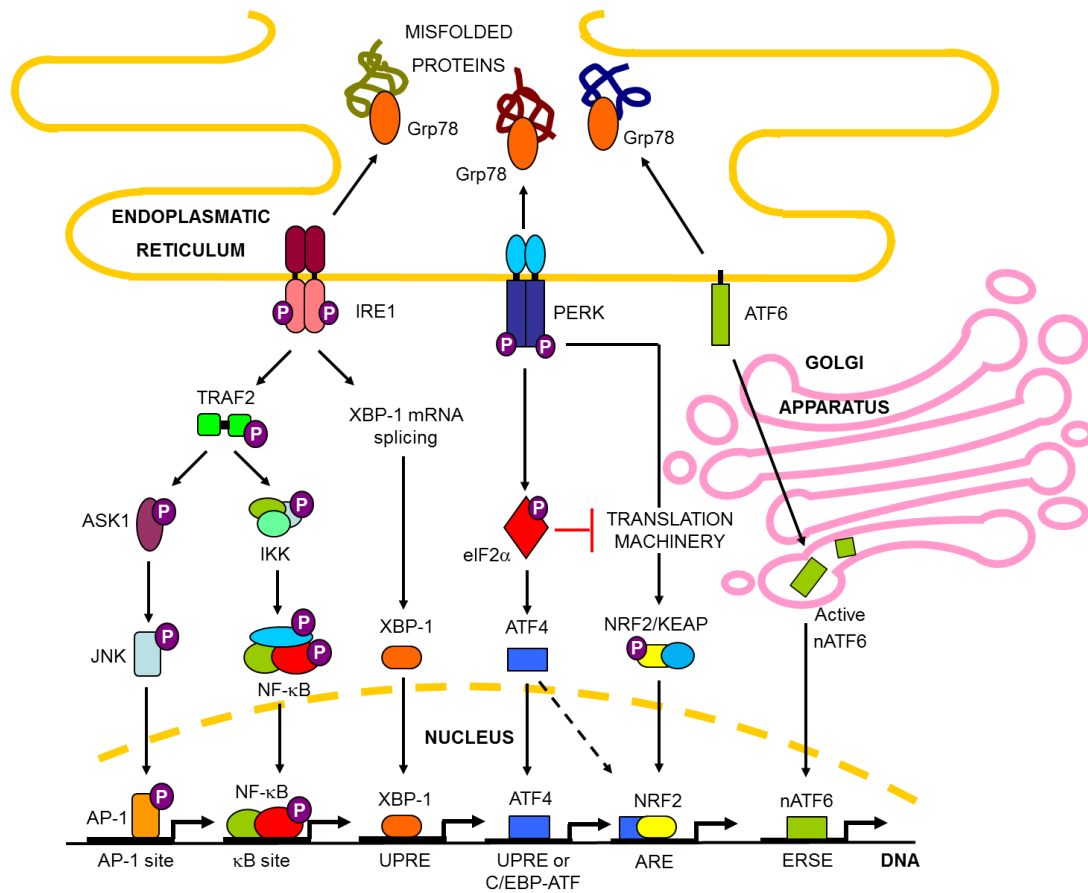
1.4.1 The ER unfolded protein response

The functions of the ER comprise lipid-, cholesterol and steroid hormone synthesis, carbohydrate storage and metabolism, calcium storage and the correct folding of proteins designated for the extracellular space, the plasma membrane and the exo- and endocytic compartments [36]. Thereby, the term “endoplasmic reticulum stress” defines any perturbation that compromises the protein folding function of the ER” [40]. Conditions that

challenge ER function and elicit ER stress responses – besides an elevated cellular demand of folded proteins – are calcium depletion and changes in redox status, energy deficiency (hypoxia, glucose deprivation), altered protein glycosylation, cholesterol deprivation and bacterial/viral infections [36]. When un-/or misfolded proteins accumulate, the ER chaperone glucose regulated protein (GRP) 78 (also referred to as immunoglobulin heavy chain-binding protein, BIP) is recruited for folding, releasing three ER transmembrane signaling proteins which are normally rendered inactive due to GRP78 binding to their ER luminal domains [41]. One of these sensor molecules, Inositol requiring enzyme (IRE) 1 α , dimerizes upon liberation from GRP78, activating its cytosolic Ser/Thr protein kinase domain and its endoribonuclease domain via trans-autophosphorylation. This activation causes the splicing of a 26-nucleotide intron out of the mRNA encoding X-box binding protein (XBP) 1 enabling the translation of this active transcription factor [42]. By binding to unfolded protein response elements (UPRE), XBP1 induces the expression of ER chaperones like P58^{IPK}, proteins involved in ER-associated degradation (ERAD), protein glycosylation [43], disulfide bond formation and ER/Golgi biogenesis [44]. As already mentioned in the previous chapter, the cytosolic domain of IRE1 can bind to TNF receptor associated factor (TRAF) 2, which activates TF activator protein (AP) 1 via cJun-N terminal kinase (SAPK/JNK) and transcription factor NF- κ B by activating the inhibitor of NF- κ B kinase (IKK); both mediating host defense responses [45, 46].

The second ER transmembrane sensor is the protein kinase R-like ER kinase (PERK) which is activated by trans-autophosphorylation upon ER stress. It phosphorylates the eukaryotic translation initiation factor (eIF) 2 α thereby inhibiting global protein translation [47, 48] and specifically inducing alternative translation of activating transcription factor (ATF) 4 [49, 50]. ATF4 binds to UPRE in the promoter of GRP78 [51] and of GADD34 which dephosphorylates eIF2 α in a negative feedback loop [52]. In addition, ATF4 binds to the C/EBP-ATF composite site in the promoter of C/EBP homologous protein (CHOP), a cell cycle arrest and apoptosis related transcription factor [53, 54]. PERK activation also promotes the dissociation of NRF2/KEAP1 dimers, subsequent nuclear translocation of NRF2, and transcription of genes harboring antioxidant response elements (ARE) in their promoters to antagonize oxidative stress [55, 56].

The third branch of the ER UPR is mediated by ATF6 α . Upon dissociation of GRP78 from its luminal domain, ATF6 translocates to the Golgi apparatus, where it is cleaved by site 1 and site 2 proteases (S1/2P) [57, 58]. The active TF nATF6 is released to the cytoplasm and migrates to the nucleus, where it binds ER stress response elements (ERSE; [59]) in the promoters of chaperones like *Grp78* [59], of *Xbp1* [60] and *Chop* [53]. Some components of the ERAD system are targets of ATF6 as well [61] (Fig. 4).

Figure 4**Fig. 4 The three branches of the ER UPR – an overview**

Acute stress demands a UPR that is relatively fast acting based on immediate reduction of the protein load, like PERK dependent inhibition of translation. However, this process is not compatible with normal cellular function for long time; therefore, they are readily reversible when the normal ER function is reestablished. In contrast, chronic ER stress occurring in cells specialized in the production and secretion of proteins like in Paneth cells demands an adaptive mechanism whereby ER stress can be persistently tolerated on a timescale ranging from days to years. In contrast to the rapid acute response, the adaptive UPR is based on the transcriptional upregulation of ER-chaperones and ER-associated degradation factors that promote ER-associated protein degradation to remove misfolded proteins and restore homeostasis [40].

1.4.2 Involvement of ER UPR mechanisms in disease pathogenesis

When adaptation fails and ER stress is excessive like during viral infection, ER stress pathways signal alarm by activating NF- κ B and SAPK/JNK dependent innate immune responses as part of the host defense to avoid spread of pathogens. Ultimately, ER stress can also lead to cell death - dependent and independent of CHOP activity [62].

The fact that the ER UPR is closely connected to inflammatory and apoptotic pathways is evolutionary feasible, but implicates that a deregulated UPR is engaged in many different chronic diseases [63]. Typical examples of pathologies that are caused by cell decay as a consequence of an accumulation of misfolded proteins in the cytoplasm are neurodegenerative disorders (e.g. Parkinson's, Alzheimer's and Huntington's disease) [64]. Obesity associated insulin insensitivity of muscle, liver and fat cells is a consequence of UPR related SAPK/JNK hyper-activation inhibiting insulin receptor signaling. The increased metabolic activity of these cells evoking ER stress, as well as free fatty acids and pathogens activating PERK-like-kinase PKR is discussed as reasons for this chronically activated UPR [65-68]. As a consequence of this metabolic syndrome, pancreatic β -cells need to dramatically increase their insulin production to fit the demand under chronic insulin resistance and hence pancreatic islets from mice and humans with type II diabetes show signs of ER UPR and apoptosis [69, 70]. Comparable to an obesity-induced metabolic syndrome, also XBP1 haplo-insufficiency results in ER stress, hyper-insulinemia, -glycemia and impaired glucose tolerance [66]. PERK-deficient mice develop severe hyperglycemia due to increased β -cell apoptosis [71] similar to the loss of function mutation in PERK causing Wallcot-Rallison syndrome, a variant of Type I diabetes, in humans [72].

Interestingly, all three arms of the UPR are implicated in tumor cell growth. Activation of PERK/ATF4 and XBP1 enables tumor cells to grow under hypoxic conditions [73-75]. ATF6 α is important for dormant tumor cells through activation of proliferative mTOR signaling [76]. Increased expression of GRP78 as a consequence of ATF6 and ATF4 activity correlates with chemotherapeutic resistance and is observed in aggressive tumors [77].

We provided first evidence that ER UPR in IEC is relevant to patients with IBD [78]. This was emphasized by an increased expression and the identification of several SNP in the human XBP1 gene in biopsies from IBD patients associated with both CD and UC by Kaser et al. [13]. Mice deficient in the TF spontaneously develop spontaneous small intestinal enteritis in a patchy pattern with variable degrees of severity [13]. Strikingly, these mice completely lack functional Paneth cells and show a marked reduction in the number and size of small intestine goblet cells, villus shortening and loss as a sign of epithelial regeneration. The absence of XBP-1 compromises the ability of Paneth cells to process and secrete anti-bacterial peptides and causes early apoptosis. Small intestinal but not colonic goblet cells show low numbers of secretory granules and low levels of MUC2 expression due to the

reduced ER folding capacity. Consequently, the mice are more susceptible to *Listeria monocytogenes* infection showing defective bacterial clearance. In addition, the XBP1 knock out shifts IRE1 activity towards activation of the SAPK/JNK dependent pro-inflammatory pathway putting IEC into a pro-inflammatory state enhancing the sensitivity of the colonic epithelium towards a DSS induced colitis and aggravating the inflammatory phenotype [13]. In the course, the generation of several mouse models targeting ER UPR signaling at different levels linked these pathways at the IEC level to promotion and perpetuation of intestinal inflammation. A constitutive deletion of *Ire1 β* [79], *P58^{IPK}* [80], total *Atf6 α* [80] and *nAtf6 α* (via missense mutation in S1P, so called “woodrat strain” [81]) results in an increased susceptibility towards development of colonic intestinal inflammation upon treatment with the detergent DSS, whereas *Chop^{-/-}* mice were largely protected against DSS induced colitis [82]. Interestingly, oral administration of either chemical chaperone PBA or TUDCA reduced signs of DSS-induced acute and chronic colitis in wild-type mice, the colitis that develops in *Il10^{-/-}* mice, and DSS-induced colitis in *P58^{IPK}^{-/-}* and *Atf6 α ^{-/-}* mice associated with significantly decreased ER stress in colonic IEC [80]. A Structure-function analysis of the tertiary bile acid and chemical chaperone TUDCA in IEC was performed by our group [83]. Tab. 3 summarizes the phenotypes of the existing UPR related mouse models in the context of IBD.

Gene	Genetic association	Model	Phenotype	Ref
<i>XBP1</i>	CD and UC	<i>Xbp1^{ΔIEC}</i>	Spontaneous enteritis; loss of Paneth cells; inflammatory hyperreactivity of the epithelium; reduction in goblet cells, increased sensitivity to DSS	[13]
<i>ARG2</i>	CD and UC	<i>Arg2^{-/-}</i> (expression in secretory IEC)	Spontaneous granulomatous ileocolitis; Increased <i>Grp78</i> expression and <i>Xbp1</i> splicing; alterations in Paneth and goblet cells due to impaired ER disulfide bound formation in secretory proteins	[84]
<i>IRE1β</i>	Not reported	<i>Ire1β^{-/-}</i> (expression epithelial specific)	Increased <i>Grp78</i> expression; increased sensitivity to DSS	[79]
<i>ATF6</i>	Not reported	<i>Atf6α^{-/-}</i>	Increased ER UPR genes and sensitivity to DSS	[80]
<i>P58^{IPK}</i>	Not reported	<i>P58^{IPK}^{-/-}</i>	Increased <i>Grp78</i> , <i>Chop</i> expression and IRE1 phosphorylation; increased sensitivity to DSS	[80]
<i>S1P</i>	Not reported	<i>S1P</i> missense mutation (woodrat mouse)	Reduced <i>Grp78</i> and <i>Grp94</i> expression in DSS colitis albeit increased susceptibility	[81]
<i>CHOP</i>	Not reported	<i>Chop^{-/-}</i>	Protected from DSS and TNBS colitis	[82]
<i>MUC2</i>	Not reported (poor GWAS coverage to gene structure)	Missense mutation in <i>Muc2</i> (Winnie and Eeyore mouse)	MUC2 precursor accumulation accompanied by ER stress; spontaneous colitis	[33]

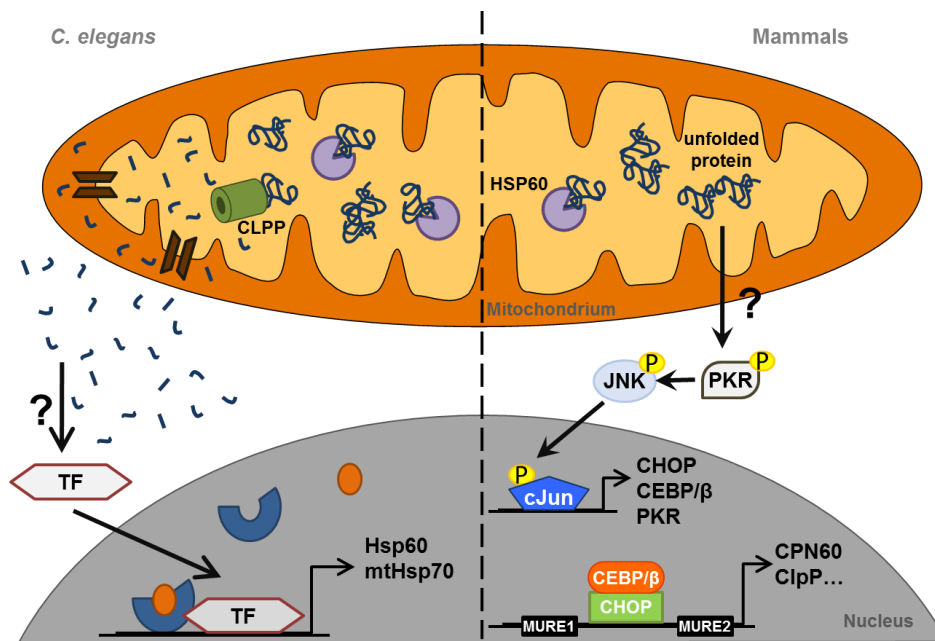
Tab. 3 Summary of available UPR related mouse models for IBD (adapted from [85])

As already mentioned, commensal bacteria are key drivers of intestinal inflammation in IBD and pathways crucial for sensing and controlling bacteria, like TLR signaling and autophagy interact with ER UPR [86]. Recent data suggest that TLR signaling can modulate ER UPR signaling and activate ER UPR-associated transcription factor [87, 88]. In line, we could show ER UPR modulation in IEC by TLR signaling using TLR2 and TLR4 deficient mice [89]. In macrophages, TLR2 and TLR4 have been demonstrated to specifically induce the IRE1/XBP1 arm of the ER UPR required for a sustained cytokine production [87]. Low doses of the TLR4 ligand LPS prior to induction of systemic ER stress, seems to suppress CHOP induction to protect TLR expressing cells from damage during host defense [88]. The involvement of ER UPR in autophagy is even more complex. ER UPR-induced autophagy might represent an alternative mechanism to respond to misfolded proteins in the ER lumen that cannot be removed by ERAD [90]. Several ER UPR pathways have been linked to the induction of autophagy – nevertheless, the necessity of different UPR components is still a matter of debate. Of note, these pathways described to be connected to ER UPR are critical for IEC to sense and control the composition of the intestinal microbiota e.g. autophagy being implicated in invasive bacterial elimination [91]. Especially for Paneth cells the network of microbiota sensing and protein quality control is eminently important. Not surprisingly, polymorphisms in sensing-related *NOD2* gene, autophagy related *ATG16L1* and UPR related *XBP1* affect Paneth cell function in human IBD. This can be confirmed by the finding that *Nod2* and *Xbp1* deficient as well as *Atg16l1* hypomorphic mice all display alterations in Paneth cell structure and function [13, 92-94]. Additional work of our group demonstrated that luminal iron impacts on the composition of the intestinal microbiota as well as epithelial UPR probably via ROS and PERK/NRF2 dependent mechanisms [95, 96].

1.4.3 The mitochondrial unfolded protein response

In mitochondria, the main source of cellular ATP, an UPR has evolved as well. Due to their prokaryotic origin, mitochondria are enclosed by two membranes. Outer and inner membranes separate two compartments, the intermembrane space and the matrix. The matrix is surrounded by the impermeable inner membrane which is folded to cristae and possesses gated channels for metabolites and protein exchange [37, 97]. Electrons from redox equivalents produced during oxidation of acetyl-CoA to CO₂ in the tricarboxylic acid (TCA) cycle within the mitochondrial matrix are transferred to five respiratory chain complexes located in the inner membrane. This transport is used to build up a proton gradient between the inner membrane space (high H⁺) and the matrix (low H⁺). Finally, the reflux of protons into the matrix drives ATP production by ATP synthase and electron transfer reduces oxygen to water - the whole process is called oxidative phosphorylation (OXPHOS) [98]. The matrix harbors several copies of the circular mitochondrial genome, enzymes for

DNA replication, transcription and translation as well as enzymes for various metabolic processes such as TCA, fatty acid oxidation, iron-sulfur cluster formation and heme synthesis [37]. Since only 13 enzymes are encoded by the mitochondrial genome itself [37], the majority of mitochondrial proteins need to be imported as cytosolically synthesized precursors [37] which need to be unfolded to transit the translocase of the outer and inner membrane (TOM/TIM), a process that is enforced by the trap-and-pull-activity of the matrix residing mtHSP70 (=GRP75) and its co-chaperone mtDNAJ (=TID1) [99, 100]. Following import, the mitochondrial target sequence is cleaved and proteins are re-folded [101], mainly by the help of HSP60 and HSP10 [37, 102]. Like during ER UPR, MT UPR is evoked by an insufficient protein folding capacity in the form of misfolded, misassembled or aggregated proteins trying to restore protein homeostasis by increasing the folding capacity and enhancing protein degradation [103]. In contrast to the nematode *C.elegans*, the MT UPR in mammals is rather poorly described. Transfection experiments with a truncated version of the enzyme ornithine transcarbamylase (OTC Δ) prone to aggregate in the MT matrix provokes a MT UPR leading to induction of chaperones HSP60, HSP10, TID1 and the proteases CLPP and YME1 in a organelle specific manner, since ER chaperones were not induced [104]. Mechanistic investigations revealed that mitochondrial stress activates JNK 2 which subsequently activates TF AP-1 to transcriptionally upregulate TF CHOP and its cofactor C/EBP β [104-106]. Consequently, CHOP induces MT UPR target genes containing a CHOP-C/EBP β binding site flanked by conserved MT UPR elements (MURE) in their promoters [105]. CHOP seems to be addressed by both ER and MT UPR but through separate pathways. Promoter analysis revealed that ER UPR uses ATF4 or ATF6 binding to C/EBP-ATF sites or ERSE respectively, whereas MT UPR induces Chop via AP-1 [105, 106] (Fig. 5). Although genetic studies in *C.elegans* identified various additional players in MT UPR, the assignability to the mammalian situation is questionable, since for some factors no obvious homologues could be found. The concept suggests that unfolded proteins are degraded by CLPP to peptides that are translocated through the mitochondrial inner membrane und diffuse to the cytoplasm. In a yet unidentified way, this signal is sensed and processed leading to the formation of a TF complex at the promoter of target genes like HSP60 [107]. Unfortunately, this concept could not (yet) be verified in mammals. Nevertheless, our group could confirm the relevance of CLPP for the mammalian MT UPR induction. We could show that dsRNA activated protein kinase R (PKR) is activated upon OTC Δ transfection in a CLPP dependent manner. Activated (meaning phosphorylated) PKR itself phosphorylates eIF2 α and SAPK/JNK leading to AP1. This TF mediated transcriptional activation of CHOP but also of PKR itself in a positive feedback loop [68]. However, the exact link between CLPP and PKR activation remains to be identified (Fig. 5).

Figure 5**Fig. 5 The mitochondrial unfolded protein response**

Left side: Proposed MT UPR in *C. elegans*. Central signal aspect is the degradation of unfolded proteins to peptides by CLPP. The release of peptides is sensed and transduced into a transcriptional response. Right side: Mammalian MT UPR with PKR as central signaling kinase (adapted from [35]).

1.4.4 The ER - mitochondrial signaling network

It has already become obvious that ER and MT UPR share common signaling molecules, but these are not the only levels of communication between these two organelles [35]. Mitochondria have to be considered as a dynamic network rather than single organelles due to constant fission and fusion events [37]. The ER is connected to mitochondria at an interface called mitochondria associated membranes (MAM) which are sites of calcium and lipid, energy and metabolite exchange [108]. Calcium fluxes may be a way of communication between the organelles ensuring the constant supply of the ER with ATP, since ER chaperones like GRP78 depend on ATP (and calcium) [109]. Interestingly, transiently increased mitochondrial calcium levels promote the activity of the ATP synthase [110]. Additionally, flavin adenine dinucleotide derived from the mitochondrial metabolism is shuttled to the ER where it serves as a cofactor for ER oxidoreductin (ERO) 1 β necessary for disulfide bond formation [111]. This vital exchange of ATP and flavin may be the reason why MAM are enriched in ER chaperones and oxidoreductases [112]. Changes in calcium homeostasis, redox status, or energy deficiency trigger ER UPR and at the same time ER stress impacts mitochondrial gene expression, morphology and function [113-115] and conversely mitochondria have been shown to modulate ER UPR [116, 117]. Nuclear genes

that encode mitochondrial proteins such as the MT matrix chaperone GRP75 and the proteases LON and YME1 are induced by ER stress [113]. Mitochondria modulate the ER UPR under conditions of glucose deprivation. Additionally, ER and mitochondria are the main sources of reactive oxygen species, which in turn can elicit ER and MT UPR [118].

IBD has been repeatedly suggested to be an energy-deficiency disease involving epithelial mitochondria and cell oxidative metabolism [119, 120]. Evidence for this hypothesis is provided by the fact that fatty acid β -oxidation is implicated in CD pathogenesis and a polymorphism in SLC22A5, encoding the carnitine transporter OCTN2 has been described as a risk factor in IBD (see chapter 1.1)[121]. Carnitine is essential for the energy metabolism of IEC since it transports long-chain fatty acids into mitochondria for β -oxidation [122]. Strikingly, gene knockout or pharmacological inhibition of fatty acid β -oxidation results in experimental colitis [123, 124]. Appropriate β -oxidation and continuous energy supply may be explicitly important for IEC upon changes in the microbial composition or energy consuming inflammatory processes [86, 125]. Of note in this context, several pathogens and their toxins specifically target mitochondria and disrupt their function [126] and cytokine-evoked ROS generation evokes a drop in mitochondrial membrane potential [127]. Additionally, enterocytes of IBD patients have been reported to display swollen mitochondria with irregular cristae pointing to impaired function [128]. In line with these observations, the ATP levels in colonocytes of some CD patients have been found to be reduced [129] and biopsies from patients with IBD were more sensitive to the application of substances uncoupling the respiratory chain from OXPHOS evoking ROS production [130]. Finally, adding relevance to the concept of integrated metabolic, inflammatory, ER and MT UPR pathways (Fig. 6), our group could show increased levels of PKR in IEC of two murine models of chronic, immune-mediated colitis as well as human IBD patients accompanied by elevated levels of GRP78 and HSP60 [68].

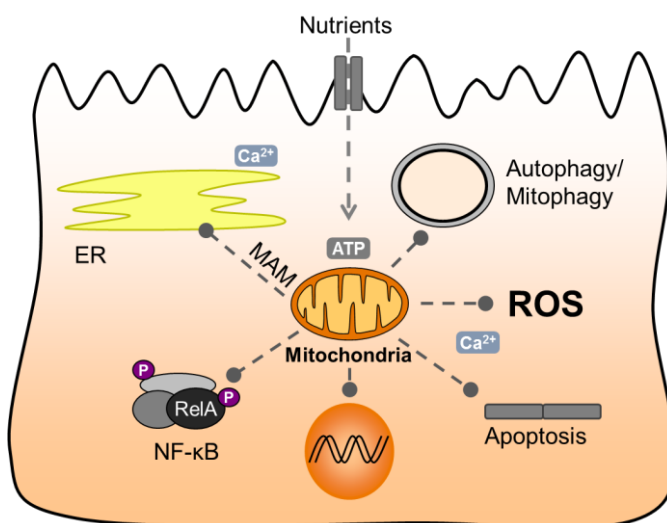


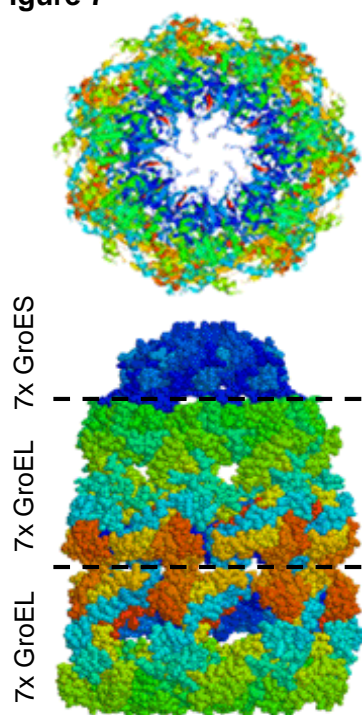
Fig. 6 Mitochondria in the center of cellular signaling

Graphical overview of the tightly interrelated cellular signaling network centering on mitochondria. Mitochondria are connected to the ER via Ca^{2+} signaling and physically via membrane associated membranes (MAM). Among other things, mitochondria are a source of ROS, initiate autophagy (mitophagy), elicit apoptotic signals and activate NF- κ B for cytokine production (adapted from [35]).

1.5 HSP60 – chaperone and danger signal

Mitochondrial HSP60 is a member of the family of type I chaperonins which enable the correct folding of newly synthesized and stress-denatured proteins in mitochondria, chloroplasts and eubacteria [131]. Studies in yeast from the late 1980s attributes an essential role to HSP60 for the folding and assembly of proteins imported into mitochondria [132, 133], for keeping proteins in an unfolded state for transport across the inner membrane of the mitochondria [134] and for the prevention of protein denaturation during heat stress [135]. Yeast studies also revealed that HSP60 interacts with single stranded mitochondrial template DNA in a complex with other factors to regulate the replication and transmission of mitochondrial DNA [136]. These essential roles are underlined by the fact that a constitutive HSP60 deficiency antagonizes cell viability in yeast [137] and leads to embryonic lethality in mice [138]. Mutations in the *HSPD1* gene were discovered to be the cause of the severe genetic neurodegenerative disorder hereditary spastic paraplegia in humans [139-141].

Figure 7



Intensive structure analysis of bacterial chaperonin has revealed that the protein folding function is executed concertedly by a barrel-shaped complex consisting of two heptameric rings of chaperonin monomers (GroEL in bacteria, HSP60 in mammals) each enclosing a large central cavity [142, 143] and two co-chaperonin heptamers (GroES in bacteria, HSP10 in mammals) binding the apical domain of the chaperonin complex [144, 145] (Fig. 7).

Fig. 7 Structure of HSP60 from bacterial origin (GroEL)

Two rings of seven chaperonin monomers each form a barrel enclosing an internal cavity for protein folding (top view). The HSP10 (GroES) heptamer (blue) attaches to one of the apical domains of the HSP60 barrel complex (adapted from [146]).

In the closed conformation of HSP60, a newly synthesized or denatured protein, which exposes hydrophobic residues to the surface, adheres to hydrophobic residues that lie on the inner surface of one of the HSP60 rings. Subsequent binding of ATP induces a conformational change, which enables the binding of HSP10. This causes an enlargement of the cavity which exposes hydrophilic residues (open conformation). These structural changes facilitate the release of the substrate protein into the enclosed cavity, where it can fold protected from aggregation [147-149].

HSP60 refolds denatured proteins exclusively with the assistance of the mitochondrial co-chaperonin, in contrast to its bacterial homolog, which is able to function with the help of co-chaperonin from any species [150]. This specificity is accomplished by special structural elements involved in direct contact of the two proteins, but also ones that are far from the binding site [146]. HSP60 and HSP10 even share a bidirectional promoter driving their expression concertedly [151].

Besides its primary function as a mitochondrial protein-folding enzyme, HSP60 has been implicated in preventing mitochondrial apoptosis signaling [152, 153] in tumor cells. Beyond that, HSP60 exerts various extra-mitochondrial activities. First, HSP60 has been localized in the cytoplasm, where it forms complexes with the pro-apoptotic factors Bax and Bak [154, 155] to prevent their activity, inactivates p53 [152] and promotes the TNF-mediated activation of the IKK/NF- κ B survival pathway via direct interaction with IKK α/β in tumor cells [156]. Nevertheless, the role of cytosolic HSP60 as a pro-or anti-apoptotic factor is still a matter of debate and may depend on the cellular context [157]. Despite the fact that HSP60 is retained after being synthesized in the cytoplasm, experimental analysis has shown that the cell is quickly capable of moving cytoplasmic HSP60 into the mitochondria upon environmental conditions which demand a higher presence of mitochondrial HSP60 [158].

Beyond its localizations in mitochondria and cytoplasm, HSP60 has also been found to be located at the extracellular side of the plasma membrane. HSP60 has been detected on the surface of normal cells, tumor cell lines [159] and primary tumors [160-162]. In mice infected with the intracellular bacterium *Listeria monocytogenes*, spleen and liver cells expressed murine HSP60 on their plasma membranes [163]. The finding that HSP60 has a lipid-binding domain, enabling it to interact with membranes [164], might explain this phenomenon. A possible function of the surface appearance of HSP60 can be seen in the activation and maturation of dendritic cells and the generation of an antitumor T-cell response [161, 165]. Moreover, it has been reported that eukaryotic cells actively secrete chaperonins into the extracellular fluid. Besides the option that HSP60 is released after cell trauma like myocardial ischemia, recent studies in tumor cells unraveled mechanisms by which mitochondrial HSP60 can be actively secreted [166-168]. Already in the late 1990s, human neuroblastoma cells for example have been shown to secrete a 60 kDa chaperonin protein [169]. Since then elevated HSP60 levels have been detected in the plasma of healthy subjects [170], under conditions of physiological and psychosocial stress [171] and in various inflammation associated diseases like periodontitis [172, 173], atopic dermatitis [174], Hashimoto's thyroiditis [175], HIV [176] obesity, insulin resistance [177] and cardiovascular disease/atherosclerosis [178-180]. It has been observed that secreted human HSP60 can stimulate vascular endothelial cells and innate immune cells to produce pro-inflammatory factors like TNF, nitric oxide, and IL-6. In addition, HSP60 was found to induce gene

expression of the cytokines IL-12(p70) and IL-15, promoting a Th₁ phenotype [181-183]. Newer studies postulate a cytokine independent activation of antigen-specific T cells by HSP60 activated innate immune cells [165]. While HSP60 from bacterial source has been reported to induce inflammatory responses through mechanisms both dependent and independent of TLR2 and TLR4 in innate immune cells [184, 185], endogenous HSP60 that appears in the serum after myocardial ischemia and reperfusion has been found to induce inflammation through activating TLR 4 signaling in cardiomyocytes [186]. Nevertheless, if TLR 4 is indeed the virtual receptor for HSP60 is still a matter of debate [187, 188]. Taking into account that HSPs like HSP60 were identified as targets of immune responses during various microbial infections [183, 189-192], HSP60 from exogenous and endogenous source can be both considered as a danger signal for the innate immune system [181].

Because of the high sequence homology between microbial HSPs and endogenous HSPs derived from damaged or stressed tissue, immunological cross-reactivity was suggested to contribute to the development of autoimmune disorders including rheumatoid arthritis, diabetes and cystic fibrosis, diseases where levels of antibodies to human HSP60 are elevated in the plasma [193, 194]. In the case of atherosclerosis, it has been hypothesized that these antibodies cross-react with the human HSP60 protein, and that this protein is expressed on the surface of stressed human vascular endothelial cells. The binding of HSP 60 antibodies to the surface of the vascular endothelial cells results in complement-mediated cytotoxicity, and the damaged areas of the vasculature then become sites of development of atherosclerosis [195].

Tab. 4 summarizes the involvements of HSP60 from different origins in human diseases.

Disease type	Disease example	HSP60 source	Evidence	Ref.
Neuro-degeneration	Hereditary spastic paraplegia	Human	Mutation in <i>hspd1</i> gene	[138, 140, 141]
Infection	Inflammation	Mycobacteria, <i>E.coli</i> , <i>Helicobacter pylori</i> , <i>Chlamydia</i> and <i>Campylobacter</i>	Activation of leucocytes, fibroblasts, epithelial cells to produce cytokines	[183, 189-192]
autoimmunity	Periodontitis, atopic dermatitis, Hashimoto's thyroiditis, HIV, obesity, insulin resistance, cardiovascular disease, ischemia/reperfusion	Human	Stimulate innate immune cells, myofibroblasts to inflammatory responses	[172-180]
	Atherosclerosis	Human	Presence of human HSP60 in atherosclerotic lesions, anti-HSP60 antibodies	[195]
	Juvenile arthritis, diabetes, cystic fibrosis	Human	Anti-HSP60 antibodies	[193, 194]

Tab. 4 Involvement of HSP60 in human diseases

In contrast to HSP60, human HSP10 was shown to stimulate the production of anti-inflammatory cytokines and suppress the production of pro-inflammatory cytokines [196]. The existence of HSP10 in the serum of pregnant women is discussed as an immunosuppressive factor during early pregnancy [197].

With respect to IBD, only little is known about the role of HSP60. Elevated levels have been found by our group in intestinal epithelial cells upon inflammation in various mouse models of chronic colitis [68] and in inflamed epithelium of CD and UC patients [68, 198]. This phenomenon could simply reflect the need for a higher rate of protein synthesis and, consequently, of protein folding for anti-pathogenetic mechanism of cytoprotection in the context of inflammation. Second, considering the possibility that HSP60 can appear extracellularly, it is possible for antibodies to encounter these molecules and react against them. Accumulation of antigen-antibody complexes in the mucosa would trigger a series of pathological events leading to perpetuation of inflammation and tissue destruction. Third, released HSP60 could activate cells of the innate immune system locally and systemically to release cytokines and chemokines and prime adaptive immune responses. Indeed, HSP60-derived peptides were found to stimulate an inflammatory response accompanied by production of pro-inflammatory cytokines in intestinal mucosa of patients with CD [199]. Consequently, HSP60 should be considered a contributor to pathogenic mechanisms mediated by the immune system [200]. To further increase the level of complexity, HSP60 was also found positively correlated with the presence of CD68⁺ macrophages in the lamina propria with a high degree of co-localization between HSP60 and this marker for cytosolic granules [200].

The fact that mitochondrial and cytosolic HSP60 favors the survival of tumor cells has already been mentioned above [152, 156]. Elevated levels of HSP60 have been linked to the ability to survive apoptotic stimuli [152], to the loss of replicative senescence [201], to uncontrolled proliferation and to neoplastic transformation [202, 203]. Conversely, *in vitro* knockdown of HSP60 stopped tumor cell growth [204]. Interestingly, tumor immunogenicity may also depend on whether tumor cells express and secrete HSP60 or not [161]. The expression level of HSP60 in/on tumors or in body fluids may be used to predict the probability that an effective immune response against a tumor will be elicited. While e.g. elevated levels of HSP60 in acute myeloid leukemia correlate with a bad prognosis in patients with unfavorable phenotype [205], in esophageal squamous carcinoma the elevated level correlates with a better five-year survival [206]. Correspondingly, decreased HSP60 levels in vesicle transitional cell carcinoma of the urinary bladder goes along with worse outcome of local treatment [207].

The following table lists examples of tumors with elevated and decreased HSP60 expression levels (Tab. 5).

Type of tumor	Tumor	HSP60 level	Method	Ref.
Nervous	Glioblastoma	Decreased	protein	[208]
Haemolympho-poietic	Acute myeloid leukemia	Elevated	protein	[205]
Respiratory	Bronchial adenocarcinoma	Decreased	protein	[209]
Digestive	Esophageal squamous carcinoma	Elevated	protein	[206]
	Gastric MALToma	Elevated	protein	[210]
	Large bowel	Elevated	RNA/protein	[211-213]
	HCV-hepatocellular carcinoma	Elevated	protein	[214]
Urinary	Vesical transitional cell carcinoma	Decreased	protein	[207]
Male reproductive	Prostate adenocarcinoma	Elevated	protein	[215]
Female reproductive	Cervical carcinoma	Elevated	protein	[216]

Tab. 5 Expression levels of HSP60 in selected tumor types (adapted from [217])

In summary, HSP60 appears only at the first glance as a “conventional” mitochondrial chaperone. In reality, HSP60 appears in various cellular compartments and is implicated in many different cellular processes. Accumulating evidence supports the concept that HSP60 serves as a cellular danger signal that appears in case of a disturbed cellular homeostasis and activates intra- and extracellular defense mechanisms to confine a potential harm to the host organism. The present work focusses on the role of HSP60 for maintaining the epithelial homeostasis in the context of chronic intestinal inflammation.

2 AIM OF THE WORK

The intestinal epithelium is the key interface between luminal factors of the gut and the mucosal immune system of the host. Receiving manifold signals from both sides the intestinal epithelium need to process these signals properly to maintain intestinal homeostasis. One set of signal processing programs are the unfolded protein responses (UPR), since the demand of properly folded and functional proteins in the cytoplasm, the ER and the mitochondria is crucial for the functionality of organelles and for the IEC as a whole. ER UPR pathways in IEC have been implicated in the pathogenesis of IBD but the impact of MT UPR signaling in this context is hardly investigated, despite the fact that an impaired energy metabolism and functional alterations of mitochondria in IEC have been associated with IBD. Therefore, the present work aims to investigate the impact of activated ER and MT UPR pathways on the epithelial homeostasis by the use of novel IEC specific mouse models. For this purpose, two approaches will be taken. First, the transgenic overexpression of the UPR relevant transcription factors *nATF6* and *CHOP*. Second, the IEC specific knockout of the mitochondrial chaperone *HSP60* representing the focus of the present work.

Chaperones are triggers and targets of the ER and MT UPR pathways. IEC from animal models of IBD and IBD patients show elevated levels of the ER chaperone *GRP78* and the MT chaperone *HSP60*. Therefore, chaperone deficiencies are supposed to be a valid tool to evoke an acute or chronic activation of UPR pathways in IEC and to study their impact on epithelial homeostasis. To target specifically IEC with an *HSP60* deficiency, *Hsp60*^{flox/flox} mice, burying conditional knockout alleles, will be crossed with *VillinCre* mice. Thus, big parts of the *ATPase* coding sequence of *Hsp60* shall be deleted from the genome of *Villin* expressing cells upon embryonic developmental stage E.10.5. In order to induce the *Hsp60* knockout specifically in adult IEC of the developed gut, *Hsp60*^{flox/flox} mice will be crossed with *VillinCreER*^{T2} mice. By administration of tamoxifen, Cre recombination gets active and performs the genetic knockout. The presence of mucosal inflammation as well as the impact on epithelial proliferation and stemness will be central matters of investigation.

To assess compensatory mechanisms of the MT UPR in IEC upon a reduction in *HSP60* levels, we will investigate haplodeficient *Hsp60*^{+/-} for the presence of intestinal tissue pathologies. To further challenge the haplodeficient intestinal tissue, two inflammatory triggers will be applied to this mouse model: First, an oral administration of the colitogenic agent DSS und second, the intercrossing of *Hsp60*^{+/-} mice with *Tnf*^{ARE/WT} mice, a genetic model for chronic Crohn's disease-like ileitis.

Overall, the use of *HSP60* deficient mouse models aims to address the question what impact an MT chaperone deficiency and the resulting MT UPR have on the epithelial homeostasis including IEC proliferation and mucosal inflammation.

3 MATERIAL AND METHODS

3.1 Supplier of experimental material

Company	City of residence	State/Country of residence
Abcam	Cambridge	UK
Active Motif	Carlsbad	CA, USA
Affymetrix	Santa Clara	CA, USA
Agilent	Böblingen	Germany
Alpha Metrix Biotech	Rödermark	Germany
ATCC	Manassas	VA, USA
BD Biosciences	Franklin Lakes	NJ, USA
BioLegend	San Diego	CA, USA
Biomers	Ulm	Germany
Biorad	Munich	Germany
Biorbyt	Cambridge	UK
Cell Biolabs	San Diego	CA, USA
Cell signaling	Danvers	MA, USA
Dako	Hamburg	Germany
Dianova	Hamburg	Germany
eBioscience	San Diego	CA, USA
Electron Microscopy Sciences	Hatfield	PA, USA
Fermentas (Thermo Fisher)	Waltham	MA, USA
Genomatix	Munich	Germany
GE Healthcare	Uppsala	Sweden
Gibbco	Cincinnati	OH, USA
InvivoGen	San Diego	CA, USA
LabVision/NeoMarkers	Fremont	CA, USA
LasVendi	Soest	Germany
Leica	Soest	Germany
Life Technologies	Karlsruhe	Germany
Macherey-Nagel	Düren	Germany
McCormick	Sparks	MD, USA
Medit	Burgdorf	Germany
Mfd diagnostics	Wendelsheim	Germany
Millipore	Billerica	MA, USA
Parr Instrument Company	Moline	IL, USA
National Diagnostics	Charlotte	NC, USA
NEB	Ipswich	MA, USA
PAN-biotech	Aidenbach	Germany
Peqlab	Erlangen	Germany
PerkinElmer	Waltham	MA, USA
Physiologic Instruments	San Diego	CA, USA
Promega	Mannheim	Germany
Qiagen	Hilden	Germany
Roche Diagnostics	Mannheim	Germany
Roth	Karlsruhe	Germany
Santa Cruz	Santa Cruz	CA, USA
Sigma-Aldrich	St. Louis	MO, USA
Ssniff	Soest	Germany
Olympus	Shinjuku	Japan
Systat	Chicago	IL, USA
Taconic	Cologne	Germany
Thermo Scientific	Waltham	MA, USA
VWR	Leuven	Germany
Zeiss	Jena	Germany

Tab. 6 Companies purchasing experimental material used for the thesis

3.2 Animal models

3.2.1 Ethics statement and animal housing

The maintenance and breeding of mouse lines and all experiments were approved by the Committee on Animal Health and Care of the local government body of the state of Upper Bavaria (Regierung von Oberbayern; AZ 55.2-1-54-2532-12-12 and 55.2-1-54-2531-214-13) and performed in strict compliance with the EEC recommendations for the care and use of laboratory animals (European Communities Council Directive of November 24, 1986 [86/609/EEC]). All mice were housed under specific pathogen free (SPF) conditions according to the criteria of the Federation for Laboratory Animal Science Associations (FELASA) except the $\Delta ARE/Hsp60^{+/-}$ mice which were conventionally housed in open cages.

3.2.2 Purchase of established mouse models

Heterozygous constitutive Grp78 knockout mice (*Grp78^{+/-}*) were provided by Prof. Amy S. Lee (USC Norris Comprehensive Cancer Center, Los Angeles) on the genetic background C57BL/6J. In this mouse model exons 5-7 of *Grp78* were excised from the genome, leading to the deletion of the C-terminal part of the ATPase domain and the N-terminal part of the peptide binding domain of the chaperone. The homozygous constitutive knockout is embryonically lethal at developmental stage E3.5 [218].

TNF^{ΔARE/WT} mice serve as a model for Crohn's disease-like ileitis and chronic inflammatory arthritis. Mice were provided by Prof. George Kollias (Alexander Fleming Biomedical Sciences Research Center, Athens, Greece). In this mouse model AU rich elements (ARE) from the 3' untranslated region of the *Tnf* mRNA required both for the re-alleviation and reinforcement of message destabilization and translational silencing were genetically deleted (genetic background mainly C57BL/6N). Upon an inflammatory trigger, various cell types express TNF in excess which leads to the manifestation of a chronic inflammation phenotype in the distal ileum and the joints. Homozygous *TNF^{ΔARE/ΔARE}* mice show a severely reduced weight and increased mortality in comparison to heterozygous and WT littermates [219].

To enable the targeted deletion or transgenic expression of genes in a specific tissue or upon a specific stimulus, three different Cre recombinase expressing mice were used. The Cre-Lox recombination system derived from bacteriophage P1 as a site-specific recombinase technology was developed by Brian Sauer *et al.* in 1987/88 to activate gene expression in mammalian cell lines and transgenic mice [220, 221]. Feil *et al.* published a mouse model in 1996 expressing a Cre recombinase that has been fused to a mutated ligand-binding domain of the human estrogen receptor (ER) resulting in a tamoxifen-dependent Cre recombinase (ER^T) which is activated by tamoxifen, but not by estradiol [222]. By introducing further mutations, ER^T was finally replaced by an improved ER^{T2} with enhanced affinity to 4-hydroxy-tamoxifen [223]. Tab. 7 summarizes the Cre expressing mice used in the experiments:

Strain	Supplier	Target tissue	background	Reference
<i>VillinCre</i>	K.P. Janssen	IEC	C57BL/6N	[224]
<i>VillinCreER^{T2}</i>	K.P. Janssen	IEC	C57BL/6N	[224]
<i>Lgr5CreER^{T2}-IRES-Egfp⁺</i>	Jackson lab	ISC	C57BL/6J	[225]

Tab. 7 Cre expressing mouse strains and their properties

The *Lgr5CreER^{T2}-IRES-Egfp* mouse serves as a reporter mouse for ISC as well, since the *Lgr5* promoter drives the expression of *CreER^{T2}* and the reporter gene *Egfp* simultaneously.

3.2.3 Generation of new mouse models

The generation process of transgenic *nAtf6* and *Chop* as well as constitutive and conditional *Hsp60* knockout mice was performed by the company Taconic-Artemis in close consultation with our lab. To generate HSP60 deficient mice, mouse genomic fragments of the *Hsp60* locus were subcloned using RPCIB-731 BAC library via ET recombination and recloned into a basic targeting vector placing a F3-site flanked puromycin resistance cassette in intron 3 and a thymidine kinase cassette downstream of the 3' UTR. LoxP sites flanked exons 4 to 8. In the case of conditional *nAtf6-HA* and *Chop-HA* transgenic mice, cDNA fragments were cloned directly from the delivered plasmids (see 3.4) into a recombinase-mediated cassette exchange (RMCE) vector harboring the indicated features. The corresponding vectors were sequenced to confirm correctness. C57BL/6N ES cells in case of *nAtf6-HA* and *Chop-HA* special RMCE ES cell line were grown on a mitotically inactivated feeder layer comprised of mouse embryonic fibroblasts (MEF) in DMEM High Glucose medium containing 20% FBS (PAN-biotech) and 1200 U/mL Leukemia Inhibitory Factor (Millipore ESG 1107).

For *Hsp60*, 1×10^7 cells and 30 μ g of linearized DNA vector were electroporated (Biorad Gene Pulser) at 240 V and 500 μ F. Puromycin selection (1 μ g/mL) started on day 2, counterselection with Gancyclovir (2 μ M) started on day 5 after electroporation. ES clones were isolated on day 8 and analyzed by Southern Blotting according to standard procedures. For *nAtf6-HA* and *Chop-HA*, 2×10^5 ES cells were plated on 3,5 cm dishes in 2 ml medium. Cells were transfected with 2 μ g circular vector and 2 μ g CAGGS-Flp plasmid in a 100 μ L lipofection batch using Eugene6 Reagent (Roche). G418 (200 μ g/mL) selection started on day 2. Seven days later single clones were isolated, expanded and molecular analyzed by Southern blotting according to standard procedures. After administration of hormones, superovulated Balb/c females were mated with Balb/c males. Blastocysts were isolated from the uterus at dpc 3.5. For microinjection, blastocysts were placed in a drop of DMEM with 15% FCS under mineral oil. A flat tip, piezo actuated microinjection-pipette with an internal diameter of 12 - 15 micrometer was used to inject 10-15 targeted C57BL/6NTac ES cells into each blastocyst. After recovery, 8 injected blastocysts were transferred to each uterine horn of 2.5 days post coitum, pseudopregnant NMRI females. Chimerism was measured in

chimeras (G0) by coat color contribution of ES cells to the Balb/c host (black/white). Highly chimeric mice were bred to strain C57BL/6 females.

In case of *Hsp60*, these female mice were transgenic for Flp recombinase (Flp-deleter mice) to excise the puromycin resistance cassette at the F3 sites (see Tab. 29, appendix). In all strains, germ line transmission was identified by the presence of black strain C57BL/6 offspring. Taconic delivered two breeder pairs for each of the four generated mouse strains.

3.2.4 Embryo preparation and genotyping

Hsp60^{flox/WT}-VillinCre⁺ and *Hsp60*^{flox/flox}-VillinCre⁻ mice were mated. When females were plug positive, embryos were assumed to be in developmental stage E 0.5 (0.5 days post conception). At the indicated stage (E 11.5-13.5) pregnant mice were killed by cervical dislocation and the uterus was removed. The embryos and the surrounding visceral yolk sac were prepared from the uterus, examined under the microscope and tail cuts were taken from the embryos for genotyping.

Tail cuts or ear punches were lysed in a 10 mM Tris-HCl buffer pH 8.0 buffer containing 50 mM KCl, 0.45% Nodidet P40, 0.45% Tween 20 and 0.5 mg/mL Proteinase K overnight (O.N.) at 65°C and inactivated at 95°C for 10 min. 2 µL of the clear supernatant was used for Crimson-Taq PCR (NEB) according to the protocol described in 3.5.

For separate genotyping of jejunal villi and crypts of *Hsp60*^{ΔIEC} mice, 10µm thick cryo-sections were H&E (Harris formulation) stained, 50.000 µm² cells were cut using the laser-microdissector (Leica DM6000 B) and lysed in RLT⁺ buffer (Qiagen). DNA was isolated using the Allprep DNA/RNA Mini kit (Qiagen). 2µL of DNA were used for Crimson-Taq PCR.

Allele	Forward primer	Reverse primer	T _A (°C)
Hsp60 KO	5'-accaagaccctgtactcttaacc-3'	5'-agtcctatgggactggatgg-3'	60
Hsp60 KO	5'-tctgcctgctcttctgcctca-3'	5'-accagaacaacctcaggcctcaat-3'	53
Hsp60 WT/flox	5'-accaagaccctgtactcttaacc-3'	5'-aacttgacctagatgttggtgg-3'	60
VillinCre	5'-caagcctggctcgacggcc- 3'	5'-cgcgaaacatcttcaggttct- 3'	55
VillinCreER ^{T2}	5'-accatatccaccgagtc- 3'	5'-aggaatgcgatgaagtag- 3'	55
Lgr5CreER ^{T2} - <i>Egfp</i>	5'-cactgcattctagtgtgg-3'	5'-cggtgccccgcagcgag-3'	58
DNA control	5'-gagactctggctactcatcc-3'	5'-ccttcagcaagagctggggac-3'	60
Grp78 KO	5'-gttgatattggaggtgggcaaaccaag-3'	5'-ttgttaggggtcgttcacctaga-3'	60
TNFΔARE	5'-aatgcacagccttctcacagag-3'	5'-aattagggttaggctcctgttcc-3'	58

Tab. 8 Primer pairs used for genotyping of mouse strains

3.2.5 Induction of postnatal genomic recombination and monitoring of animals

Male 8 weeks old *Hsp60*^{flox/flox}-VillinCreER^{T2+} or *Hsp60*^{flox/flox}-Lgr5CreER^{T2+} mice and their CreER^{T2-} littermates received phytoestrogen free chow feed (ssniff) for two weeks before they received 400mg tamoxifen per kg chow feed (LASvendi) in pellets *ad libitum* for seven days. Body weight was monitored before (day 0 -7), during (day 8 - 14) and after (day 15 -

16) oral administration of tamoxifen. Body weight, general condition, behavior and intestinal symptoms were assessed by a score between 0 and 10 each and were summarized in an affection index - according to the demands of the approved application for animal experiments. The animals were either killed at the indicated time point or when they reached an affection index of 20 by CO₂ inhalation.

3.2.6 Nutrient uptakes in small intestinal everted gut rings

Measurements were performed by Pia Röder in the lab of Prof. Hannelore Daniel (TUM), according to standard protocols. In principle, the whole small intestine was excised, adhesive mesenteric fat was carefully removed and the entire intestine was everted cautiously and washed in ice cold Krebs buffer (119 mM NaCl, 4.7 mM KCl, 2.5 mM CaCl₂, 1.2 mM MgSO₄, 1.2 mM KH₂PO₄, 25 mM NaHCO₃, pH 7.4). After discarding the first 5 cm, intestinal segments of approximately 1 cm were produced. Three consecutive segments were incubated for 2 minutes at 37 °C in 1 mL of the C14 radiolabeled incubation solutions (50 mM glucose + 1 µM ¹⁴C glucose (11.1 kBq/mL) ± 2 mM phloretin; 1 mM α-methyl-glucopyranoside (α-MDG) + 1 µM ¹⁴C α-MDG (11.1 kBq/mL) ± 0.2 mM phlorizin; 1 mM glycylsarcosine (Gly-Sar) ± 100 mM Gly-Sar. After 2 minutes, segments were removed from the radiolabeled incubation solutions and washed thoroughly in ice cold Krebs buffer. They were blotted on absorptive tissue and each segment was dried separately in a scintillation tube at 50°C overnight. After digestion in 100 µL Biosol (National Diagnostics) at 50°C overnight and decoloration with 20 µL H₂O₂ at RT for 1h, samples were mixed with 3 mL Bioscint (National Diagnostics) and vortexed well. Incorporation of radioactivity was measured using a liquid scintillation counter (PerkinElmer).

3.2.7 Calorimetry of fecal samples

Fecal samples were collected from individual mice between d₀ and d₂. Samples were dried at 60 °C for 3 days and stored airtight at RT until being assessed. Fecal pellets were manually ground and pressed into pellets and the gross energy content was determined using a 6300 Calorimeter (Parr Instrument Company).

3.2.8 Ussing chamber measurements

Ussing chamber systems (Easy mount chambers, Physiologic instruments) were used in the lab of Prof. Schemann (TUM) to investigate the colonic transepithelial electrical resistance (TER) and the translocation of sodium fluorescein (NaF) from the luminal to the basolateral side. The technical details and the principle of the measurements have been described previously [226]. Proximal and distal colon pieces were prepared as whole mount into slider with a recording area of 0.25 cm². Apical and basolateral sides were bathed separately in 3

mL Krebs buffer (37°C; aerated continuously with carbogen (95% O₂ and 5% CO₂)). After an equilibration period of 45 min, the Krebs solution in both compartments was replaced by 3 mL fresh Krebs solution containing 500 µg/mL NaF in the mucosal compartment and plain Krebs solution in the basolateral compartment. TER was calculated from the short circuit current and the resulting voltage difference. Translocated sodium fluorescein was measured in 100 µL aliquots from basolateral compartments using a fluorimeter (Thermo Scientific).

3.2.9 Tissue processing, H&E-, alcian blue-, IHC- and IF staining, ISH

The intestine was removed immediately after killing, trimmed free of adjacent tissue and cleaned of stool. Parts of the gastrointestinal tract were cut open and prepared as a “swiss role” [227], fixed in 10% phosphate buffered formaldehyde, dehydrated (Leica TP1020) and embedded in paraffin (McCormick; Leica EG1150C).

Step	Reagent	Time (min)	Step	Reagent	Time (min)
1	70% EtOH	60	7	100% EtOH	60
2	70% EtOH	60	8	100% EtOH	60
3	80% EtOH	60	9	Xylen	60
4	96%EtOH	60	10	Xylen	60
5	96%EtOH	60	11	Paraffin	60
6	100% EtOH	60	12	Paraffin	60

Tab. 9 Dehydration and paraffin embedding of formalin fixed tissue

5 µm sections (Leica RM2255) were deparaffinized and rehydrated in an automated manner (Leica ST5020). Staining with hematoxylin (of Mayer) and 0.2% eosin (ethanolic solution; both Medite) was performed using the same automate. Slides were mounted with Histokitt (Roth) and covered with a glass slip (VWR).

Deparaffinization+Rehydration			H&E staining		
Step	Reagent	Time (min)	Step	Reagent	Time (min)
1	Xylen	3	6	dH ₂ O	1
2	Xylen	3	7	Hematoxylin	4
3	100% EtOH	2	8	Running dH ₂ O	2
4	96%EtOH	2	9	Eosin	2
5	70% EtOH	1	10	70% EtOH	1
			11	96%EtOH	1
			12	100% EtOH	1
			13	100% EtOH	1,5
			14	Xylen+100% EtOH	1,5
			15	Xylen	2
			16	Xylen	2
			17	Xylen	various

Tab. 10 Deparaffinization, rehydration and H&E staining of tissue sections

After deparaffinization, acidic mucus was stained with alcian blue according to the protocol:

Step	Reagent	Time (min)	Step	Reagent	Time (min)
1	dH ₂ O	2	6	Running tap water	1
2	Alcian blue	30	7	95%EtOH	3
3	Running tap water	2	8	100% EtOH	3
4	dH ₂ O	1	9	100% EtOH	3
5	Nuclear fast red	5	10	Xylene	various

Tab. 11 Alcian blue staining of acetic mucus

Alcian blue solution	
Alcian Blue, 8GX	1 g
Acetic acid, 3% solution	100mL
Acetic acid	adjust to pH 2.5
0.1% Nuclear fast red Solution	
Nuclear fast red	0.1 g
Ammonium sulfate	5 g
dH ₂ O	100 mL

Mucus area was assessed using the laser microdissection microscope (Leica DM6000 B) and the associated software.

Immunohistochemical (IHC) and immunofluorescence (IF) staining was performed on 2-5 µm sections of formalin fixed and paraffin embedded tissue. After deparaffinization and rehydration, antigen unmasking was performed by cooking the sections in 10mM citrate buffer pH 6.0 in a pressure cooker for 23 min. After cooling to RT, sections were rinsed twice in PBS for 5 min. In case of an immunohistochemical staining, endogenous peroxidases were blocked by a 10 min incubation with 3% H₂O₂ (Sigma-Aldrich, St. Louis, MO), rinsed three times in dH₂O and one time in PBS. Specimens were blocked in blocking buffer for 60 min at 4°C.

Blocking buffer	
Normal serum from the same species as the secondary AB	1.25 mL
Triton X-100	75 µL
PBS	ad 25 mL

Primary antibodies were diluted in antibody diluent (1% BSA in PBS) and incubated on specimens O.N.

After rinsing three times with PBS, the according secondary antibody, diluted 1:200 in antibody diluent, was applied for 1h at RT. For immunohistochemistry, antigen detection was performed using the DAB enhanced liquid substrate system (Sigma-Aldrich). Slides were finally counterstained with hematoxylin for 7-10 sec, sealed with Histokitt (Roth) and covered

with glass slides (VWR). Sections were viewed on a Zeiss Axioskop 40 (Zeiss) microscope and imaged using a Zeiss AxioCam and the Axiovision software. For immunofluorescence, slides were mounted with Aquatex (Merck) and covered with glass slips (VWR) before visualization with the Fluoview FV10i microscope (Olympus).

Primary antibodies				Secondary antibodies		
Antigen	Supplier	Dilution	Species	Species	Supplier	Dilution
HSP60	Santa Cruz	1:200	goat	Goat Anti-Rabbit-HRP	Dianova	1:200
KI67	Abcam	1:100	rabbit	Rabbit Anti-goat-HRP	Sigma	1:200
OLFM4	Biorbit	1:100	rabbit	Donkey Anti-Rabbit-647	Dianova	1:200
c-Myc	Cell signaling	1:200	rabbit	Donkey Anti-Rabbit-Cy3	Dianova	1:200
GFP	Cell signaling	1:100	rabbit	Donkey Anti-Goat-488	Dianova	1:200
CD3	LabVision	1:300	rabbit	Donkey Anti-Goat-549	Dianova	1:200
B220	BD	1:3000	rat			
Ly6G	BD	1:600	rat			
CD11c	BD	1:5000	hamster			
F4/80	BioLegend	1:20	rat			
Lysozyme	Dako	1:2000	rabbit			
P-Stat 3	Cell signaling	1:100	rabbit			

Tab. 12 Primary and secondary antibodies used for IHC and IF

IF was also used for the detection of apoptosis on paraffin embedded tissue sections. For this purpose the Apo-BrdU *In Situ* DNA Fragmentation Assay Kit (Bio Vision) was used according to the manufacturer's instructions. For positive controls, 5 µm tissue sections were treated with DNaseI (Macherey-Nagel) for 15 min immediately after antigen retrieval. Further steps were done following the manufacturer's instructions.

RNA *in situ* hybridization (ISH) with digoxigenin-UTP labeled mRNA probes (assembled by *in vitro* transcription) for *Olfr4* was performed by Michael Allgäuer in the lab of Prof. Markus Gerhard (TUM) according to standard protocols.

3.2.10 Isolation of total primary IEC and jejunal villus tip and crypt bottom epithelium

Primary IEC were purified as previously described [29]. Approx. 7 cm of intestine (e.g. colon or jejunum) were inverted on a needle, vortexed vigorously for 1 min in 20 mL Dulbecco's modified Eagle's medium (DMEM; Gibco) containing 10% fetal calf serum (FCS), 1% L-glutamine and 0.8% antibiotics/antimycotics (see 3.3.1) supplemented with 1 mM dithiothreitol (Roth) and incubated (37 °C, 15 min) under continuous shaking. After vortexing, the IEC suspensions were centrifuged (7 min, 300 g, RT) and cell pellets were resuspended in DMEM containing fetal calf serum, L-glutamine and antibiotics. The remaining tissue was vortexed and incubated in 20 ml PBS (10 min, 37 °C) containing 1.5 mM EDTA. After vortexing again, the tissue was discarded and the cell suspension from this step was centrifuged as above. Finally, primary IEC were resuspended in 5 mL medium and purified

by centrifugation through a 20%/40% (in medium/PBS) discontinuous Percoll gradient (GE) at 600 g for 30 min. The IEC fraction at the interface between the Percoll phases was collected and washed once with medium and once with PBS.

The isolation of primary jejunal villus tip and crypt bottom IEC was adapted from a protocol published by Ferraris *et al.* [228] and Mariadason *et al.* [229]. The jejunum was cut in two ~5 cm pieces, inverted, cleaned of stool and beaded on a needle. Gut tissue was incubated (15 min, 37°C) in citrate buffer (96 mM NaCl, 1.5 mM KCl, 27mM NaCitrate, 8 mM KH₂PO₄, 5.6 mM Na₂HPO₄, pH 7.3) to vigorously remove mucus and stool remnants. The gut tissues fixed on the needles were then transferred into 10 ml of isolation buffer (1.5 mM EDTA, 0.5 mM DTT, 1 mg/ml BSA) and incubated for 10 min at 37°C while rocking (fraction 1). Gut tissues were transferred into 10 ml fresh isolation buffer and incubated as above (fraction 2). Fractions 1 and 2 of each jejunum were centrifuged (300g, 5 min, 4°C), resuspended and combined in 1 ml cold PBS and recentrifuged (300g, 5 min, 4°C). To gain fractions 3-10, the isolation procedure was repeated for 6, 5, 5, 9, 10, 15, 25 and 30 min always transferring the gut to a fresh tube with isolation buffer. Fraction 10 refers to the crypt bottom IEC.

IEC pellets of isolated primary IEC were lysed in 350 µl RA1 buffer (Macherey-Nagel) for subsequent RNA and/or protein isolation. Alternatively, IEC were lysed in a urea containing buffer for later protein detection only.

Protein lysis buffer	
Urea (7M)	8,4 g
Thiourea (2M)	3,04 g
CHAPS (2%)	0,4 g
Protease Inhibitor Cocktail	1 tablet
Phosphatase Inhibitor Cocktail	1 tablet
DTT	0,202 g
dH ₂ O	ad 20 mL

3.3 Cell lines and bacteria

3.3.1 Mode K

The Mode K cell line was obtained immortalizing small intestinal epithelial cells from the C3H/HeJ mouse by SV40 large T gene (oncogene) transfer through a murine ecotropic retrovirus. The resulting cell line express the SV40 large T mRNA and exhibit stable morphological and phenotypic characteristics of normal enterocytes over 56 passages, including intercellular junctions, and expression of cytokeratin, villin, slgA-receptor and vasoactive intestinal peptide receptors. All express cell surface major histocompatibility complex class I molecules. Interferon-γ treatment of Mode K cells results in a high level of class II molecule expression, and the ability to process and present native protein antigens to specific CD 4⁺ T-cells, via functional class II molecules. This indicates that Mode K cells

exhibit the antigen presentation characteristics of normal intestinal epithelial cells and are therefore a suitable model for the analysis of intestinal epithelial cell function in mucosal immunity [230].

DMEM (Gibbco) containing 4500 mg/L glucose (High glucose) is supplemented with other components, above all FCS, as it provides numerous growth factors and other stimulants for the epithelial cells. FCS has to be inactivated at 56°C for 30 min prior use. Additionally, 4mM L-Glutamine (Gibbco) and a mix of antibiotics and antimycotics (Gibbco) are added to the medium.

Mode K cells medium		Stock Conc.	Volume [mL]
DMEM medium		-	500
FCS superior		10% (w/v)	50
L-glutamine		4 mM	5
Antibiotic/ antimycotic mix	Penicillin	10000 U/mL	4
	Streptomycin	10000 µg/mL	
	Amphotericin B	25 µg/mL	

IEC are adherent cells, therefore require the following steps for passaging:

After withdrawal of medium and washing of cells twice with 12 mL PBS, 4 mL of trypsin-EDTA (Gibbco) was added. Incubation at 37°C causes the detachment of the cells from the bottom of the flask. The addition of 10 mL of medium stops the reaction. After centrifugation of the cell suspension at 350x g for 5 min, the cell pellet was resuspended in 2 mL medium.

The determination of the cell number is accomplished by mixing 20 µl of the cell suspension with 80 µl Tripan Blue solution (1:5 diluted in ddH₂O). After loading an aliquot of this dilution to a Neubauer chamber, living cells in the big squares of the chamber, with a volume of 0.1 µL (10⁻⁴ L) each, are counted using a light-microscope.

Finally, the number of cells per mL suspension can be calculated by the following equation:

$$\text{Cells/mL in medium} = \frac{\text{Ø cells counted} \times \text{dilution factor} \times 10^4/\text{mL}}{\text{Number of big squares counted}}$$

2x10⁵ Mode K cells per mL medium are seeded in order to get 80% confluence next day.

3.3.2 Competent *E. coli*

XL1-Blue Competent *E. coli* cells (Agilent) used for transformation of plasmid vectors possess the following genotype:

recA1 endA1 gyrA96 thi-1 hsdR17 supE44 relA1 lac [F' proAB lacIqZΔM15 Tn10 (Tetr)].

Transformed *E. coli* cells were spread on agar plates based on lysogeny broth (LB) [231], to which 1.7 % (w/v) agar-agar is added prior to sterilization.

LB-Medium (Luria/Miller)

Trypticase Pepton	10 g
Yeast extract	5 g
NaCl (Lenox formulation)	5 g
dH ₂ O	up to 1L

The medium was autoclaved for at least 20 min at 120°C and 1 bar overpressure for germ elimination. Temperature sensitive additives like antibiotics were filtered and added (100µg/mL ampicillin) after cooling the medium to 50°C in case of solid media or, in case of liquid media, prior to inoculation with single colonies picked from agar plate. Inoculated LB-medium is incubated O.N. at 37°C on continuous shaking (~250 rpm).

3.4 Plasmids

The following plasmids were used for different purposes:

Plasmid	Size [kb]	Resistance	Usage	Origin
pBluescript-CAG-lox-CAT-lox	6.5	Amp	Cloning	K.P. Janssen
pBluescript-HA-nAtf6	6.0	Amp	Transfection	Self-made
pBluescript-nAtf6-HA	6.0	Amp	Transfection	Self-made
pBluescript-HA-Chop	5.5	Amp	Transfection	Self-made
pBluescript-Chop-HA	5.5	Amp	Transfection	Self-made
pCAGGS- <i>Otc</i> Δ	5.0	Amp	Transfection	N. Hoogenraad
pCAGGS- <i>Otc</i>	5.2	Amp	Transfection	N. Hoogenraad

Tab. 13 Plasmids and their properties

The plasmid pBluescript-CAG-lox-CAT-lox was used as an eukyrotic expression vector, since it bears the CAG promoter, which also drives transgen expression in the later mouse model.

Figure 8

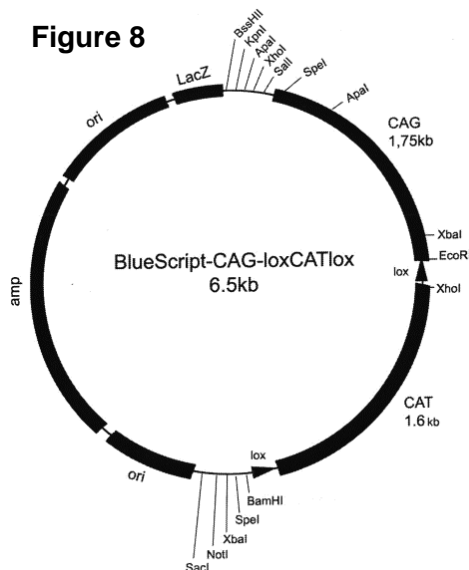


Fig. 8 Vector map of pBluescript-CAG-lox-CAT-lox

For cloning of *nAtf6-HA* and *Chop-HA* CDS, the vector pBluescript-CAG-lox-CAT-lox was used which bases on the pBluescript vector backbone (fermentas). Into the multiple cloning site the CAG promoter was inserted consisting of a CMV enhancer, a chicken β-actin promoter and a γ-globin splice acceptor for strong constitutive gene expression. The adjacent floxed CAT cassette was replaced by *nAtf6-HA* or *Chop-HA* (see 3.5).

3.5 Molecular cloning

The *nAtf6*- and *Chop*-coding sequence was amplified from full length cDNA of embryonic stem cells (Bl/6 strain) provided by Dr. Klaus-Peter Janssen. The primer design for the nuclear fragment of the *Atf6* CDS was performed according to de Almeida *et al.* [232].

Tab. 14 shows the nested primers used for this purpose.

<i>nAtf6-HA</i>	amplicon: 1079 bp		
Forward	ATF6_Nested_F	21 bp	$T_m = 57^\circ\text{C}$
	5'-TCACCCATCCGAGTTGTGAGG-3'		
Reverse	ATF6_Nested_R	20 bp	$T_m = 56.9^\circ\text{C}$
	5'-TTGCTCCAGCATGCTCATGG-3'		

<i>Chop-HA</i>	amplicon: 506 bp		
Forward	Chop_Nested_F	24 bp	$T_m = 57.7^\circ\text{C}$
	5'-TATCATGTTGAAGATGAGCGGGTG-3'		
Reverse	Chop_Nested_R	24 bp	$T_m = 57.4^\circ\text{C}$
	5'-CAATGTACCGTCTATGTGCAAGCC-3'		

Tab. 14 Nested primers and their properties used for amplification of coding sequences

HotStar HiFidelity Polymerase (Qiagen) with proof reading activity was used to amplify the coding sequences from cDNA:

PCR Mix	Volume [μL]	Final concentration
5x buffer	10	1x
Forward primer (20 μM)	2.5	1 μM
Reverse Primer (20 μM)	2.5	1 μM
HotStar HiFidelity Polymerase (2.5 U/ μL)	1.0	2.5 U
Full length cDNA (~20 ng/ μL)	3.0	60 ng
RNAse-free ddH ₂ O	31	-
TOTAL VOLUME	50	

The annealing temperature is largely dependent on the properties of the primers and is typically 5°C below the melting temperature. The extension time is defined as one minute per thousand base pairs, if the PCR product is shorter than 2 kb.

	Temperature [°C]		Time [min]		Number of cycles	
	<i>nAtf6</i>	<i>Chop</i>	<i>nATF6</i>	<i>Chop</i>	<i>nAtf6</i>	<i>Chop</i>
Initial activation	95		5		1	
Amplification						
Denaturation	94		0.25		35	
Annealing	52		1			
Extension	72		1			
Completing synt.	72		10		1	
Cooling	4		various		1	

Tab. 15 PCR-conditions for CDS amplification from cDNA

PCR products were separated on a 1XTAE-agarose gel (2%) containing 0.001% Gelred (InvivoGen) for DNA band visualization under UV light.

50x TAE buffer

Tris Base	242 g
Glacial Acetic Acid	57,1 mL
500 mM EDTA, pH=8,0	100 mL
ddH ₂ O	up to 1L

Bands were cut out and DNA was released from the gel using Wizard SV Gel and PCR Clean-Up System (Promega) according to the manufacturer's instructions. In order to introduce restriction sites at the 5'- and 3'-end of the coding sequence, a second PCR was performed. The PCR-mix is composed as for the first PCR, but now extended primers are used in combination with ~35 ng of the first PCR product as DNA-template.

	Temperature [°C]				Time [min]		Number of cycles	
	<i>HA-nAtf6</i>	<i>nAtf6-HA</i>	<i>HA-Chop</i>	<i>Chop-HA</i>	<i>nAtf6</i>	<i>chop</i>	<i>nAtf6</i>	<i>chop</i>
Initial activation	95				5		1	
Amplification								
Denaturation	94				0.25		35	
Annealing	62.5	65	64.1	65	1			
Extension	72				1			
Completing synt.	72				10		1	
Cooling	4				various		1	

Tab. 16 PCR conditions for addition of restriction sites on CDS

Tab. 17 shows the primers for the introduction of restriction sites at the 3' and 5'-end of *nAtf6*- and *Chop* CDS. Start and stop codons are printed in bold and cutting sequences are underlined. Nucleotides marked with light grey facilitate the cutting of the restriction enzyme, whereas those marked with dark grey are necessary to maintain the frame of the coding sequence.

MATERIAL AND METHODS

HA-nAtf6	amplicon: 1096 bp			
Forward	HA_ATF6_F	27 bp	$T_m = 68.8^\circ\text{C}$	Not I
	5'- <u>AGCGGCCGCT</u> ATGGAGTCGCCTTTTAG-3'			
Reverse	HA_ATF6_R	29 bp	$T_m = 66.2^\circ\text{C}$	BamH I
	5'- <u>GGGATCC</u> CTAAGTTGGGACTTTGAGCCTC-3'			

nAtf6-HA	amplicon: 1098 bp			
Forward	ATF6_HA_F	32 bp	$T_m = 69.7^\circ\text{C}$	EcoR I
	5'- <u>AGAATTC</u> ACCATGGAGTCGCCTTTTAGTCCGG-3'			
Reverse	ATF6_HA_R	25 bp	$T_m = 70.2^\circ\text{C}$	Not I
	5'- <u>AGCGGCCGC</u> ACTTGGGACTTTGAGC-3'			

HA-Chop	amplicon: 523 bp			
Forward	HA_Chop_F	25 bp	$T_m = 70.3^\circ\text{C}$	Not I
	5'- <u>AGCGGCCGCT</u> ATGGCAGCTGAGTCC-3'			
Reverse	HA-Chop_R	26 bp	$T_m = 67.8^\circ\text{C}$	EcoR I
	5'- <u>GGGATCC</u> CTATGCTTGGTGCAGGCTG-3'			

Chop-HA	amplicon: 525 bp			
Forward	Chop_HA_F	29 bp	$T_m = 69.2^\circ\text{C}$	EcoR I
	5'- <u>AGAATTC</u> ACCATGGCAGCTGAGTCCCTGC-3'			
Reverse	Chop_HA_R	22 bp	$T_m = 70.6^\circ\text{C}$	Not I
	5'- <u>AGCGGCCGC</u> TGCTTGGTGCAGG-3'			

Tab. 17 Primers and their properties used for introduction of restriction sites

PCR products were again separated and purified. Isolated PCR products were treated with the restriction enzyme Not I (NEB) to enable ligation to the tag sequence later on. The cloning vector was treated with EcoR I and BamH I to remove the lox-CAT-lox cassette.

Restriction Mix	PCR product	pBluescript-CAG-lox-CAT-lox
DNA	25 μL	5 μg
NEBuffer	4 μL	4 μL
BSA (10mg/mL)	0.4 μL	0.4 μL
Restriction enzyme	10 U (each)	10 U
Sterile ddH ₂ O	-	up to 40 μL

The restriction reaction takes place for at least 2h to O.N. After inactivation (65°C, 20 min), the restricted PCR products were again purified using Wizard SV Gel and PCR Clean-Up System (Promega), whereas the linearized cloning vector was treated with shrimp alkaline phosphatase (SAP) to dephosphorylate the 5'-end of the vector to prevent later re-ligation.

Dephosphorylation mix	Volume [μ L]
Restriction batch (0.5 μ g DNA)	40
10xSAP buffer	4,6
SAP (1U/ μ l)	1

SAP was added to the dephosphorylation mix on ice and was incubated for 1h at 37°C. After inactivation for 15 min at 85°C, the cut vector (4.9 kbp) was separated from uncut remnants on a 0.8% agarose gel, cut and extracted from the gel.

The tag sequences were ordered as single stranded oligo-nucleotides (Biomers) and had to be annealed to double stranded pieces of DNA.

HA_Nterm	40 bp	EcoR I / Not I
5'- <u>AATTC</u> ACC ATG TACCCATACGATGTTCCAGATTACGCT <u>GC</u> -3'		
5'- <u>GGCCGC</u> AGCGTAATCTGGAACATCGTATGGGTAC CAT GGT <u>G</u> -3'		

HA_Cterm	38 bp	Not I / BamH I
5'- <u>GGCCGCT</u> TACCCATACGATGTTCCAGATTACGCT TAG <u>G</u> -3'		
5'- <u>GATCC</u> CTA AGCGTAATCTGGAACATCGTATGGGTA <u>AGC</u> -3'		

Tab. 18 N- and C-terminal HA-tag sequences

Therefore, 100ng of each single stranded oligo-nucleotide was mixed in annealing buffer (total volume 50 μ L), heated to 95°C for 5 min, gradually cooled to 75°C, incubated at 75°C for 30 min and then slowly cooled to RT in a water bath.

Annealing buffer	
Tris-HCl pH 7.5	100mM
NaCl	1mM
EDTA	10mM

Afterwards, tag-sequences were phosphorylated at their 5'-end using T4 Kinase (NEB) to enable ligation with the cut CDS.

MATERIAL AND METHODS

Restriction Mix	
dsTag	5 pmol
10x Buffer A	2 µL
10 mM ATP	2 µL
T4 Kinase	1 µL
Sterile ddH ₂ O	up to 19 µL

Ligation reaction was used for connecting the cut coding sequences of *nAtf6* and *Chop* with the corresponding N- or C-terminal tag sequences in an equimolar ratio. Since 15 ng of tag was used for the ligation reaction, the resulting amount of insert can be calculated by the following equation.

$$m(\text{CDS}) = \frac{L(\text{CDS})}{L(\text{Tag})} \cdot m(\text{Tag}) \quad L = \text{length of nucleic acid in bp. } m = \text{mass of nucleic acid in ng}$$

In a 10 µL batch the following components are mixed and incubated O.N. at 4°C:

Ligation Mix	
Tag	15 ng
CDS	X ng
10XBuffer	1,5 µL
T4 ligase	1 µL
Sterile ddH ₂ O	up to 10 µL

After inactivation of ligase at 65°C for 10 min, 1µL of the ligation mixture was inserted in a PCR which amplifies the tag-CDS fusion product to gain higher amounts of DNA for the following steps. The PCR program was equivalent to Tab. 16.

HA-CDS	amplicon: 1134 bp (<i>HA-nATF6</i>); 561 bp (<i>HA-Chop</i>)			
Forward	HA_Nterm_all	35 bp	T _m = 66.9°C	EcoR I
	5'- <u>AGAATTC</u> ACCATGTACCCATACGATGTTCCAGATT -3'			
Reverse 1	HA_ATF6_R	29 bp	T _m = 66.2°C	BamH I
Reverse 2	HA-Chop_R	26 bp	T _m = 67.8°C	BamH I

CDS-HA	amplicon: 1134 bp (<i>nATF6-HA</i>); 561 bp (<i>Chop-HA</i>)			
Forward 1	ATF6_HA_F	32 bp	T _m = 69.7°C	EcoR I
Forward 2	Chop_HA_F	29 bp	T _m = 69.2°C	EcoR I
Reverse	HA_Cterm_all	35 bp	T _m = 69.8°C	BamH I
	5'- <u>AGGATCC</u> CTAAGCGTAATCTGGAACATCGTATGGG -3'			

Tab. 19 Primers and their properties used for amplification of tagged CDS

The corresponding four separated PCR products were purified from an agarose gel and cut with the restriction enzymes EcoR I and BamH I to enable ligation with the cloning vector.

For ligation reaction of PCR products and cloning vector, a fivefold molar excess of insert was added compared to approx. 100 ng of vector.

$$m(\text{CDS}) = \frac{L(\text{CDS})}{L(\text{Tag})} \cdot m(\text{Tag}) \cdot 5 \quad L = \text{length of nucleic acid in bp. } m = \text{mass of nucleic acid in ng}$$

Ligation Mix	
pBluescript-CAGΔloxCATlox	100 ng
CDS	X ng
10XBuffer	1,5 µL
T4 ligase	1 µL
Sterile ddH ₂ O	up to 10 µL

The ligase reaction was stopped by incubation at 65°C for 10 min before transformation of electrocompetent *E.coli* XL-1 blue (Agilent). 50 µL of cells were incubated with 2 µL ligation mix (10-20 ng plasmid), incubated for 1-2 min on ice, transferred into a electroporation cuvette and pulsed with 1.8 kV (25 µF, 200 Ω) in the Gene Pulser (Biorad) for approx. 4.7 ms. Immediately after the pulse, 1 mL pre-warmed SOC medium was added to the cells and incubated at 37°C for exactly 1 h under continuous shaking at 225 rpm.

100 µL and 900 µL of the cell suspension was spread in two petri discs with LB-Agar medium containing 100 µg/mL ampicillin to select for transformed *E.coli* (37°C O.N.).

E. coli colonies were picked from the agar plates with pipette tips and dipped into a PCR mix to check for the presence of the tagged CDS in the vector plasmid. For this purpose, the primers listed in Tab. 19 were used in the following PCR mix:

Control-PCR Mix	Volume [µL]	Final concentration
5x buffer	5	1x
Forward primer (10 µM)	0.5	1 µM
Reverse Primer (10 µM)	0.5	1 µM
dNTPs (10 mM each)	0.5	6 µM
MgCl ₂ (25 mM)	1.5	
CrimsonTaq Polymerase (5 U/µL)	0.125	2.5 U
Plasmid DNA (colony)	-	
RNAse-free ddH ₂ O	16.9	
TOTAL VOLUME	25	

The PCR program is optimized for the use of CrimsonTaq polymerase (NEB).

	Temperature [°C]				Time [min]		Number of cycles	
	HA-nAtf6	nAtf6-HA	HA-Chop	Chop-HA	nAtf6	Chop	nAtf6	Chop
Initial activation	95				5		1	
Amplification								
Denaturation	95				0.5		45	
Annealing	62.5	65	64.1	65	0.33			
Extension	68				1			
Completing synt.	68				5		1	
Cooling	4				various		1	

Tab. 20 PCR conditions for colony PCR

After control-PCR the mix is loaded on an agarose gel and separated to check whether the corresponding amplicon can be detected.

Positive clones were transferred into 10 mL LB-medium (+100µg/mL ampicillin) and incubated O.N. at 37°C under continuous shaking. From this overnight culture plasmid DNA was purified using the Wizard Plus SV Miniprep DNA Purification System kit (Promega) according to the manufacturer's instructions (~100-500ng/µl) and sent for sequencing (Qiagen) using the primers in Tab. 19 for N- and C-terminal sequencing.

From clones with the correct sequence high amounts of plasmid DNA from ~200 mL *E.coli* culture were purified using the NucleoBond Xtra Midi Plus kit (Machery Nagel) according to the manufacturer's instructions.

3.6 Transfection of adherent cell lines

The following conditions are needed for transient transfection:

Transfection mix	6-well plate	24-well plate
FuGENE 6 Reagent	6µl	1,5 µl
DNA	2µg	0,5 µg
Serum free medium	until 100µl	until 25 µl

FuGENE 6 Reagent must come to R.T. and be vortexed prior to dilution in serum-free medium (without antibiotics or fungicides). It is important to mix by pipetting up and down without letting FuGENE 6 Reagent come into contact with the plastic wells of the tube containing the medium. After incubation for 5min at R.T., the DNA-vector was added. The batch was mixed by pipetting up and down and incubated for 40 min at R.T. In the meanwhile, cells medium can be changed. 100 µL of FuGENE-DNA-complex per well in case of a six well plate or 25 µL per well in case of a 24 well plate are added to the cells in a drop-wise manner, followed by swirling of the wells to ensure distribution over the entire plate surface.

3.7 Chromatin Immunoprecipitation for analysis of DNA-protein-interaction

Chromatin Immunoprecipitation (ChIP) is a tool for the study of protein-DNA interactions. In this method, intact cells are fixed using formaldehyde, which cross-links and preserves protein-DNA interactions. The DNA is then sheared into small fragments using either sonication or enzymatic digestion and specific protein-DNA complexes are immunoprecipitated using an antibody directed against the DNA-binding protein of interest. Following immunoprecipitation, cross-linking is reversed, the proteins are removed by treatment with Proteinase K and the DNA is purified. The DNA is then analyzed to determine which DNA fragments were bound by the protein of interest. The experiments were performed using the ChIP-IT Express Enzymatic (Active Motif) kit according to the manufacturer's instructions. Chromatin was prepared from three T75 flasks per treatment. This corresponds to approximately 4.5×10^7 70-80% confluent cells. Fixation with formaldehyde lasted for 10 min. at RT. Isolated nuclei were incubated for an optimized time (20 min) at 37°C with the shearing enzyme under periodical flicking or vortexing the tubes to ensure the chromatin is evenly shared. 10 µL sheared chromatin is reserved for use as input control in later PCR analysis. For Chromatin Immunoprecipitation, 6.3 µg sheared chromatin were incubated with 2 µg of the corresponding antibody and protein G coated magnetic beads O.N. at 4°C while continuously flipping of the tubes. Anti-ATF6 and Anti-Chop antibodies were purchased from Santa Cruz (Heidelberg).

After reverse crosslinking and digestion of proteins, the precipitated DNA and the input controls were used in PCR reaction. When performing real time quantitative PCR with LightCycler the following mixture was prepared (LightCycler Fast StartDNA Master SYBR Green; Roche)

ChIP PCR mix	Final Conc.	Volume (µL)/Sample
ddH ₂ O	-	1.4
MgCl ₂	4 mM	1.2
Forward primer	0.4 µM	0,2
Reverse primer	0.4 µM	0,2
Master Mix, 10xconc	1 x	1.0
DNA		6.0
TOTAL VOLUME		10,0

For assessing the CHOP and nATF6 binding, Genomatix software was used to predict potential TF binding sites. Accordingly, the following primers were designed:

Gene	nATF6 binding	CHOP binding
<i>Grp78</i>	5'-CATTGGTGGCCGTTAAGAATGAC-3'	-
	5'-AGTATCGAGCGCGCCGTCGC-3'	-
<i>Hsp60/ Hsp10</i>	5'-CAATGAGCCCGAGTCCCCTCC-3'	5'-CAATGAGCCCGAGTCCCCTCC-3'
	5'-GGAAATGACGCCACTTGACCTTTC-3'	5'-GGAAATGACGCCACTTGACCTTTC-3'
<i>Grp75</i>	5'-TTCAAGCCATGGTTGTATCTTAAGTCATG-3'	-
	5'-CCAGTCTTCTGGACTGATTTTCCTATTACTC-3'	-
<i>Tid1</i>	5'-CGCTACAGGTTTGGAGAA-3'	-
	5'-GCGGCGTCAGTATCAGA-3'	-
<i>ClpP</i>	5'-CGTGGACCTGATTGCT-3'	-
	5'-GGCGGGGATAAGTCTGT-3'	-
<i>mtCK</i>	5'-CGCACCCAAACCTCAG-3'	-
	5'-TGGCTTGCTAAGGCAG-3'	-

Tab. 21 Primers used for amplification of ChIP gained promoter fragments

3.8 Quantitative real time PCR

Reverse transcription (RT) PCR was performed using RNA-dependent DNA polymerase (reverse transcriptase), an enzyme that uses RNA molecule as a template for the synthesis of a complementary DNA strand (cDNA). 1 µg total RNA per sample (up to 12 µL with ddH₂O) was mixed with random hexamer primers offering 3'-hydroxyl groups for elongation and was heated to 70°C for 5 min to denature RNA secondary structures. After cooling on ice for 5 min. the reaction mix was added containing Moloney murine leukemia virus (MMLV) reverse transcriptase with point mutation (promega).

RT-PCR Mix 1	Final Conc.	Volume (µL)/Sample
Random hexamers (0.2µg/µL)		1.0
RNA		1µg
ddH ₂ O		Up to 14

RT-PCR Mix 2	Final Conc.	Volume (µL)/Sample
5xMMLV Buffer	1x	5
dNTP's (10mM)		1.25
RNAse Inhibitor		0.65
MMLV PM RTase (2000U/µL)		1
ddH ₂ O		3.1
TOTAL VOLUME		11

Reverse transcription is performed at 37°C for 60 min followed by denaturation at 99°C for 1 min. Final theoretical concentration of cDNA should be 1000 ng/25 µL (40 ng/µL).

To analyze relative gene transcript amounts of certain genes of interest, quantitative real-time PCR (qPCR) was performed using 1 µl cDNA in a Light Cycler® 480 system (Roche Diagnostics) applying the Universal Probe Library system.

qPCR mix	Final Conc.	Volume (μL)/Sample
ddH ₂ O	-	3,4
Forward primer (20μM)	0.4 μM	0.2
Reverse primer (20μM)	0.4 μM	0.2
Probe (10μM)	0.2 μM	0.2
Master Mix, 2xconc.	1 x	5.0
DNA	~ 25 ng	1.0
TOTAL VOLUME		10.0

	Temperature [°C]	Time [min]	Number of cycles
Initial activation	95	300	1
Amplification			
Denaturation	95	10	50
Annealing	60	20	
Extension	72	2	
Cooling	40	10	1

Tab. 22 Reaction conditions for probe based qPCR

Primer sequences were as follows:

Gene	Forward primer	Reverse Primer	Probe #
<i>Hsp60</i>	5'-tcttcaggtgtggcagtca-3'	5'-cccctcttctccaaactg-3'	1
<i>Hsp10</i>	ggcccaggttcagagtcc	tgtcaaagagcggaagaaactt	77
<i>Grp75</i>	gttatggagggcaaacaagc	aggggtagtctggcacctt	80
<i>Tid1</i>	agtcaccacacaagcactg	ccagcctctcgctatcc	4
<i>ClpP</i>	gcaacaagaagcccattcat	gtactgcattgtgtcgtagatgg	26
<i>Atf3</i>	gctggagtcagttaccgtcaa	cgctccttttctctcat	80
<i>Trib3</i>	gtcgtttgtcttcagcaact	tcatctgatccagtcacacg	67
<i>Ero1l</i>	gcgccagatttcagctct	tcaaagtgcaggaaatga	48
<i>Bcl2</i>	gggatgcctttgtggaact	gctgagcagggtcttcagag	2
<i>Grp78</i>	ctgaggcgtatttgggaag	tcatgacattcagtcagcaa	105
<i>Chop</i>	gcgacagagccagaataaca	gatgcacttcttctggaaca	91
<i>sXbp1</i>	tgacgaggttcagagggtg	tgcacctgctgaggactcag	49
<i>uXbp1</i>	gcagcactcagactatgt	ggccaactgttcagaatgcc	62
<i>Pkr</i>	gttgttgggagggagttgac	agaggcaccgggtttgtat	99
<i>Gadd34</i>	tctgtactggaaatgccttct	agctgaatccaaatcgctgt	6
<i>P58lph</i>	agaagacgattcaagaaagtgc	gctgagactcgggttcctt	15
<i>nuCoxIV</i>	tactgctgctcgttctgat	cgatcgaaagtatgagggatg	7
<i>mtCoxI</i>	cagaccgcaacctaaacaca	ttctgggtgcccagaagaat	25
<i>Pgc1α</i>	gagcgaaccttaagtgtgaa	tcttggttgctttatgagga	52
<i>Tfam</i>	ccaaaaagacctcgttcagc	caagcctcattacaagcttca	79
<i>Cpt1α</i>	gctgtcaaagataccgtgagc	tctccctccttcacagtgg	109
<i>OTC</i>	gctgtcatggtatccctgct	tttcttttgacaggcatca	99
<i>Hif1α</i>	gcactagacaaagttcacctgaga	cgctatccacatcaaagcaa	95
<i>Ho1</i>	gtcaagcacagggtgacaga	atcacctgcagctcctcaaa	4
<i>Cat</i>	ccttcaagttggttaatgcaga	caagttttgatgccctgg	34
<i>Sod2</i>	gaccattgcaaggaacaa	gtagtaagcgtgctccacac	3
<i>Tnf</i>	tgccatgtctcagcctcttc	gaggccatttgggaacttct	49
<i>Ifnγ</i>	cctttggaccctctgacttg	agcgttcattgtctcagagcta	63
<i>Il6</i>	gatggatgctacaaactggat	ccaggtagctatggtactcaga	6
<i>KC</i>	agactccagccacactccaa	tgacagcgcagctcattg	83
<i>Mcp1</i>	catccacgtgttggtcga	gatcatcttgctggtgaatgagt	62
<i>Ip10</i>	gctgccgtcattttctgc	tctcactggcccgtcatc	3
<i>Egf</i>	ttgtgacacctggaaaactga	gtttgagaagttcgggggtca	26

<i>Tgfα</i>	cctggtggtggtctccatt	cagtgtttgctggagctga	81
<i>Wnt3</i>	ctcgctggctacccaattt	gaggccagagatgtgtactgc	81
<i>Rspo1</i>	cgacatgaacaaatgcatca	ctcctgacacttgggtcaga	5
<i>Olfm4</i>	gaaattcgagagagagtttctaagg	gaccttactcggaccgtca	5
<i>Lgr5</i>	cttcactcgggtgcagtgc	cagccagctaccaaatagggtg	60
<i>Ki67</i>	gctgtcctcaagacaatcatca	ggcgttatccaggagact	80
<i>Socs9</i>	gtacccgcactctgcacaac	ctcctccacgaagggtctct	66
<i>c-Myc</i>	cctagtgtgcatgaggaga	tccacagacaccacatcaattt	77
<i>Ccnd1</i>	tttcttccagagtcacatcaagtgt	tgactccagaagggtctcaa	72
<i>Gapdh</i>	tccactcatggcaaattcaa	tttgatgtagtgggtctcg	9

Tab. 23 Primers and probes used for qPCR

Relative induction of gene mRNA expression was calculated by the $\Delta\Delta C_p$ method using the expression of *Gapdh* for normalization.

3.9 Discontinuous denaturing polyacrylamid gel electrophoresis

By discontinuous polyacrylamid gel electrophoresis (PAGE), proteins are separated while migrating through a cross-linked polyacrylamid matrix in an electric field. Prior to separation, the proteins are denaturated by heat treatment and disulfide bounds are dissolved by DTT. Besides DTT, a further component of the so called “Laemmli buffer” [233] is the anionic detergent sodium dodecyl sulphate (SDS), which binds hydrophobic regions of proteins with its aliphatic alkyl-tail, linearizes and confers them a negative charge due to their sulphate groups. Consequently, in presence of SDS denaturated proteins migrate to the anode in an electric field and are separated according to differences in their molecular mass.

An especially high resolution of the protein mixture is possible by using a discontinuous buffer system. For this purpose the samples first migrate through a stacking gel with large pores, are then focused on the borderline between stacking gel and resolving gel, before being separated in the small pores of the resolving gel. Focusing is possible, as the migrating proteins slow down and concentrate on the border between stacking and resolving gel caused by a sieve effect. This process is supported by the fact that the stacking gel has a pH value that lies under the value of the resolving gel.

The gel solutions are prepared as follows (volumes are given for two gels):

Resolving Gel	Volume [mL]	
	10%	15%
ddH ₂ O	4.1	2.4
30% Acrylamid/ 0.8% Bisacrylamid	3.3	5.0
Resolving gel buffer (1.5M Tris) pH 8.8	2.5	2.5
10% w/v Sodiumdodecylsulfate (SDS)	0.1	0.1
25% w/v Ammoniumpersulfate (APS)	0.05	0.05
TOTAL VOLUME	10	10

3% Stacking Gel	Volume [mL]
ddH ₂ O	3.25
30% Acrylamid/ 0.8% Bisacrylamid	0.5
Stacking gel buffer (1.5M Tris) pH 6.8	1.25
10% w/v SDS	0.05
25% w/v APS	0.025
TOTAL VOLUME	5

5 µL of TEMED were added to start polymerization. After polymerization, the gel was placed in the electrophoresis chamber filled with 1x running buffer. 5x Laemmli buffer was added to the samples, boiled at 95°C for approx. 5-10 min. and equal amounts of protein were loaded on the gel. Electrophoresis was performed with 15 mA per gel.

10x running buffer	
Tris	30 g
Glycerin	144 g
SDS	10 g
ddH ₂ O	up to 1L

5xLaemmli Buffer	
Tris-HCl, pH 6.8	1.82 g
20% w/v SDS	10 mL
99% Glycerol	14 mL
1M DTT	2,5 mL
Bromophenol Blue	4 mg
ddH ₂ O	up to 40 mL

3.10 Western blot

The Western Blot combines gel-electrophoretic separation of proteins (cell extract) with the specificity of an immunochemical detection. The protein of interest, fixed on a Polyvinylidendifluorid (PVDF) membrane, serves as an antigen for a specific mono- or polyclonal primary antibody. The complex between first antibody and its antigen is detected by a secondary antibody binding the first antibody's Fc-part and is chemically linked to horse radish peroxidase, which catalyzes a luminescence reaction.

Prior to blotting, the PVDF membrane was equilibrated in 100% methanol for one min. and in Semi-Dry-Blotting buffer afterwards.

Semi-Dry-Blotting Buffer	
Glycin	14,4 g
Tris	3,03 g
Methanol	200 mL
ddH ₂ O	up to 1 L

MATERIAL AND METHODS

In the Semi-Dry Transfer Cell, first a filter paper were placed on the anode-plate, followed by the membrane, the gel and finally a filter papers on top, all soaked in semi-dry blotting buffer. Blotting lasted for 45-50 min. at 14 V.

After removal of filter paper and gel the membrane was briefly incubated in 0.5% Ponceau-dye for protein detection, to test whether the blotting worked properly.

0.5% Ponceau		
Ponceau S		1 g
Acidic acid		2 mL
ddH ₂ O		up to 200 mL

After removal of Ponceau with dH₂O, the membrane surface is blocked in 15 mL TBST containing 5% milk protein for 1h.

10x TBS (Tris Buffer Saline)		
Tris		12.1 g
NaCl		40 g
ddH ₂ O		500 mL

TBST		
10x TBS		200 mL
Tween20		2 mL
ddH ₂ O		up to 2 L

The blocked membrane was washed once with TBST before 10 mL of the first antibody solution were added. The incubation can last for 1 h at 37°C or O.N. at 4°C with agitation.

The antibody stock solutions were diluted in TBST containing 5% milk protein typically 1:1000, but the adequate dilution depends on the antibody.

After rinsing with TBST, the membrane was washed three times à 10 min. under agitation and then incubated in the secondary antibody solution for 1h. After washing three additional times, the luminescence reaction was detected on a photo-film.

Primary antibodies				Secondary antibodies		
Antigen	Supplier	Dilution	Species	Species	Supplier	Dilution
HSP60	Santa Cruz	1:2000	goat	Goat Anti-Rabbit-HRP	Dianova	1:200
Grp78	Sigma	1:2000	rabbit	Rabbit Anti-Goat-HRP	Sigma	1:200
PKR	Santa Cruz	1:1000	rabbit			
CHOP	Santa Cruz	1:1000	rabbit			
HA-Tag	eBioscience	1:1000	-			
β-Actin	Cell signaling	1:2000	rabbit			

Tab. 24 Primary and secondary antibodies used for Western Blot visualization

For densitometric band quantification, the Western blot photo-films were scanned (GS-800 Calibrated Densitometer; Biorad) and analyzed using QuantityOne software (Biorad).

3.11 Electron microscopy

1 cm long segments of the jejunum or distal colon from four *Hsp60*^{ΔIEC} and three *Hsp60*^{flox/flox} mice were fixed in 2.5% glutaraldehyde (Electron Microscopy Sciences). After washing in buffered saccharose and osmication for 1h, tissues were dehydrated in acetone and then processed for Epon embedding. The tissues were then trimmed so that ultrathin sections of gut rings could be cut and counterstained with uranyl acetate and lead citrate. Electron micrographs from each gut specimen were obtained at 19000 fold magnification from each animal. Of these, up to nine images for each specimen and animal were randomly selected and mitochondrial abundance and diameter were measured using the analySIS Dock System (Soft Imaging System) by Ori Staszewski (lab of Prof. Macro Prinz, Fribourg).

3.12 RNA Microarray

Total RNA was prepared from isolated colonic epithelial cells of *Hsp60*^{ΔIEC} and *Hsp60*^{flox/flox} mice at day d₂ (n = 5 per group) with column-based NucleoSpin RNAII kit (Macherey-Nagel) according to the manufacturer's instructions. RNA concentration and quality was determined by spectrophotometric analysis (ND-1000, PEQLAB). RNA integrity number (RIN) was >8 for all samples (Agilent 1200 bioanalyzer, Alpha Metrix Biotech). Labelling of total RNA (100 ng) was performed with the Ambion WT Expression kit (Life Technologies), samples were hybridized to Affymetrix GeneChip Mouse Gene 1.1 ST arrays (Affymetrix) and scanned on an Affymetrix GeneTitan instrument. Probe sets were defined according to Dai *et al.* [234]. In this method, probes are annotated using up-to-date databases and assigned to unique gene identifiers, in this case Entrez IDs. The probes present on the Mouse Gene 1.1 ST arrays represent 21,225 Entrez IDs. Arrays were normalized with the Robust Multi-array Average (RMA) method [235, 236]. Only probe sets with normalized signal intensities above 20 on at least five arrays, interquartile range > 0.2 and at least 5 probes per probeset were selected for further analysis. This filter was passed by 7,827 probesets. Differentially expressed probe sets were identified using intensity-based moderated t-statistics [237]. *P* values were corrected for multiple testing using a false discovery rate (FDR) method (*Q* value) [238]. *Q* values <0.01 were considered as significant. Processing of the data was performed as previously described [239]. Heat maps of significantly regulated genes (signal log₂ ratio) were performed using TIGR MeV software. Enriched pathways and gene ontology (GO) groups represented by significantly regulated genes were identified by using the GeneRanker tool in the Genome Analyzer (Genomatix). Microarray analysis was performed by Dr. Mark Boekschoten in the lab of Prof. Müller (Wageningen University, the Netherlands).

3.13 Statistical analysis

Data of at least 3 animals per experimental group are indicated. Statistical significant differences were determined by the parametric unpaired t-test or One-Way-Anova, respectively (treatment vs. control group(s)). If the data did not fulfill the prerequisites of parametric statistics (not normally distributed or discontinuous data), a Mann-Whitney/Rank-Sum test or an Anova-On-Ranks test, respectively, was performed. If groups were compared with respect to two independent variables (parametric data), a Two-Way-Anova analysis followed by an appropriate multiple comparison procedure was performed. Differences reached statistical significance with p values < 0.05 (*), <0.01 (**) and <0.001 (***). Statistical analyses were performed using SigmaStat (Systat).

4 RESULTS

4.1 Interrelation of ER- and MT UPR signaling

4.1.1 Promoter analysis of ER- and MT UPR responsive genes

To investigate the signaling network of ER- and MT UPR, a promoter analysis of several ER- and MT UPR responsive genes was performed using genomatix software. The presence or absence of bioinformatically predicted binding sites for ATF6 (CREB, Ebox) and CHOP is summarized in Tab. 25.

Table 25

	<i>Hsp60</i>	<i>Hsp10</i>	<i>Grp78</i>	<i>Grp75</i>	<i>Tid-1</i>	<i>ClpP</i>	<i>mtCk</i>
<i>ATF6</i>	yes	yes	yes	yes	yes	yes	yes
<i>CHOP</i>	yes	yes	no	no	no	no	no

Tab. 25 Bioinformatical promoter analysis of UPR responsive genes

Orange fields indicate putative binding sites for ATF6 (CREB or Ebox site) and CHOP. Blue fields indicate that no such binding site could be found in the analyzed promoter fragment.

To transfer the *in silico* prediction of transcription factor binding to a biological system, the IEC line Mode K was either treated with the ER stressor Tm or transfected with a plasmid encoding the MT UPR inducer OTC Δ . In two previous reports, we were able to show that the anti-inflammatory cytokine IL-10 exerts inhibitory effects on the UPR activation [68, 78]. Therefore, Mode K cells were preincubated with IL-10 prior to UPR induction by Tm or OTC Δ . Subsequently, ChIP analysis was performed on isolated chromatin of these cells (Fig. 9). The ChIP analysis revealed that upon induction of ER UPR, transcription factor ATF6 binds not only to the ERSE of the *Grp78* promoter – a classical ER UPR responsive gene - but also to CREB and Ebox elements in the promoter of MT UPR responsive genes like the mitochondrial chaperones *Grp75* and *Tid-1*, the MT protease *ClpP* and of *mtCk*, a part of the mitochondrial transition pore. This binding was inhibitable upon an IL-10 preincubation. Binding of ATF6 at these elements was not observed upon *Otc1* transfection. On the contrary, Tm as well as OTC Δ both caused the binding of the transcription factor CHOP to the bidirectional promoter of the MT chaperones *Hsp60* and *Hsp10*.

Figure 9

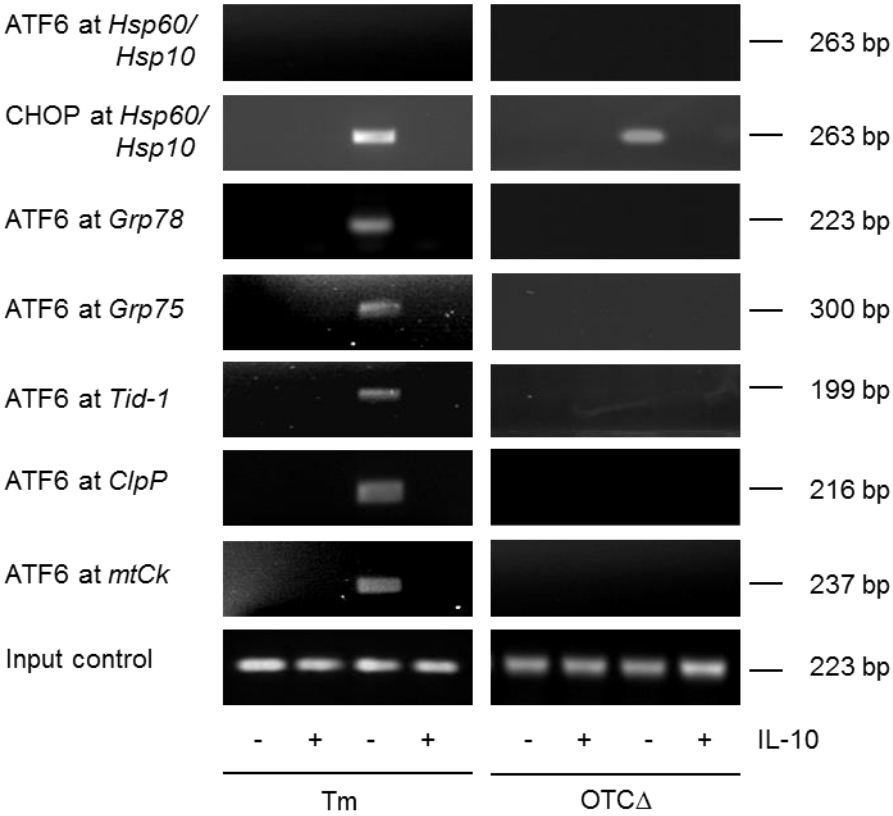


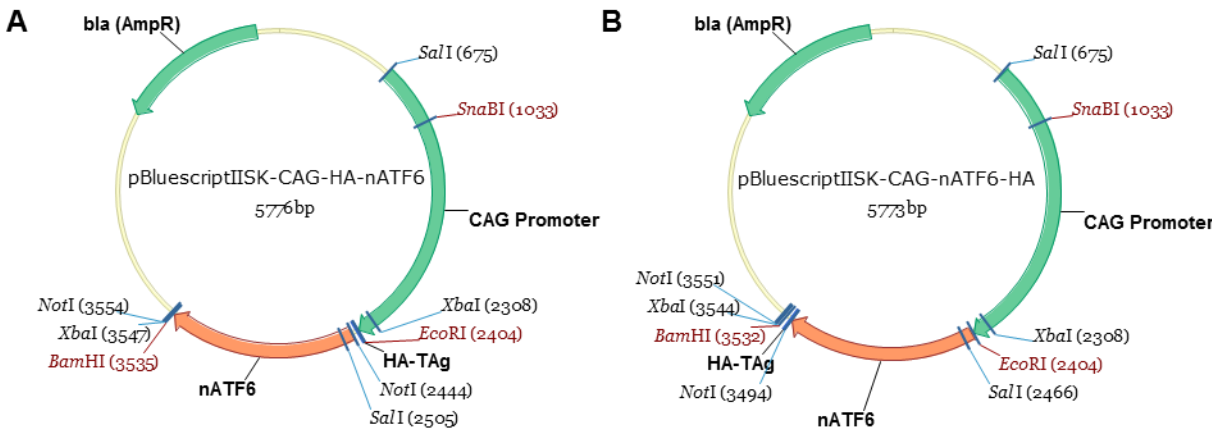
Fig. 9 Crosslink between ER and MT UPR via TF ATF6 and CHOP

Mode K cells were pre-incubated with IL-10 and subsequently treated with Tm or transfected with *OtcΔ*. ChIP was performed after chromatin isolation and enzymatic sheering. PCR products for specific promoter fragments are shown after electrophoresis on agarose gels. Input controls served to show equal amounts of chromatin upon all treatments.

4.1.2 Construction and *in vitro* validation of *Chop* and *nAtf6* overexpressing vectors

To further investigate the possible cross-communication of the ER and MT UPR via the TF CHOP and nATF6, vectors were constructed that enable the overexpression of N- or C-terminally HA-tagged transcription factors (Fig. 10).

Figure 10



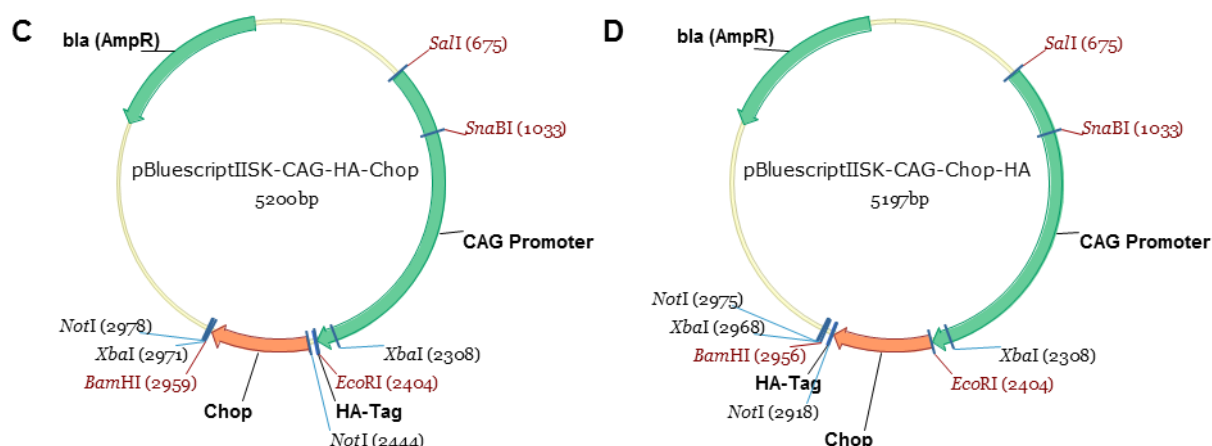


Fig. 10 Vector maps for the overexpression of HA-tagged CHOP and nATF6

The pBluescriptIIISK plasmid served as backbone for the expression system. A CAG promoter was inserted to drive the overexpression of the CDS of the corresponding TF. (A+C) The HA-tag was placed at the 5' end of the CDS. (B+D) the HA-tag was placed at the 3' end of the CDS.

An *in vitro* validation of the overexpression system by transfection of Mode K cells with the corresponding vector revealed an approx. 400-700 fold increase in expression compared to control transfected cells for both the N-and C-terminally tagged TF (Fig. 11A). Notably, only the C-terminal HA-tag could be detected by the anti HA-tag antibody in case of both TF (Fig. 11B). CHOP-HA was obviously present to a greater extent than nATF6-HA. HA-tag and 3xAla-linker add approx. 1.5 kDa to the molecular weight of the endogenous TF.

Figure 11

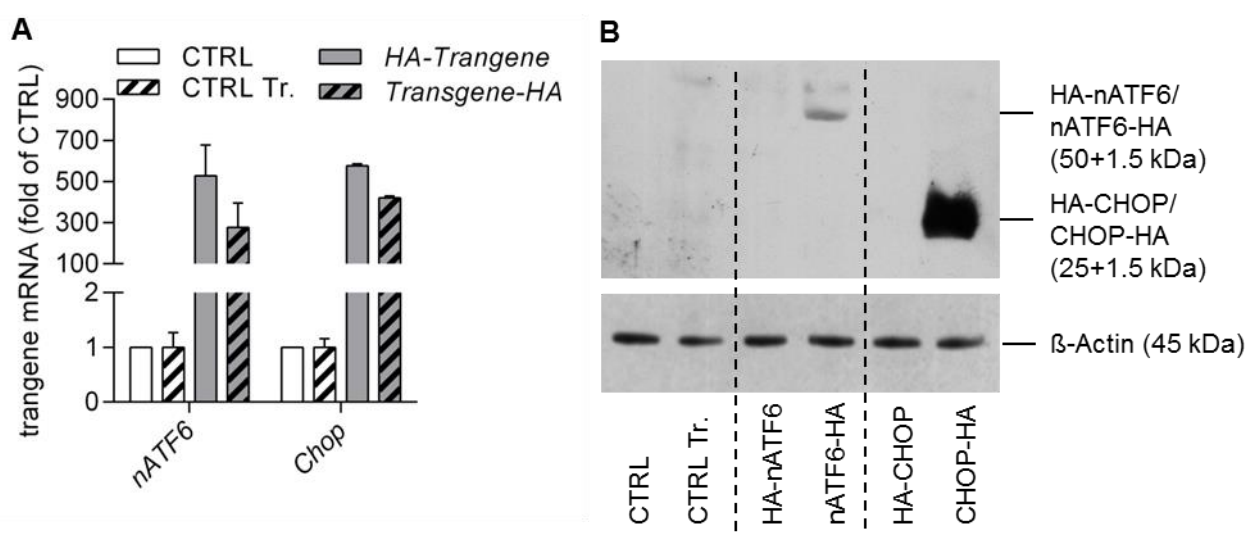


Fig. 11 Validation of TF overexpression *in vitro*

Mode K cells were transfected with the corresponding overexpression plasmid for 30h. (A) qPCR analysis of the exogenous TF mRNA levels. Columns represent independent triplicates. (B) Western Blot analysis using the anti HA-tag antibody to detect expression of the exogenous fusion protein. Pooled protein from triplicates was used.

RESULTS

Due to the exclusive binding of the antibody to the C-terminal HA-tag, only these constructs were used for further *in vitro* validation and for the generation of transgenic mouse models. To validate the functional consequence of a TF overexpression in the complex network of ER and MT UPR signaling, Mode K cells were stimulated with Tm or OTCΔ in combination with a transient transfection of the corresponding TF overexpression plasmid (Fig. 12). 36h after transfection, *nATF6-HA* and *Chop-HA* transfection *per se* only marginally induced UPR target genes e.g. endogenous *Chop*. Notably, *nATF6-HA* overexpression further elevated the transcript levels of *Grp78*, *Chop* and *Grp75* upon Tm stimulation. In contrast, *Chop-HA* overexpression elevated the transcript levels of *Grp78*, *Chop* and *Hsp60* upon *OtcΔ* transfection. In accordance with the ChIP data (Fig. 9), *Chop-HA* also induced *Hsp60* in combination with Tm.

Figure 12

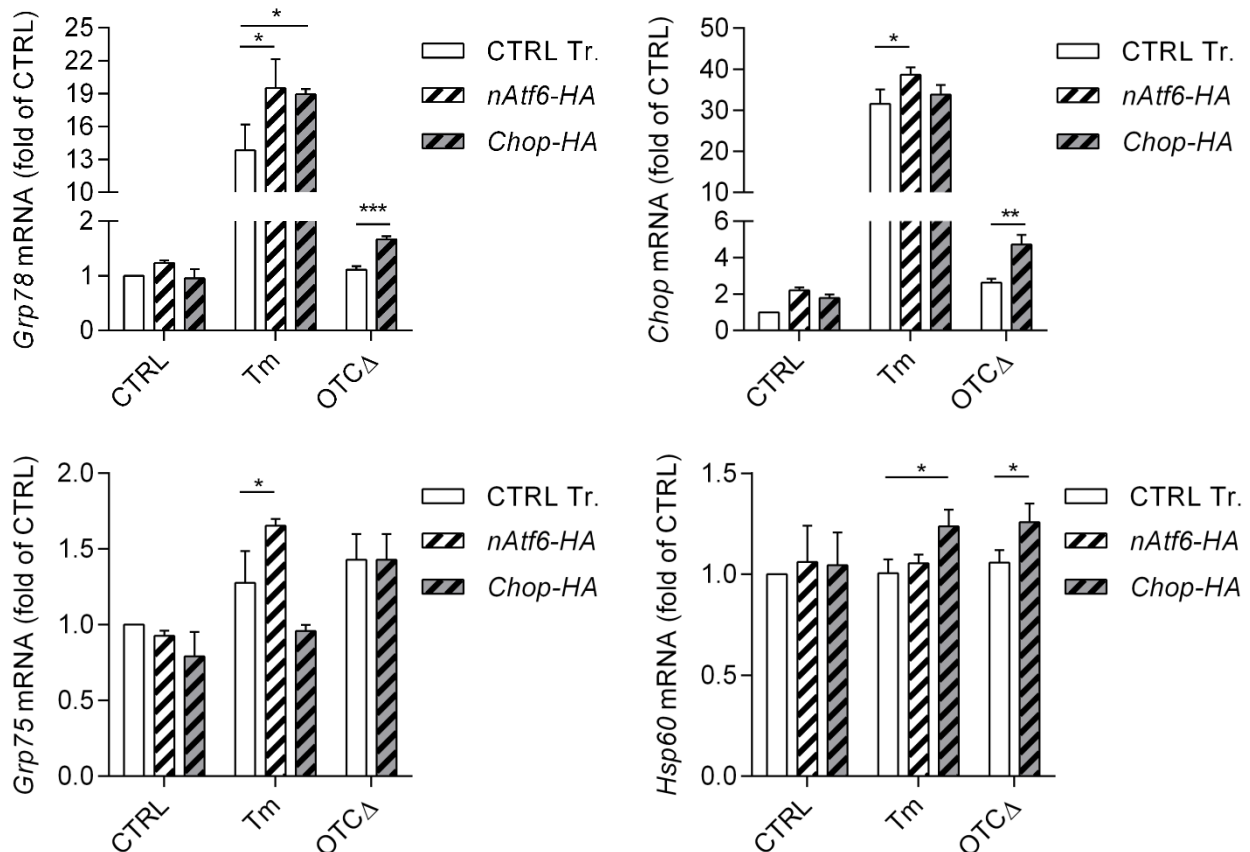


Fig. 12 Validation of the functionality of nATF6-HA and Chop-HA overexpressing plasmids

30h after transfection with the OTCΔ-, nATF6-HA- or CHOP-HA encoding plasmid and the transfection control respectively, Mode K cells were stimulated with Tm for 6h. qPCR analysis for ER- and MT UPR responsive genes was performed. Bar charts represent mean values of treatment triplicates \pm SD. *P<0.05, **P<0.01, ***P<0.001 (One-way-Anova).

4.2 Generation of the *nAtf6-HA* and *Chop-HA* conditional transgenic mouse models

The plasmids encoding *nAtf6-HA* and *Chop-HA* were used as basis for the generation of the *nAtf6-HA*^{Tg flox/flox} and *Chop-HA*^{Tg flox/flox} mouse by Taconic-Artemis. The generation was carried out in several steps (milestones) documented in Tab. 27 and Tab. 28 (Appendix).

Mice carrying the conditional allele for the according transgene (floxed mice) were crossed with VillinCre transgenic mice [224], to finally generate the epithelial specific *nAtf6-HA*^{IEC Tg/Tg} and *Chop-HA*^{IEC Tg/Tg} transgenic mouse models. This work opened out into the PhD projects of M.Sc. Elena Lobner (ATF6) and M.Sc. Nadine Waldschmitt (CHOP).

4.3 Generation of the constitutive and conditional *Hsp60* knockout mouse model

To investigate the impact of a mitochondrial chaperone deficiency in particular on the intestinal epithelium, a constitutive and a conditional knockout model of mitochondrial *Hsp60* were created. Tab. 29 (Appendix) summarizes the generation procedure of the conditional (*Hsp60*^{flox/flox}) and the constitutive (*Hsp60*^{+/-}) knock out mouse model of *Hsp60*.

Of note, *Hsp60*^{flox/WT} mice of the G1 generation still carry the allele for Flp recombinase expression and *Hsp60*^{+/-} mice in the G1 generation still express Cre recombinase. These alleles were crossed out in the course of the subsequent generations.

4.4 Characterization of the constitutive *Hsp60*^{+/-} mouse model

4.4.1 Genotyping

Murine DNA from tail cuts or ear punches was used for genotyping PCR. The distance of primers 1 and 3 is too big for amplification in WT mice, but not in the KO situation.

Figure 13

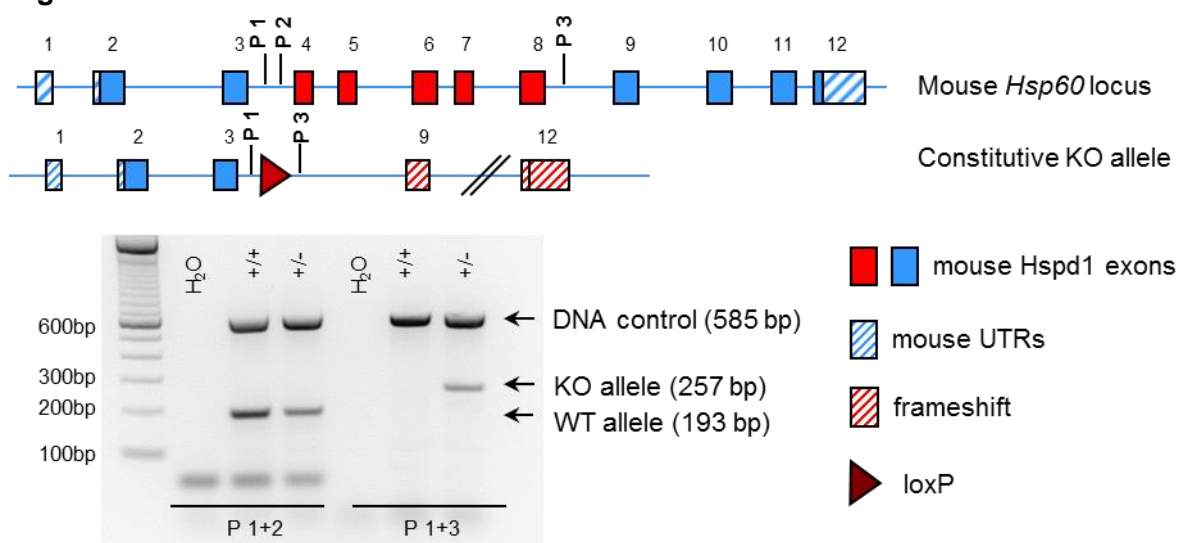


Fig. 13 Genotyping of *Hsp60*^{+/-} mice

Schematic illustration and agarose gel of the genotyping PCR products. Deletion of exons 4-8 enables the amplification of a PCR fragment enclosed by Primers P1+3, whereas the binding site for P2 has been excised in the KO allele.

4.4.2 Embryolethality of *Hsp60*^{-/-} mice

From the G2 generation on, *Hsp60*^{+/-} mice were inter-crossed to generate homozygous KO mice. According to the Mendelian law, one fourth of the offspring should be homozygous for the KO. As shown in Tab. 26, no homozygous offspring could be genotyped. Since in a formerly published report about a model of Hsp60 deficiency [138], the dieback of *Hsp60*^{-/-} embryos has already been dated between day 6.5 and 7.5 of gestation, embryolethality has not been further investigated in our model.

Table 26

<i>Hsp60</i> ^{+/-} X <i>Hsp60</i> ^{+/-}	
Genotype	Number of offspring
<i>Hsp60</i> ^{+/+}	16
<i>Hsp60</i> ^{+/-}	33
<i>Hsp60</i> ^{-/-}	0

Tab. 1 Embryolethality of *Hsp60*^{-/-} offspring

Three pairs of *Hsp60*^{+/-} mice were set up for intercrossing. 49 viable offspring from eleven litters were genotyped for the presence of an *Hsp60* KO allele.

4.4.3 Phenotypic screening of selected organs of *Hsp60*^{+/-} mice

To assess pathological consequences of a constitutive *Hsp60* haplodeficiency, two male *Hsp60*^{+/-} mice, one eight and one twelve months of age, were sent to a company (mfd diagnostics) specialized on a histopathological screening of a broad range of organs.

Figure 14

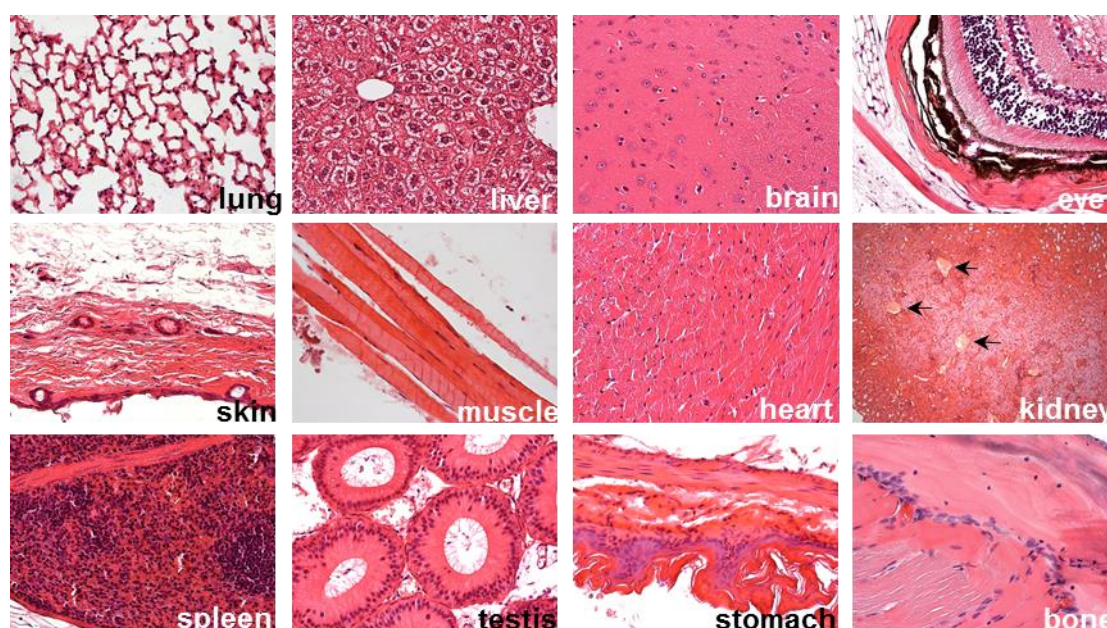


Fig. 14 H&E stainings of selected organ sections from old *Hsp60*^{+/-} mice

Pictures show representative pictures of H&E stainings of various organs in a 400x magnification. Black arrows indicate fibrin deposits in kidney.

All inspected organs were inconspicuous except the kidney. There, white fibrin deposits were visible between the renal glomeruli. Since this phenomenon could only be observed in the 12 months old mouse, it could be an effect of renal senescence as well and was not further investigated.

4.4.4 Basic characterization of the intestine of *Hsp60*^{+/-} mice

To direct the focus on the intestine, the different compartments of the intestinal tract – duodenum (Duo), jejunum (Jej), ileum (Ile), caecum (Caec), proximal colon (CP), and distal colon (CD) – were histopathologically evaluated. Neither alterations in the villus-crypt architecture nor the presence of ulcers nor elevated infiltrations of leukocytes were observed compared to WT intestinal tissue.

Figure 15

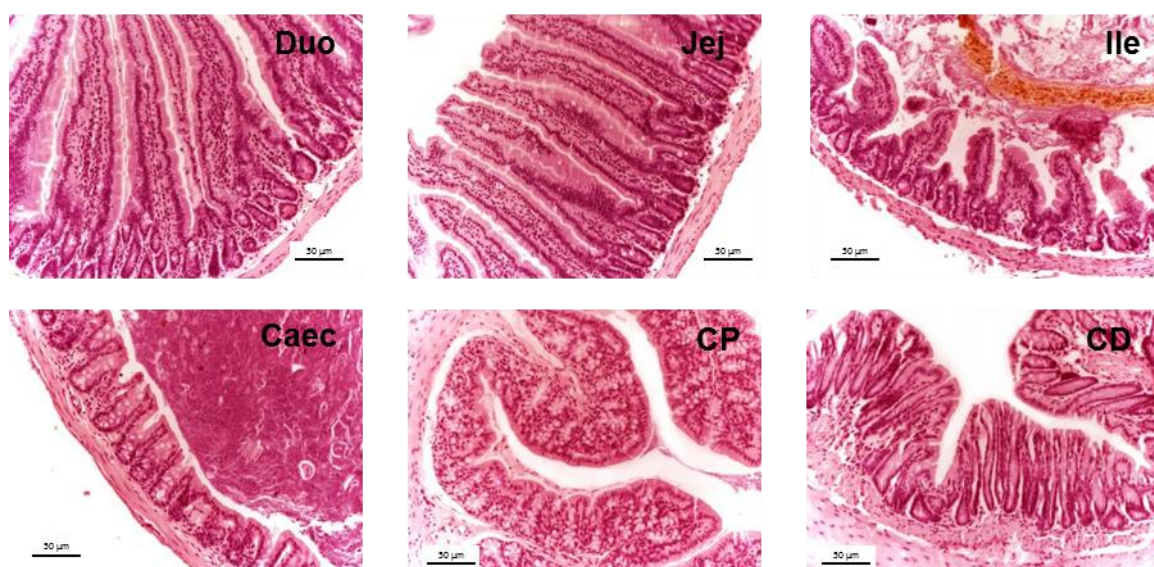


Fig. 15 Histopathological evaluation of different gut compartments of *Hsp60*^{+/-} mice

Tissue sections from WT and *Hsp60*^{+/-} mice along the GI tract were H&E stained and evaluated by the pathologist (Scores 1-12). Representative pictures from *Hsp60*^{+/-} mice show gut sections in a 250x magnification.

From the intestine as a whole, the focus now turns to the intestinal epithelium. To investigate, if the *Hsp60* haplodeficiency is compensated by an increased expression of the chaperone on the WT allele, the mRNA and protein levels of *Hsp60* in the small and large intestinal epithelium of male and female *Hsp60*^{+/-} mice were compared to WT mice (Fig. 16).

Figure 16

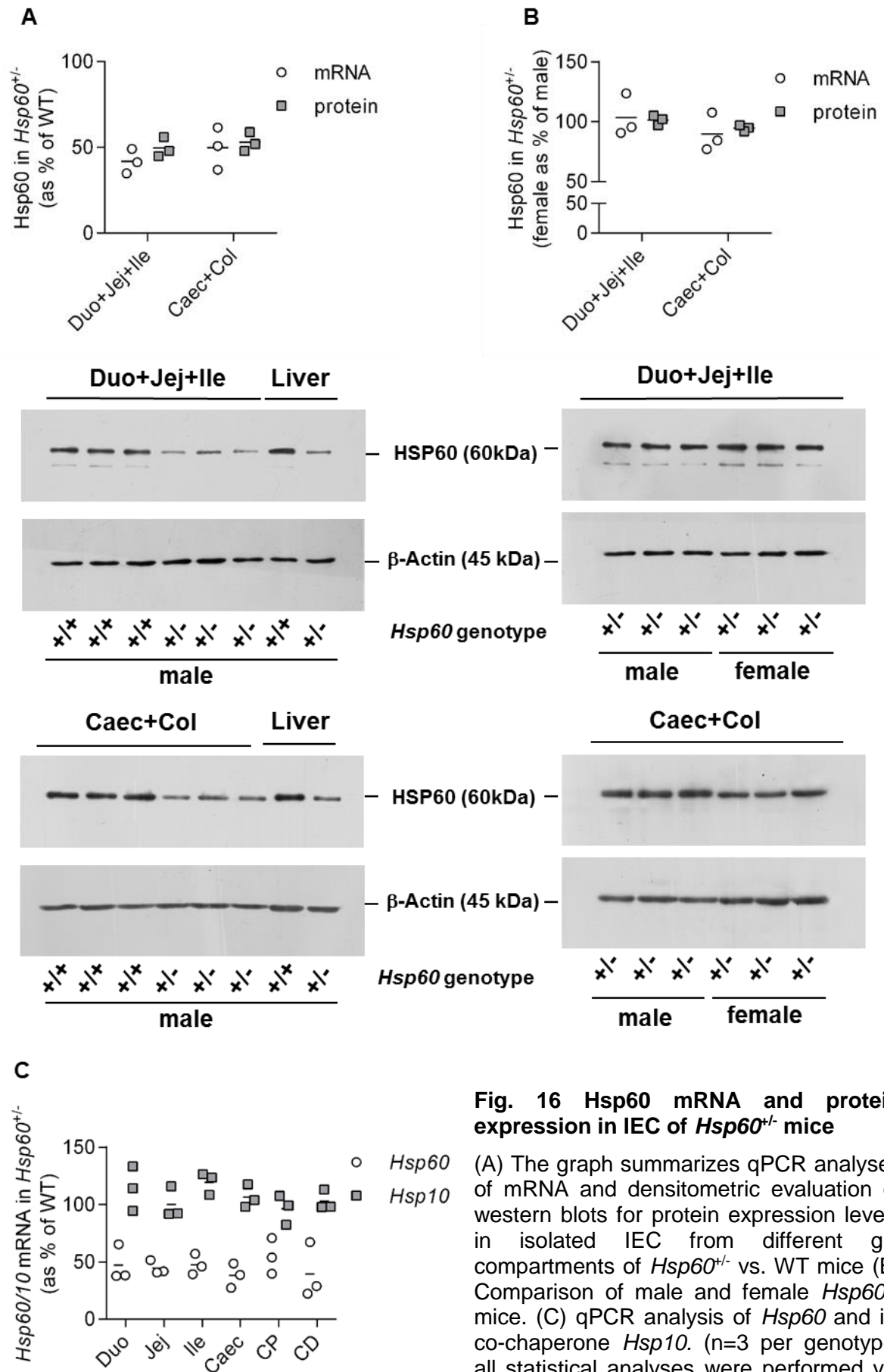


Fig. 16 Hsp60 mRNA and protein expression in IEC of *Hsp60*^{-/-} mice

(A) The graph summarizes qPCR analyses of mRNA and densitometric evaluation of western blots for protein expression levels in isolated IEC from different gut compartments of *Hsp60*^{+/-} vs. WT mice (B) Comparison of male and female *Hsp60*^{+/-} mice. (C) qPCR analysis of *Hsp60* and its co-chaperone *Hsp10*. (n=3 per genotype; all statistical analyses were performed via t-test comparing genotypes).

Western blot analysis confirmed that the 50% reduced HSP60 expression was not compensated by the remaining allele – neither in the intestinal epithelium nor in a gut unrelated organ like liver. Accordingly, no compensatory upregulation of the co-chaperone *Hsp10* and other ER- and MT UPR related genes could be observed (Fig. 16C).

Finally, with respect to the application of DSS induced colitis described in 4.4.5, the integrity of the colonic barrier in *Hsp60*^{+/-} mice was assessed by using chamber measurements. By this technique, the transepithelial electrical resistance (TER) was measured and additionally the penetration of a small sized molecule sodium-floureszin (NaF) through the mucosa of the proximal and distal colon. No significant difference in the intestinal colonic barrier integrity could be observed in *Hsp60*^{+/-} mice compared to WT mice. However, in the distal colon a trend towards reduced barrier integrity was apparent.

Figure 17

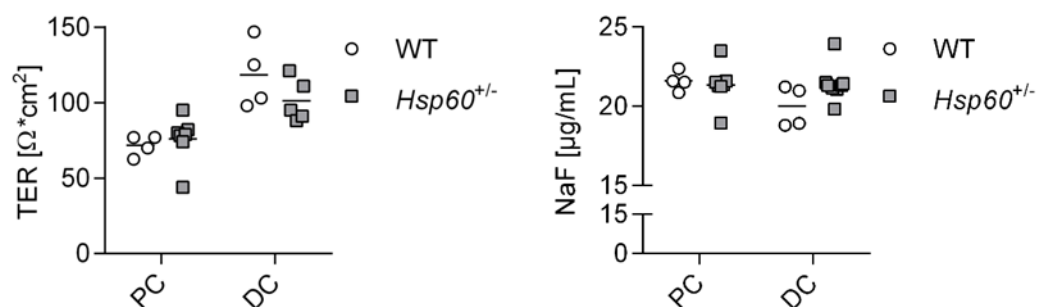


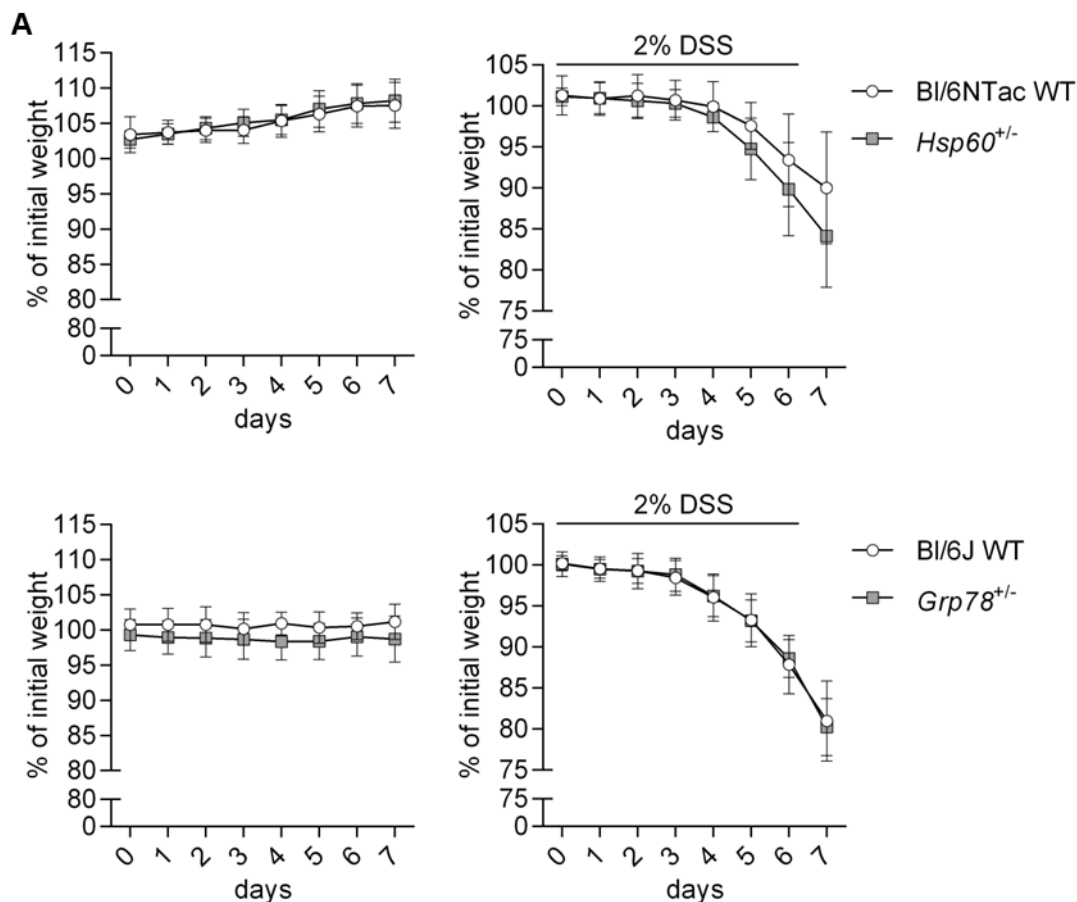
Fig. 17 Integrity of the colonic mucosal barrier in *Hsp60*^{+/-} mice

Ussing chamber measurements to assess the TER of the colonic epithelium of 4-8 mucosal explants per genotype. The NaF translocation was quantified using fluorescence spectroscopy (n=4-5 per genotype; statistical analyses were performed via t-test comparing genotypes).

4.4.5 *Hsp60*^{+/-} mice in an acute and a chronic model of intestinal inflammation

We observed so far, that a 50% reduction of HSP60 did not lead to compensation in expression from the remaining allele and that this reduction has no significant impact on the overall organism and on the intestine in particular. To study, if the haploinsufficiency leads to an altered response towards an intestinal inflammatory trigger, BI/6NTac WT and *Hsp60*^{+/-} mice were treated with the colitogenic reagent DSS (2% in the drinking water for seven days) and sampled one day later. As an additional control, *Grp78*^{+/-} – a well described model of a heterozygous ER chaperone deficiency – and corresponding BI/6J WT mice were treated the same way to compare models of ER and mitochondrial chaperone deficiency. Upon DSS colitis, *Grp78*^{+/-} mice decreased in weight exactly like WT controls, whereas *Hsp60*^{+/-} mice lost more weight than their WT controls by trend. This trend towards an elevated susceptibility towards DSS colitis can also be seen in the disease activity index and in the histological score of the colon, but was not pronounced enough to become manifest in an shorter colon length or increased spleen weight compared to WT mice on DSS. *Grp78*^{+/-} mice in comparison showed no trend towards an altered susceptibility towards DSS in none of the assessed parameters (Fig. 18).

Figure 18



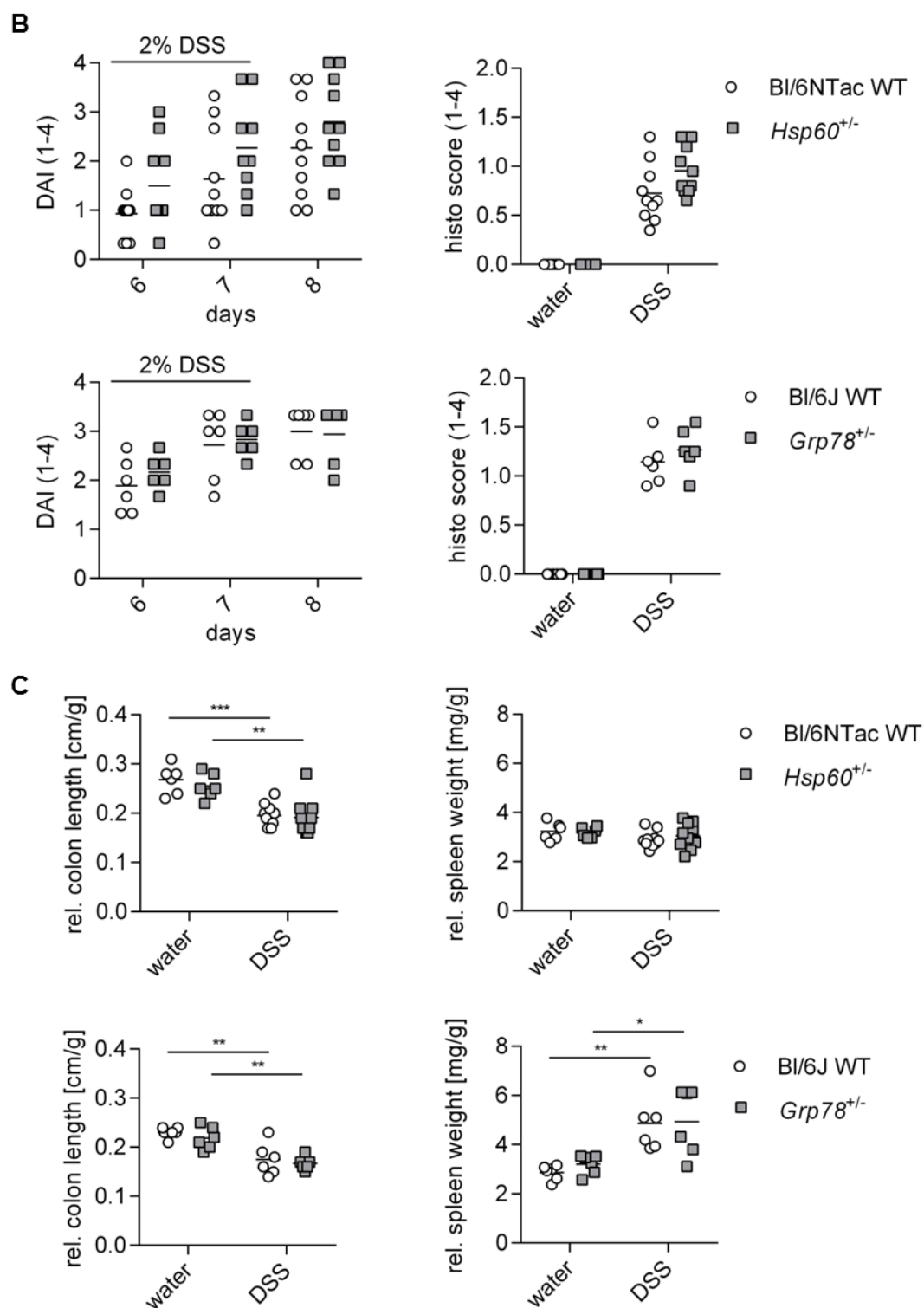


Fig. 18 DSS colitis in *Grp78*^{+/-} and *Hsp60*^{+/-} mice

(A+B) Weight and disease activity index (DAI) development of *Grp78*^{+/-} and *Hsp60*^{+/-} mice on a seven days treatment with 2% DSS with corresponding WT and water controls. A Mann-Whitney/Rank-Sum statistical test was performed to compare genotypes on DSS. (C) Colon length and spleen weight was related to the initial body weight of mice before start of treatment. Graphs represent 6 *Grp78*^{+/-}, 6 BI/6J WT, 10 *Hsp60*^{+/-} and 10 BI/6NTac WT mice. A Two-Way-Anova statistical test was performed to compare treatments and genotypes.

RESULTS

In addition to the acute colitis caused by administration of the chemical substance DSS, the *Grp78*^{+/-} as well as the *Hsp60*^{+/-} mouse was challenged by crossing them to a genetic model of chronic ileal inflammation, the *Tnf*^{ΔARE/WT} (ΔARE) mouse and held under conventional (non SPF) housing conditions. The histopathology of the terminal ileum was not different in ΔARE/*Hsp60*^{+/-} and ΔARE/*Grp78*^{+/-} mice in comparison to the ΔARE mouse at an age of 18 weeks. In contrast, in the proximal colon, where inflammation is mild compared to the distal ileum, *Hsp60* deficiency caused an increased tissue pathology and elevated signs of local and systemic inflammation like MLN- and spleen weight (Fig. 19A). Deeper analysis of the tissue pathology of the proximal colon identified elevated leucocyte infiltration into the mucosa, submucosa and epithelial damage (crypt loss) as contributors to the elevated histo score (Fig. 19B) in ΔARE/*Hsp60*^{+/-} mice.

Figure 19

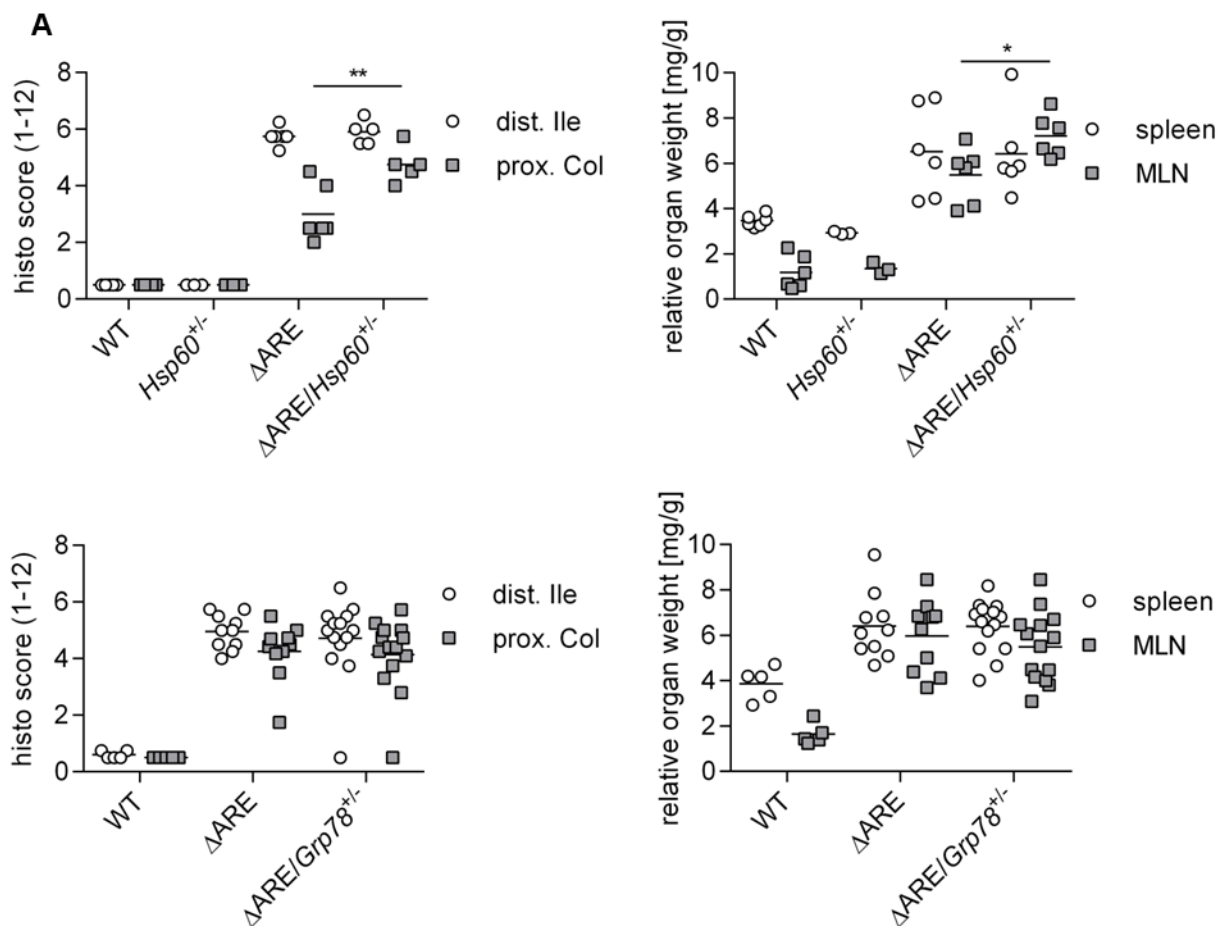


(Figure continued on next page)

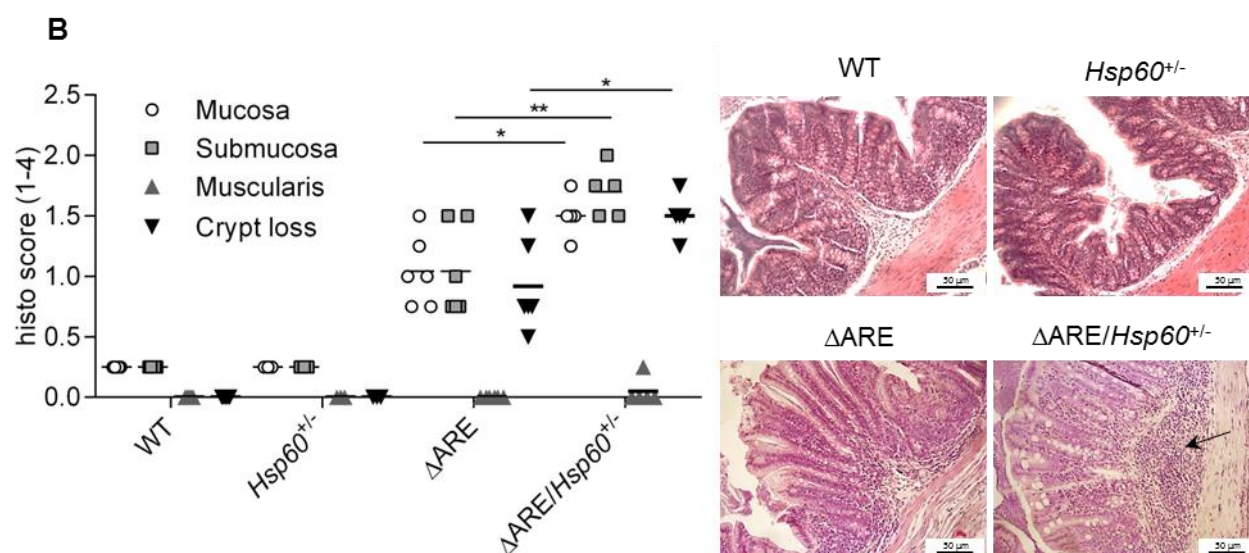


Fig. 19 Chronic ileitis in *Grp78*^{+/-} and *Hsp60*^{+/-} mice

(A) Histological analysis of the distal ileum and proximal colon and immune organ weight analysis in 18 weeks old Δ ARE/*Grp78*^{+/-} (n=14) and Δ ARE/*Hsp60*^{+/-} (n=6) mice compared to Δ ARE mice (n=10/6). An Anova-On-Ranks statistical test (for histopathology) and a Two-Way-Anova test (for organ weights) were performed to compare Δ ARE and *Hsp60* genotypes (B) Detailed view on the proximal colon of the Δ ARE/*Hsp60*^{+/-} model. An Anova-On-Ranks statistical test was performed. Pictures show H&E stainings in a 250x magnification. The arrow indicates accumulated infiltration of leucocytes into the submucosa.

4.5 Characterization of the *Hsp60*^{ΔIEC} mouse

4.5.1 Genotyping of the conditional knock out allele

To investigate the impact of a homozygous *Hsp60* deficiency specifically in the intestinal epithelium, the *Hsp60*^{flox/flox} mouse was crossed with different Cre recombinase expressing mice (*VillinCre*, *VillinCreER*^{T2} and *Lgr5CreER*^{T2}) to generate a tissue specific conditional knockout. In all cases, the presence of the flox allele was checked via genotyping PCR).

Figure 20

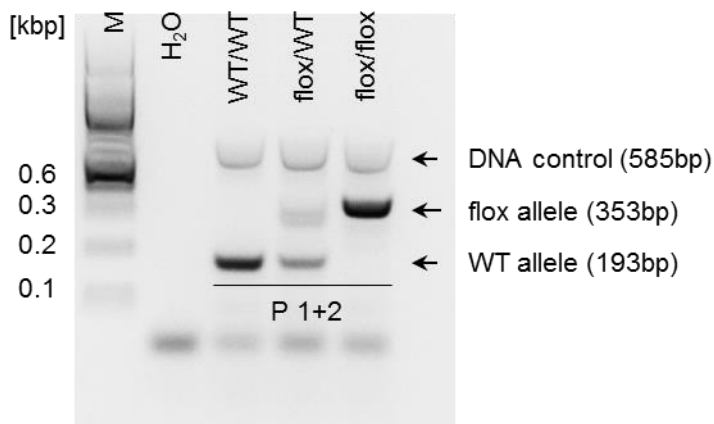
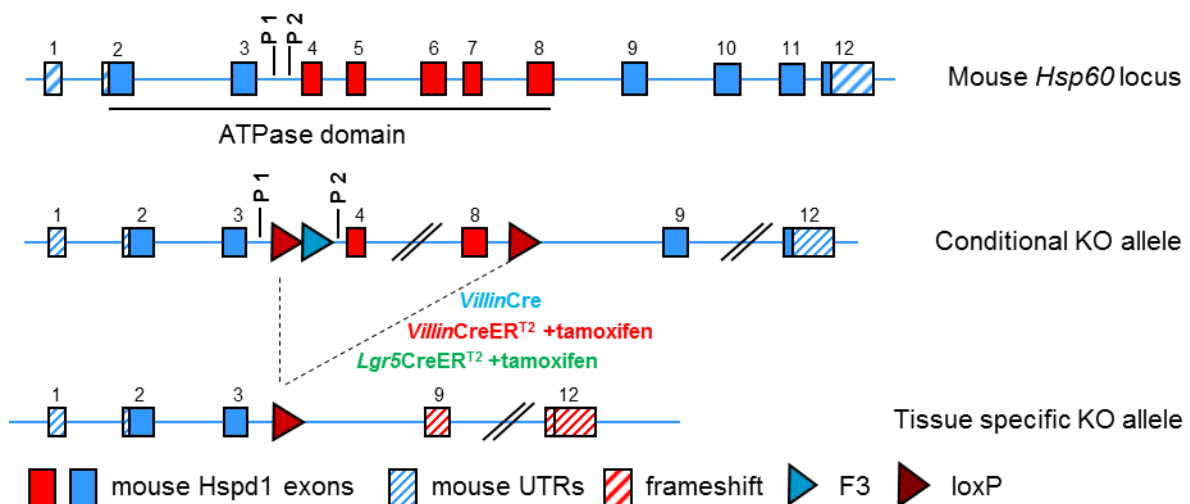


Fig. 20 Genotyping of *Hsp60*^{flox/flox} mice

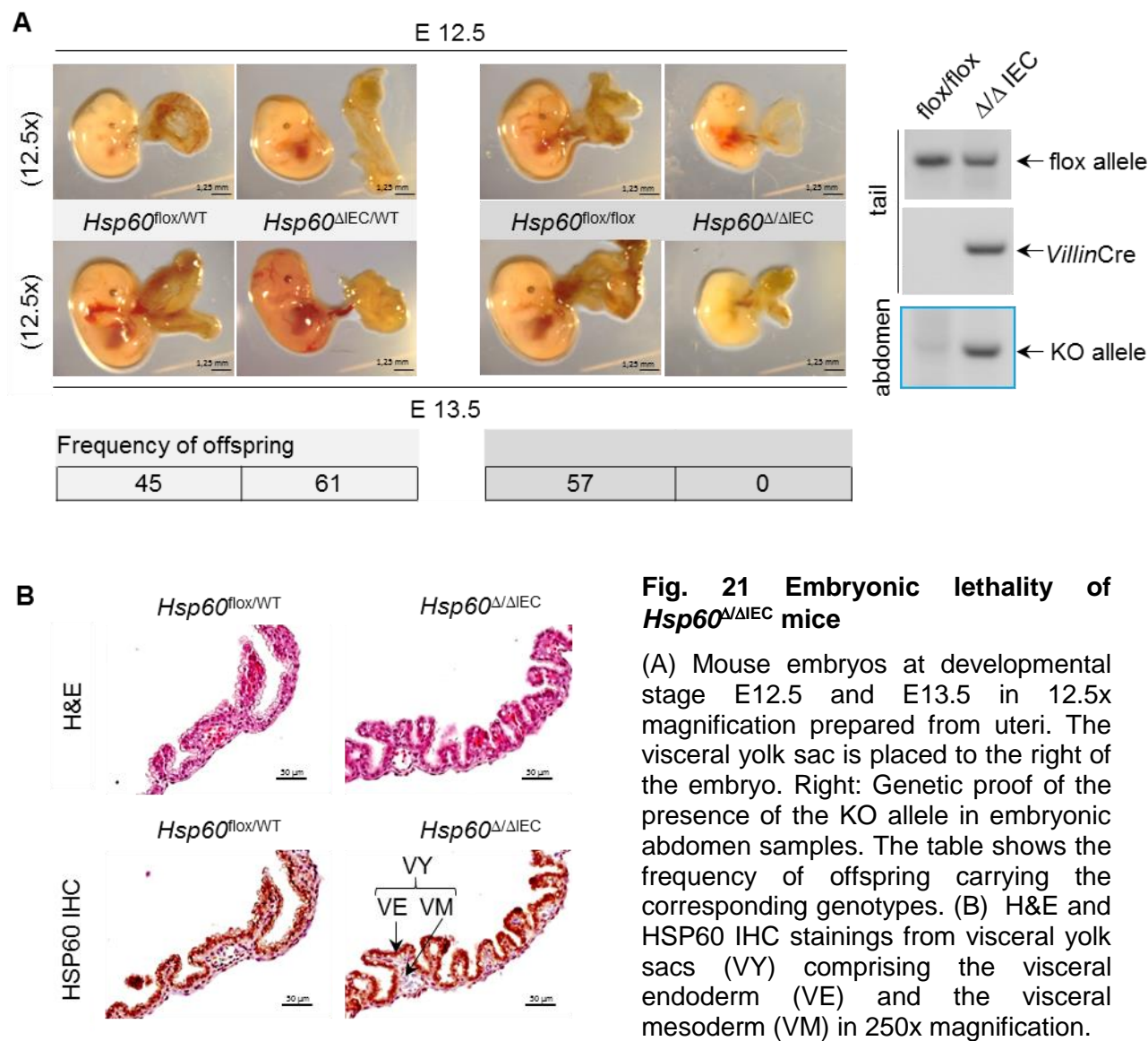
Schematic illustration and agarose gel of the genotyping PCR products. The insertion of a loxP and a F3 site between exons 3 and 4 increases the amplicon size for 160bp. A water control was performed to exclude contaminations of PCR reagents with foreign DNA.

4.5.2 Embryolethality of the *Hsp60*^{ΔIEC} mouse

After crossing the *Hsp60*^{flox/flox} mouse with the *VillinCre* transgenic mouse, the epithelial specific *Hsp60* knock out starts to establish with the beginning of Villin expression at approx. E10.5 of embryonic development [224]. According to the Mendelian law, a crossing of *Hsp60*^{flox/flox} mice with *Hsp60*^{flox/WT}-*VillinCre*^{Tg} (in short *Hsp60*^{ΔIEC/WT}) is supposed to deliver 25% offspring carrying the homozygous epithelial KO (*Hsp60*^{ΔIEC}).

As shown in Fig. 21A, no homozygous offspring could be genotyped. Instead embryos at stage E12.5 and 13.5 showed obvious signs of developmental retardation (like missing eyes) compared to control embryos of the same age.

Figure 21



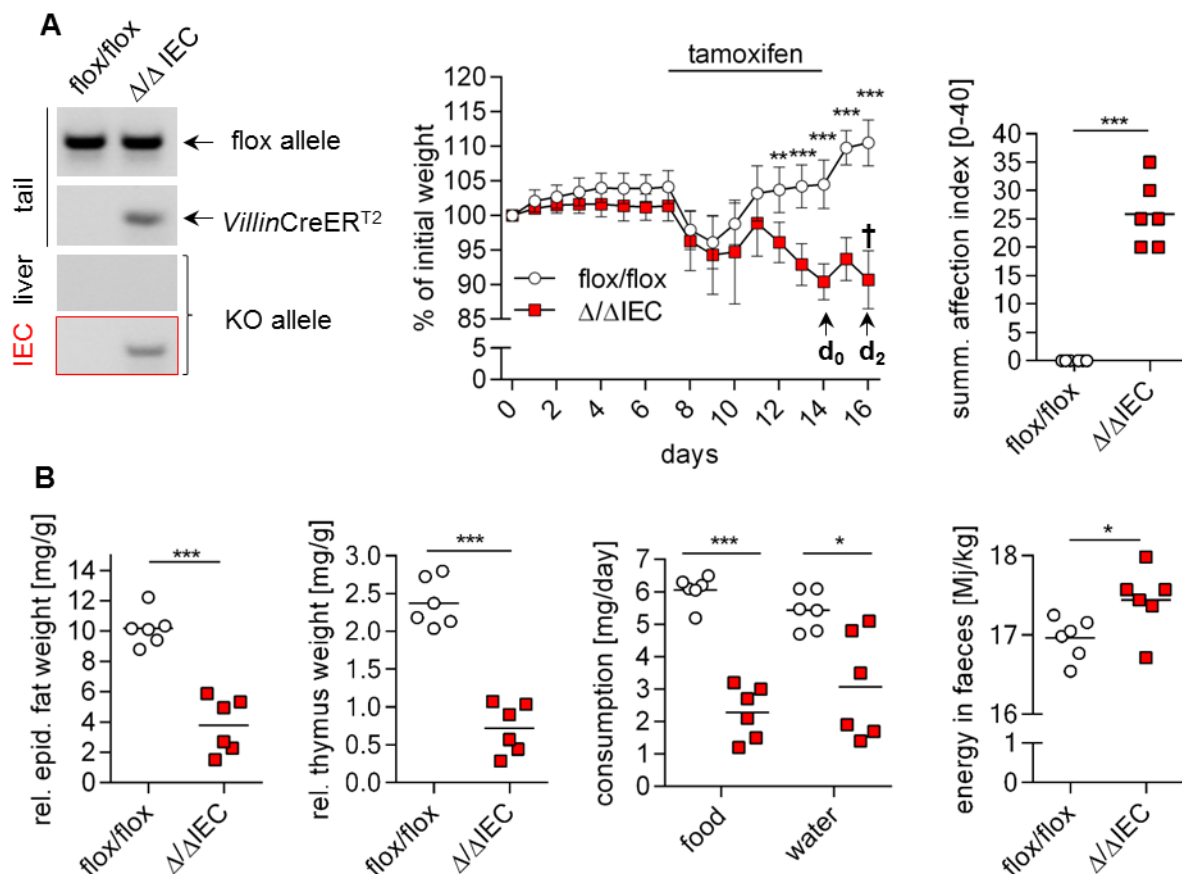
According to Marjou *et al.* [224], Villin driven Cre recombination is already present at embryonic developmental stage E10.5 strongly in the extraembryonic visceral endoderm (VE). This extraembryonic cell layer forms - together with the visceral mesoderm (VM) - the visceral yolk sac (VY) to provide the early embryo with nourishment. To investigate if a lack of HSP60 in this cell layer caused the embryo lethality, H&E and HSP60 IHC stainings on the respective tissue was performed. Unexpectedly, the IHC did not reveal a reduction of the HSP60 protein levels in VE compared to control tissue. Accordingly, the VY showed a normal folded architecture according to the H&E stainings (Fig. 21B).

4.6 Characterization of the tamoxifen inducible *Hsp60*^{ΔIEC} mouse

4.6.1 Phenotypic, metabolic and intestinal characterization of the *Hsp60*^{ΔIEC} mouse

To be able to generate an IEC specific homozygous *Hsp60* knock out in adult mice and thereby circumvent embryolethality, we created *Hsp60*^{lox/lox}-*VillinCreER*^{T2} Tg mice. Upon oral administration of tamoxifen to 10 weeks old male mice, the knock out could be detected in isolated IEC (Fig. 22A). Mice lost weight rapidly and had to be sacrificed two days after putting them back on chow diet. The sum of abortion criteria had passed the threshold of 20 comprising an untended coat (general condition), reluctant movement (behaviour) and sticky stool (intestinal symptoms; Fig. 22A). The rapid weight loss was accompanied by a drop in feed and water consumption at day 15 and 16 leading to a wasting of the epididymal fat and the thymus mass. Not only the intake of feed and water was diminished, also the intestinal nutrient uptake was disturbed, as the increased fecal energy content (combined feces of day 15+16) revealed (Fig. 22B). This metabolic disturbance was accompanied by several morphological abnormalities of the GI tract. The stomach of *Hsp60*^{ΔIEC} mice were densely filled with food, a phenomenon that is often observed when starving mice are fed *ad libitum*. The small intestinal tract was shortened, whereas the colon was not, pointing to a inflammatory pathology located in the small intestine. In 30% of the cases the cecum was filled with water and thin mucus, extending the caecum wall and putting the mucosa under severe tension (Fig. 22C). These mice developed sticky stool as an intestinal symptom.

Figure 22



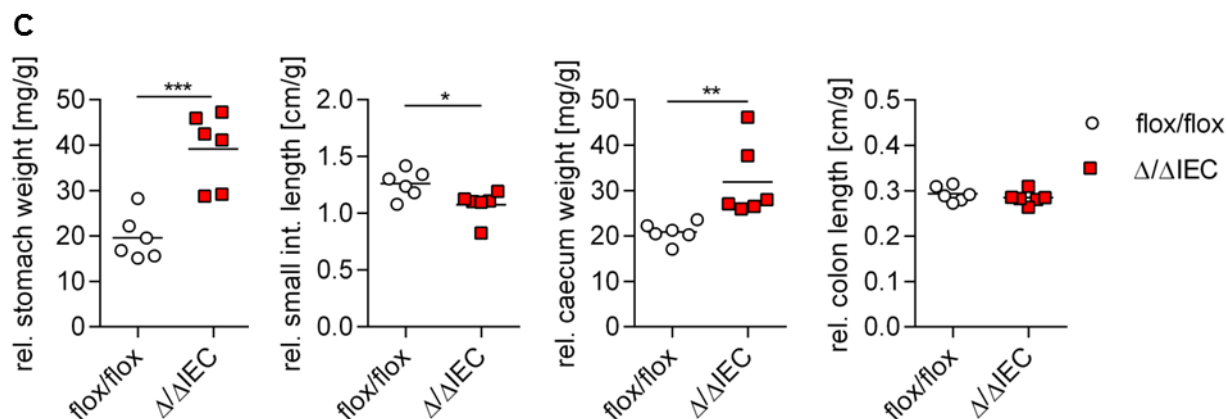
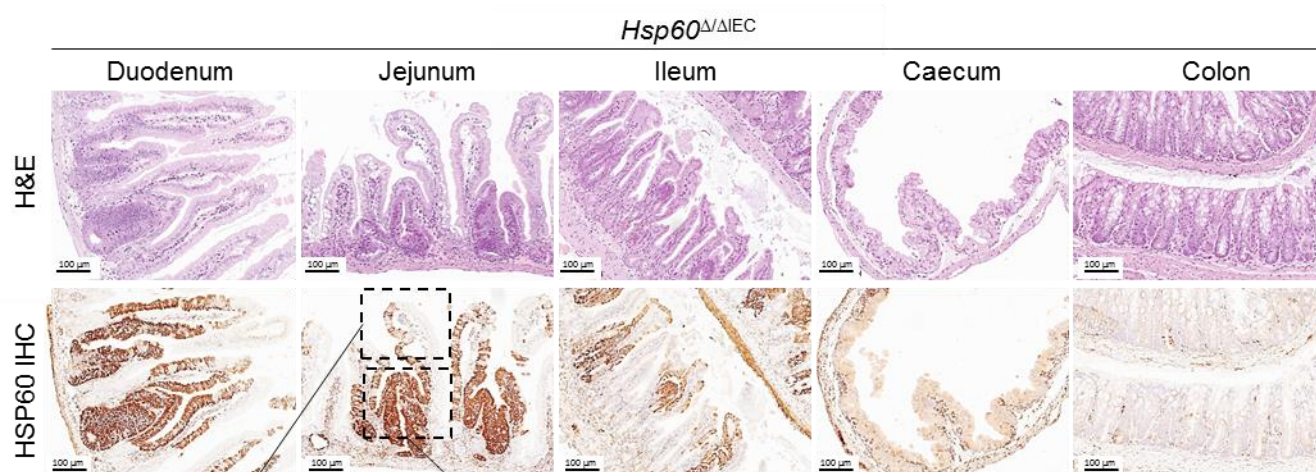
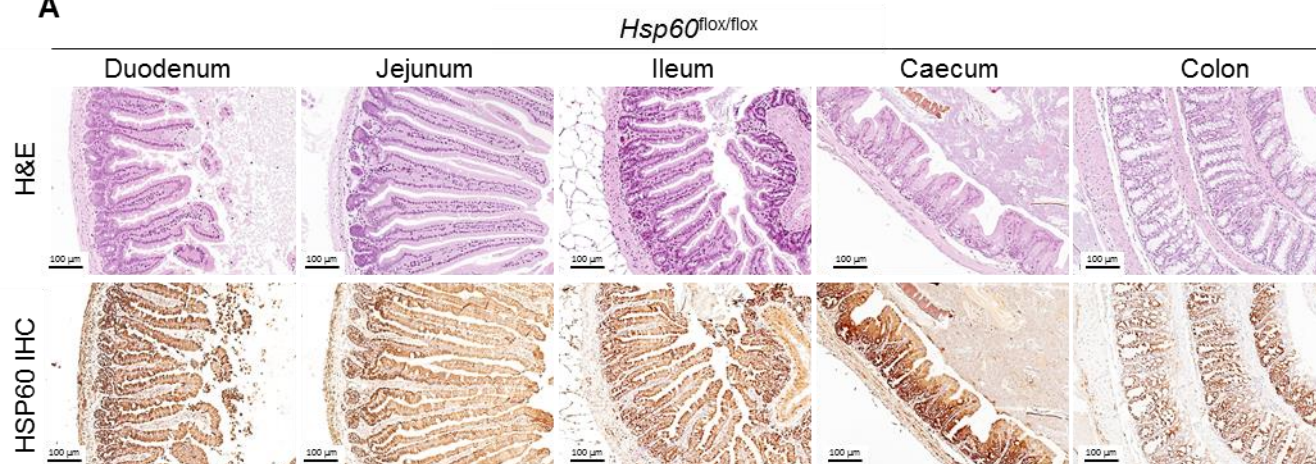
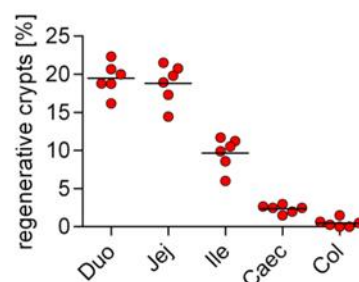
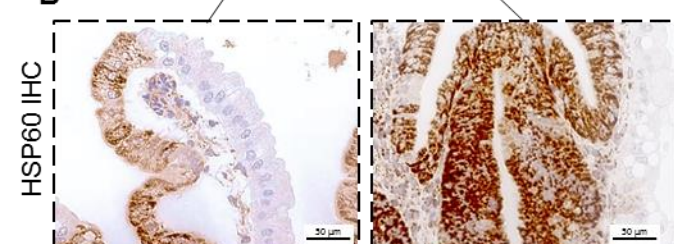


Fig. 22 Characterization of the phenotypic, metabolic and morphologic appearance of tamoxifen inducible *Hsp60* $\Delta\Delta\text{IEC}$ mice

(A) Genetic proof of IEC specific knock out and weight development in the course of oral administration of tamoxifen. Summarized affection index at d_2 considering four macroscopic criteria. Abortion threshold is a score of 20. (B) Metabolic status and excess of wasting measured by food and water consumption at d_2 , the epididymal fat and thymus weight and by assessing the energy content of fecal samples (d_0 - d_2) by calorimetry. (C) Morphologic appearance of the GI tract. Length and weight measurements were normalized to the body weight of mice at d_0 . Graphs represent six animals per group. Statistical analysis was performed via t-test comparing genotypes at each time point.

At the level of histopathological evaluation of relevant tissue sections revealed alterations most prominent in the upper small intestinal tract. Numerous hyperproliferative crypts were identified with decreasing densities from the duodenum to the colon. Immunohistochemical staining of HSP60 reveals that the genetic knock out indeed led to an abolishment of HSP60 – most clearly visible in the colon – whereas hyperproliferative crypt foci are strongly expressing HSP60 (Fig. 23A+B).

On high magnification pictures of the H&E stained tissue sections, mild infiltration of leucocytes into the mucosa of *Hsp60* $\Delta\Delta\text{IEC}$ can be observed. To identify the type of leucocytes infiltration a staining for CD3 (T-cells), B220 (B-cells), Ly6G (granulocytes), CD11c (dendritic cells) and F4/80 (macrophages) was performed on jejunal tissue. The infiltrates could be identified as mainly macrophages and dendritic cells (Fig. 24A). Moderate macrophage infiltration appeared along the entire GI tract to a similar extent (Fig. 24B). Profiling of selected cytokine and chemokine mRNA expression both in jejunal and colonic mucosa (total tissue) revealed a pronounced *Il-6* induction in the jejunum and a *Tnf* induction in the colon. Although no infiltration of T-cells and neutrophils is apparent in the mucosa of *Hsp60* $\Delta\Delta\text{IEC}$ mice, chemokines attracting neutrophils (*Kc*) and monocytes (*Mcp-1*) were upregulated in both jejunum and colon of this mouse model. In jejunum, levels of *Ip-10* attracting T-cells were upregulated as well (Fig. 24C).

Figure 23**A****B****Fig. 23 Histologic characterization of the GI tract in tamoxifen inducible *Hsp60^{Δ/ΔIEC}* mice**

(A) Representative H&E and corresponding HSP60 IHC stainings along the different compartments of the GI tract in a 125x magnification. (B) Representative section (400x) of HSP60 IHC of villus tips and hyperproliferative crypts. Perceptual amount of HSP60 positive regenerative crypts along the GI tract assessed from the H&E and HSP60 IHC stainings. The graph represents tissue sections from six animals.

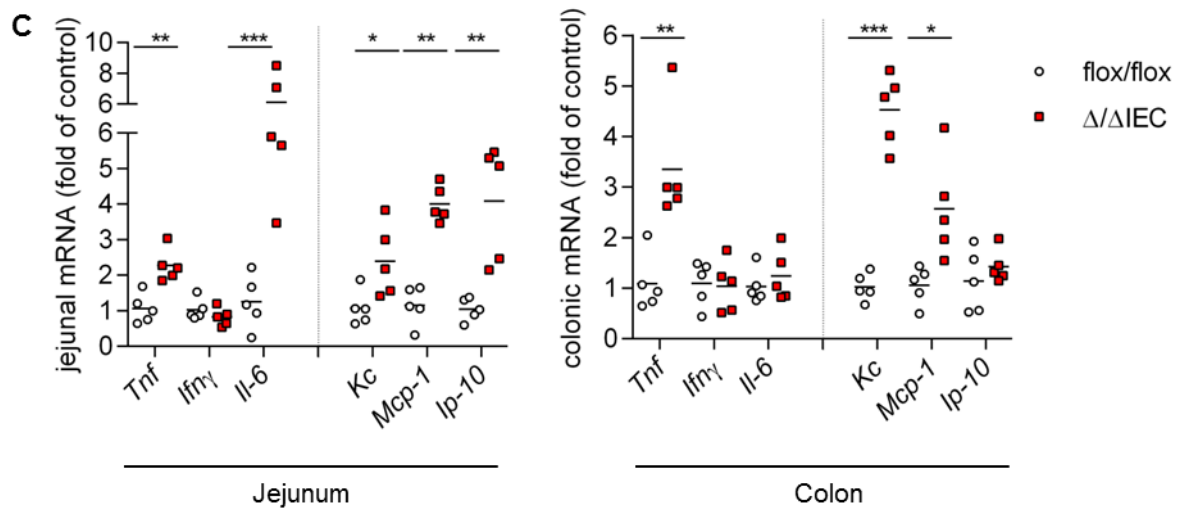


Fig. 24 Characterization of mucosal inflammation in tamoxifen inducible *Hsp60*^{Δ/ΔIEC} mice

(A) IHC screening to identify the type of leucocyte infiltration into the jejunal mucosa (representative stainings; 125x). (B) Representative stainings for macrophages (F4/80) along the GI tract (200x) in jejunum and colon including magnifications of relevant areas (400x). (C) Cytokine (left panel) and chemokine (right panel) mRNA profile (selection) of jejunal and colonic mucosa (n=5 per genotype). Statistical analysis was performed via t-test.

4.6.2 Functional characterization of the epithelium in *Hsp60*^{Δ/ΔIEC} mice

To exclude the possibility that a deletion of the mitochondrial chaperone HSP60 induces epithelial apoptosis, a TUNEL assay was performed to detect DNA degradation as a marker for programmed cell death. This phenomenon could not be observed in representative jejunal sections of *Hsp60*^{Δ/ΔIEC} mice (Fig. 25).

Figure 25

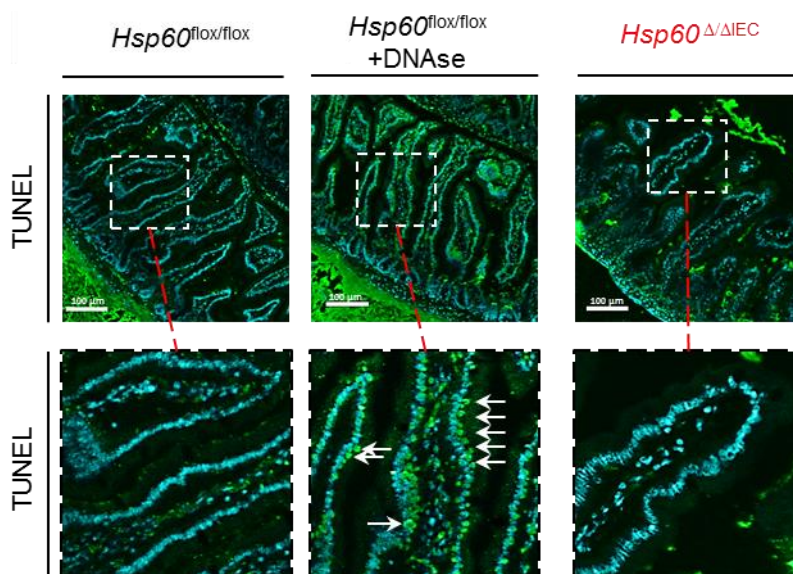


Fig. 25 Epithelial apoptosis in tamoxifen inducible *Hsp60*^{Δ/ΔIEC} mice

TUNEL staining (green) to assess DNA fragmentation upon apoptosis on intestinal sections of control and *Hsp60*^{Δ/ΔIEC} mice. DNase treated sections of control mice served as positive control. Upper row: Representative pictures in 200x magnification. Lower row: Details in 600x magnification. Nuclear staining (dapi) in cyan.

To investigate if the small intestinal epithelium of *Hsp60*^{Δ/ΔIEC} mice is functionally intact, the uptake of nutrients into ileal tissue sections by specific epithelial transporters was measured. Since the absolute amount of substrate taken up during a certain time period is not sufficient to assess the specificity of a transporter, the uptake in the presence of a specific transport inhibitor was measured as well. The difference between the absolute uptake and the remaining uptake after addition of an inhibitor is called the inhibitable uptake. The activity of the basal glucose transporter GluT2, assessed by the inhibitable glucose uptake was not diminished in *Hsp60*^{Δ/ΔIEC} mice. As well, the apical glucose transport activity of SGLT1, assessed by the inhibitable α -MDG uptake was not altered. However, the activity of the dipeptide transporter PepT1 was reduced by half (Fig. 26).

Figure 26

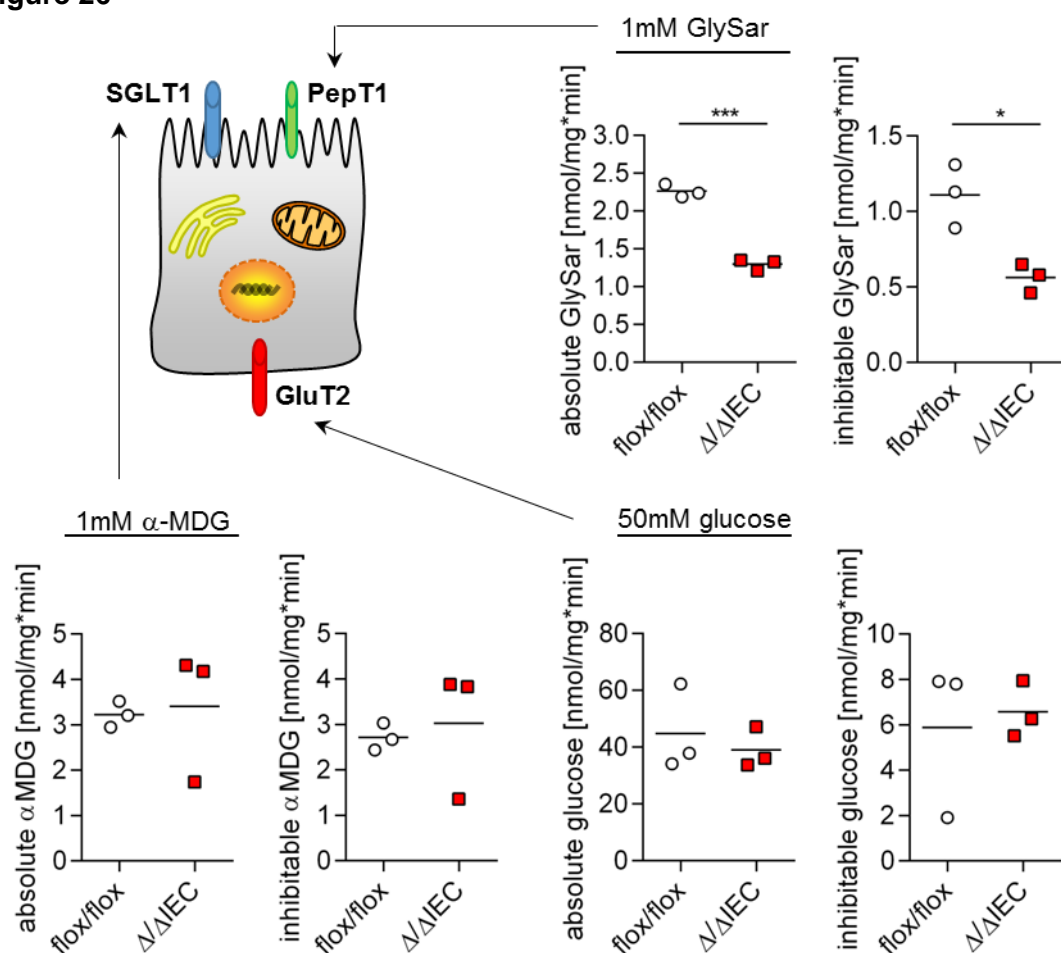


Fig. 26 Functionality of the ileal epithelium of tamoxifen inducible *Hsp60*^{Δ/ΔIEC} mice

2cm ileal gut sections were incubated with radioactively labeled nutrients and nutrient analogues with or without addition of inhibitors of uptake (inhibitable uptake = uptake without inhibitors – uptake with inhibitors). Graphs represent sections from 3 animals per genotype. Statistical analysis was performed via t-test comparing genotypes.

4.6.3 Characterization of the epithelial stress responses in *Hsp60*^{ΔIEC}

To characterize the impact of a HSP60 deletion in IEC at the transcriptional level, a mRNA microarray analysis was performed on isolated colonic epithelial cells derived from *Hsp60*^{fllox/fllox} and *Hsp60*^{ΔIEC} mice. In this tissue where HSP60 is homogenously absent in the knockout mice, 2,512 genes were differentially regulated compared to the control group (Fig. 28A). According to the gene ontology (GO) term analysis, highly significantly regulated genes belong to the group “metabolic processes” among the term “biological processes”. All “primary metabolic processes” except carbohydrates are overrepresented in regulated genes (Fig. 28B). The MeSH term analysis revealed that the profile of regulated genes is typical for “digestive system diseases” and for “neoplasms”. Among the “digestive system diseases” the profile fits most significantly to “digestive system neoplasms” (Fig. 28C). A closer look at the GO term “response to stimulus” revealed that numerous cellular stress responses (ER stress, protein folding stress, and oxidative stress) were represented by the regulated genes (Fig. 28D) in this global approach of gene expression profiling.

Figure 27

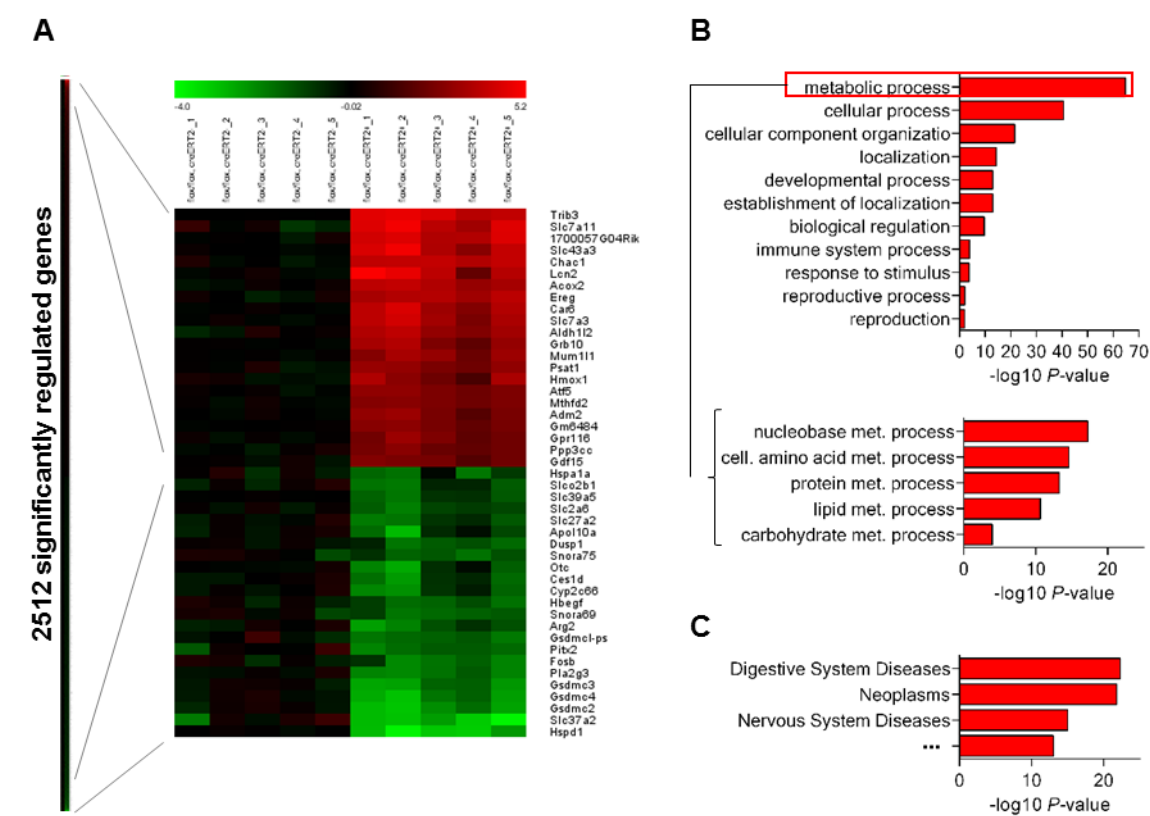


(Figure continued on next page)

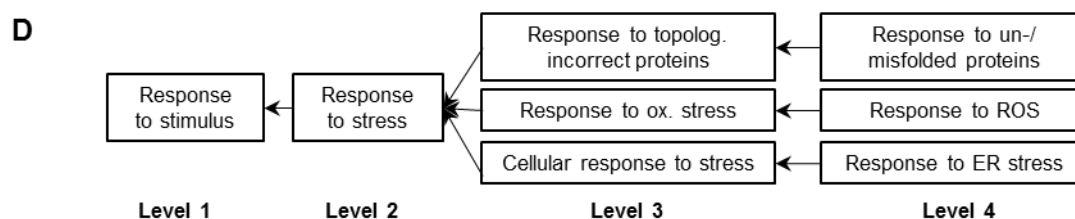
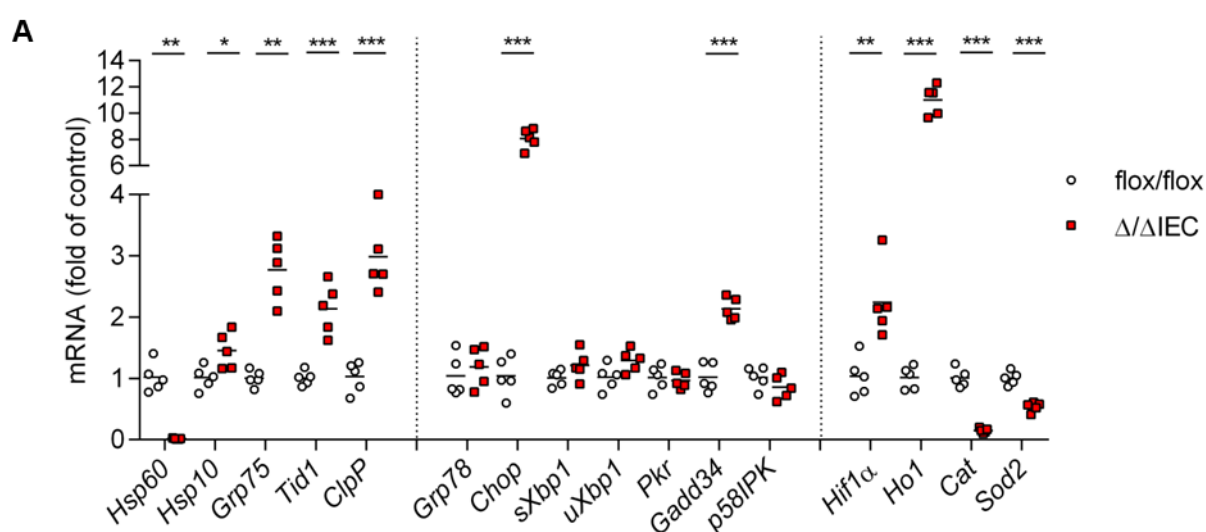


Fig. 27 mRNA expression profiling of colonocytes from *Hsp60*^{Δ/ΔIEC} mice

(A) The 22 most up- and downregulated among 2,512 significantly ($q < 0.01$) regulated genes on the mRNA microarray ($n=5$ per genotype) shown in a heat map (red=up; green=down). The scale indicates signal log2 ratios (-4.0 - +5.2). (B) GO term analysis of regulated genes under the head term “biological processes”. Deep analysis of regulated “primary metabolic processes”. (C) MeSH term analysis of diseases represented by the regulated genes. (D) Represented GO terms on all levels contributing to the term “response to stimulus”.

To specifically verify expression changes of cellular stress responses upon deletion of HSP60 in colonocytes on mRNA level revealed an upregulation of MT chaperones and proteases (MT UPR), a selective ER UPR activation namely *Chop* and *Gadd34* and an extensive response to oxidative stress and hypoxia (Fig. 28A). The high induction of *Chop* was verified on protein expression levels (IHC) and caused induction of several CHOP responsive genes like *Trib3*, the highest upregulated gene on the microarray (Fig. 28A+Fig. 28B). To assess if the colonic goblet cells which are highly active in secretory protein synthesis are affected by the induction of the UPR pathways, an alcian blue staining of acetic mucus was performed. In essence, the colonic epithelium showed no alteration with respect to mucus production compared to control mice (Fig. 28C).

Figure 28



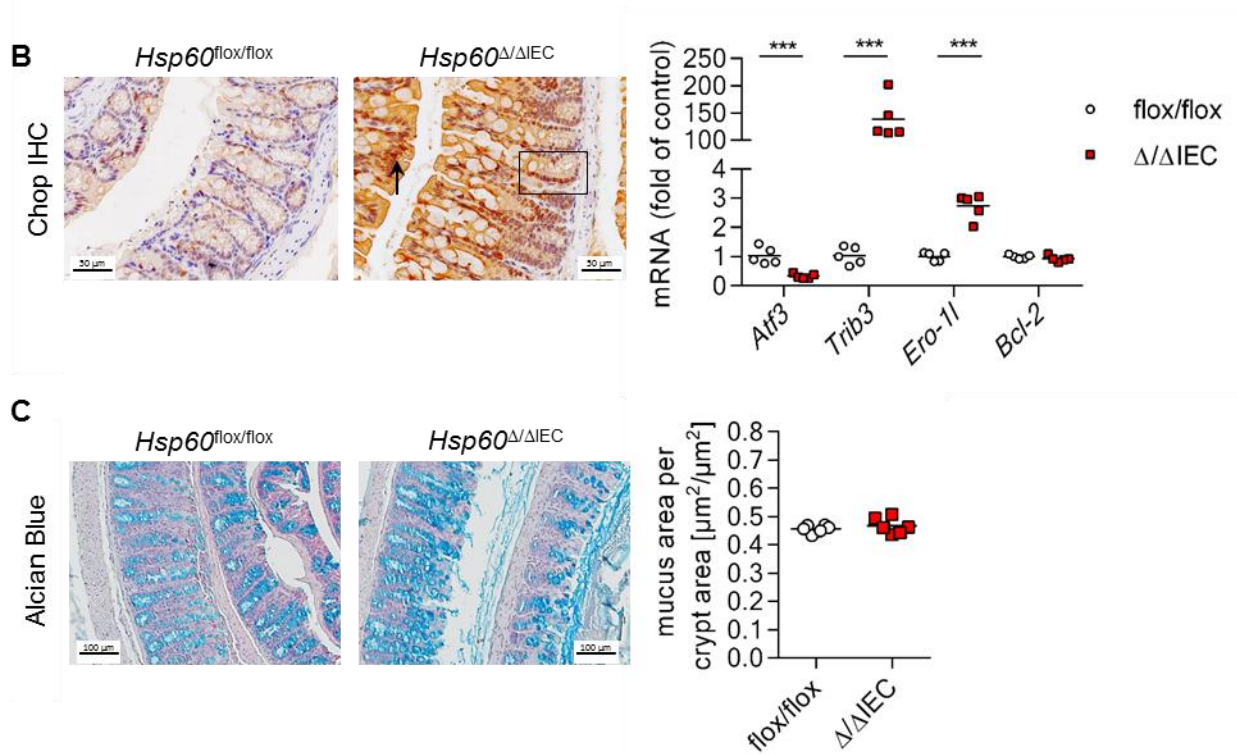
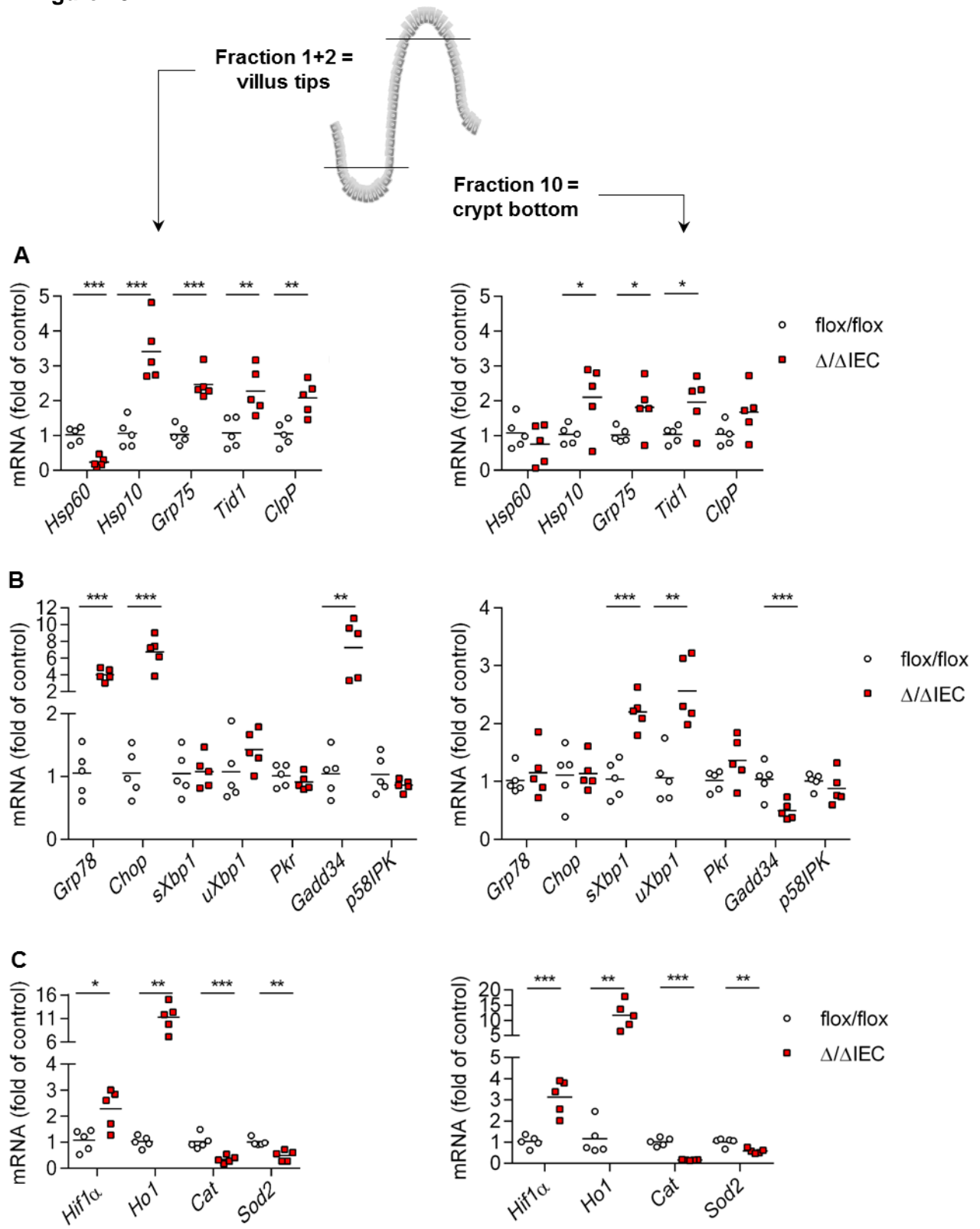


Fig. 28 mRNA expression profiling of colonocytes from *Hsp60*^{Δ/ΔIEC} mice

(A) qPCR profiling of MT-, ER- and oxidative stress responses (n=5 per genotype). (B) Chop IHC staining (representative picture; 250x; box and arrow indicate nuclear localization of CHOP) and pPCR analysis of CHOP responsive genes. (C) Alcian blue staining of acetic mucus (150x) and quantification of mucus (blue) area. All statistical analysis was performed via t-test comparing genotypes

The characterization of the UPR-related gene expression in the small intestine is more difficult compared to the colon, since hyperproliferative crypts that can be large in size, express high amounts of HSP60 (Fig. 23B). Therefore, the epithelium from villus tips was isolated separately from the crypt bottom. Villus tips show a clear reduction of *Hsp60* compared to control epithelium. This reduction is accompanied by an induction of the MT UPR marker genes comparable to the induction in the colonic epithelium (Fig. 29A). For the ER UPR, levels of *Grp78* were elevated in addition to those *Chop* and *Gadd34* which already showed up in the colonic epithelium (Fig. 29B). The expression pattern of genes in response to oxidative stress and hypoxia were also comparable to those detected in colonic IEC. This is also true for the crypt bottom compartment of the IEC (Fig. 29C). However, clear differences in UPR gene expression could be detected compared to the villus tips. The expression levels of some genes seem diluted by the signals originating from the hyperproliferative crypts e.g. the MT UPR genes. Here, *ClpP* induction does not reach significance whereas it does in the villus tips (Fig. 29A). In case of *Gadd34*, the gene is even adversely regulated compared to the villus tips and the colon IEC (Fig. 29B). The restricted induction of *Chop* in the villus tips (Fig. 29B) could be confirmed on protein level via IHC stainings of corresponding jejunal tissue sections (Fig. 29D).

Figure 29



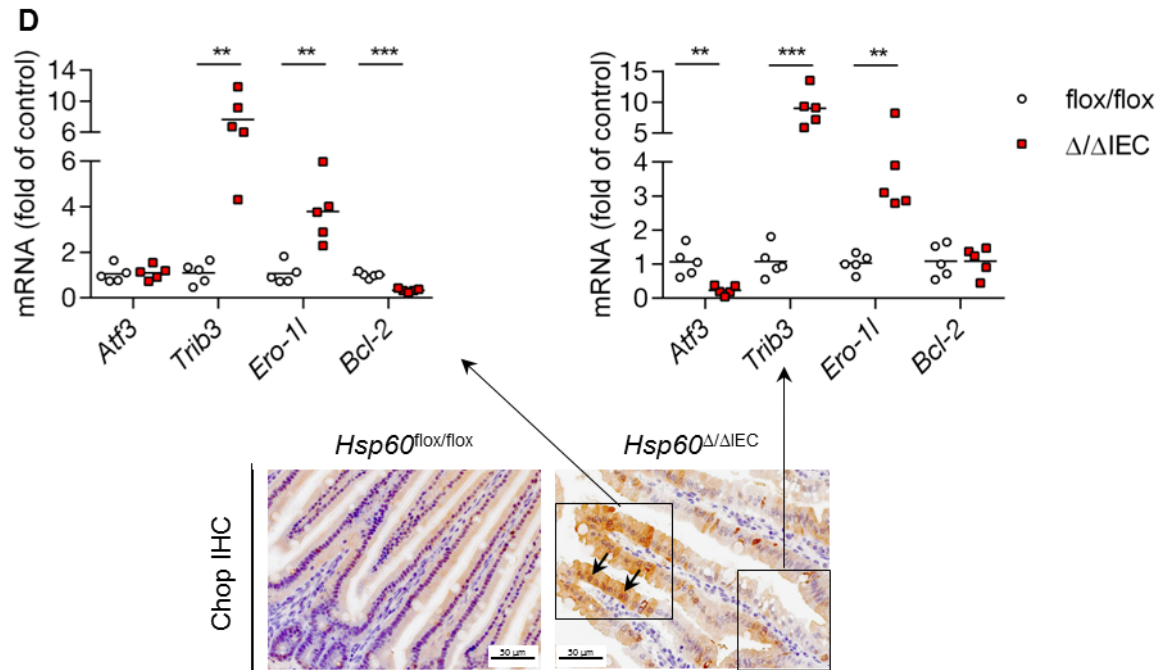
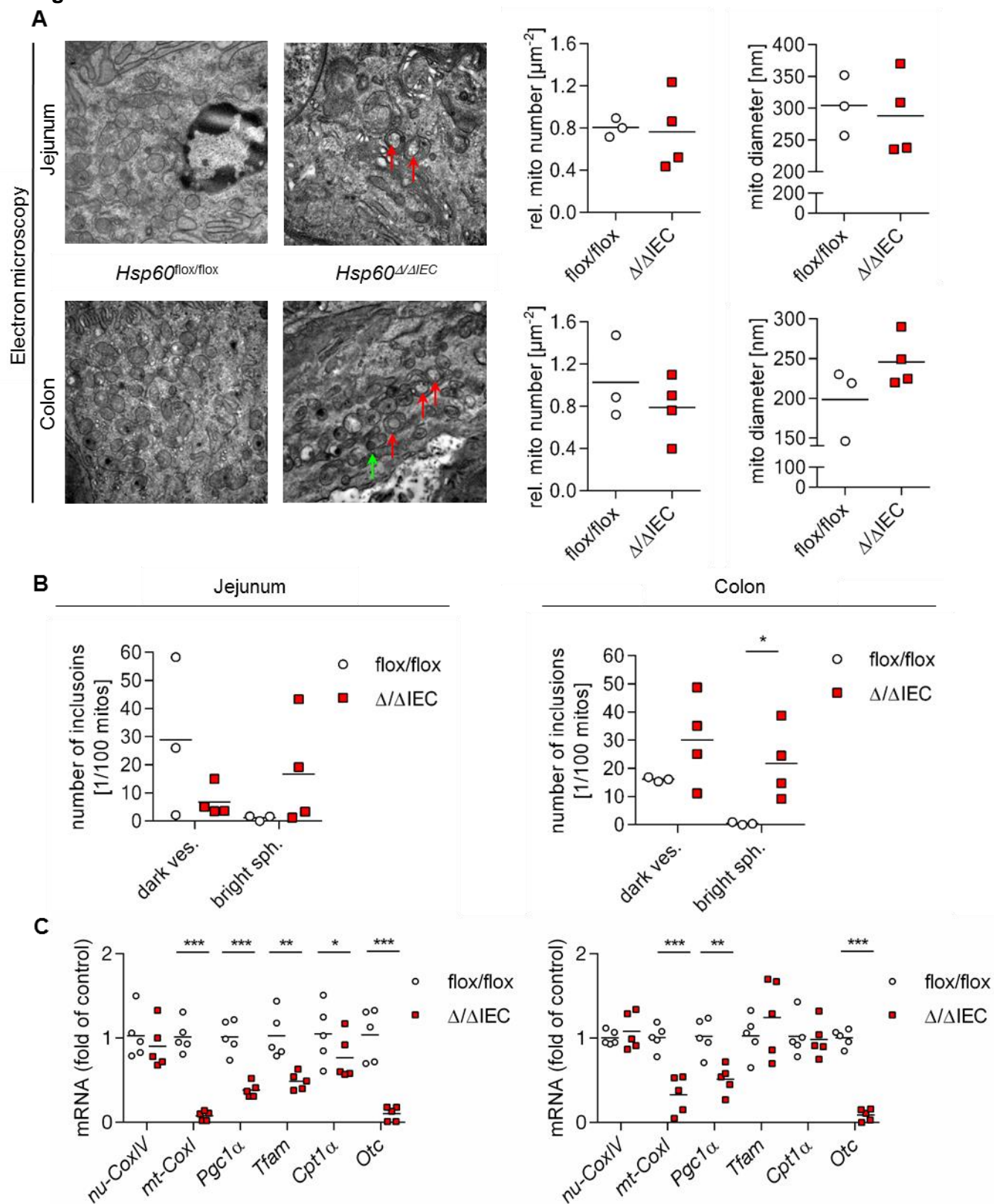


Fig. 29 Differential (villus vs. crypt) UPR profiling of jejunal epithelium in *Hsp60*^{Δ/ΔIEC} mice

(A-D) Left panel: Villus tip epithelium (fraction 1+2). (A-D) Right panel: Crypt bottom epithelium (fraction 10). qPCR profiling of the (A) MT UPR, (B) ER UPR and (C) oxidative stress response (n=5 per genotype). (D) qPCR of CHOP responsive genes and CHOP IHC (250x). Boxes indicate villus tip region with high CHOP expression (arrow: nuclear localization) and crypt bottom with mild/absent CHOP expression (representative pictures). Statistical analysis was performed via t-test comparing genotypes.

4.6.4 Characterization of the mitochondrial appearance in IEC of *Hsp60*^{Δ/ΔIEC} mice

Finally, the consequences of a HSP60 depletion on the mitochondrial morphology and functionality was investigated. Evaluation of electron microscopic images from the colonic and jejunal epithelium revealed no alterations in the mean number or in the mean diameter of the mitochondria (Fig. 30A). The analysis was restricted to a relatively low number of individuals (n=3-4), since this set of tissue specimen was available for parallel preparation for electron microscopy and batch to batch differences in the complex procedure of preparation should be avoided. Nevertheless, two types of inclusions in the mitochondrial matrix could be observed: including dark vesicles and bright membrane enclosed spheres. The number of these spheres, which are almost absent in control mice, was significantly elevated in colonocytes of *Hsp60*^{Δ/ΔIEC} mice (Fig. 30B). The qPCR profiling of mitochondrial functionality genes revealed an abolishment of the MT encoded cytochrome C oxidase (Cox) subunit I of respiratory chain complex IV and the urea cycle enzyme ornithinetranscarbamylase (*Otc*) in both colonic and villus tip epithelium. *Pgc1α*, a marker of MT biogenesis, is inversely regulated in the two compartments, whereas, *Tfam*, a transcription factor for MT genes, is downregulated in the villus tips but not in the colonocytes (Fig. 30C).

Figure 30**Fig. 30 Mitochondrial morphology and functionality in IEC of *Hsp60*^{Δ/ΔIEC} mice**

(A) Transmission electron microscopy (TEM; 19.000x) of colonic and jejunal epithelium with evaluation of MT number and diameter based. Green arrow: dark vesicles; Red arrow: bright spheres (B) Quantification of dark and bright inclusions based on the TEM images. (C) qPCR profiling of MT functionality genes in villus tip and colon epithelium (n=5 per genotype). Statistical analysis was performed via t-test.

4.6.5 Effects of HSP60 depletion on epithelial proliferation

As already indicated in Fig. 23A+B, the *Villin*CreER^{T2} driven knock out of *Hsp60* is incomplete. To proof this observation on the genomic level, villi and hyper-regenerative crypts were cut out separately via Laser Microdissection (LMD), genomic DNA was isolated and used for genotyping. Although both epithelial regions carried the allele for CreER^{T2} recombinase, no knock out allele could be observed in the isolated crypts in contrast to the villi (Fig. 31A) meaning that these cells have escaped the recombination process. *Hsp60* highly correlates with the proliferative capacity of the crypt cells. *HSP60*⁻ crypt cells also lack the proliferation marker Ki67, whereas hyper-regenerative *HSP60*⁺ crypts consist of numerous Ki67 expressing cells – five times more than in a control crypt (Fig. 31B).

Figure 31

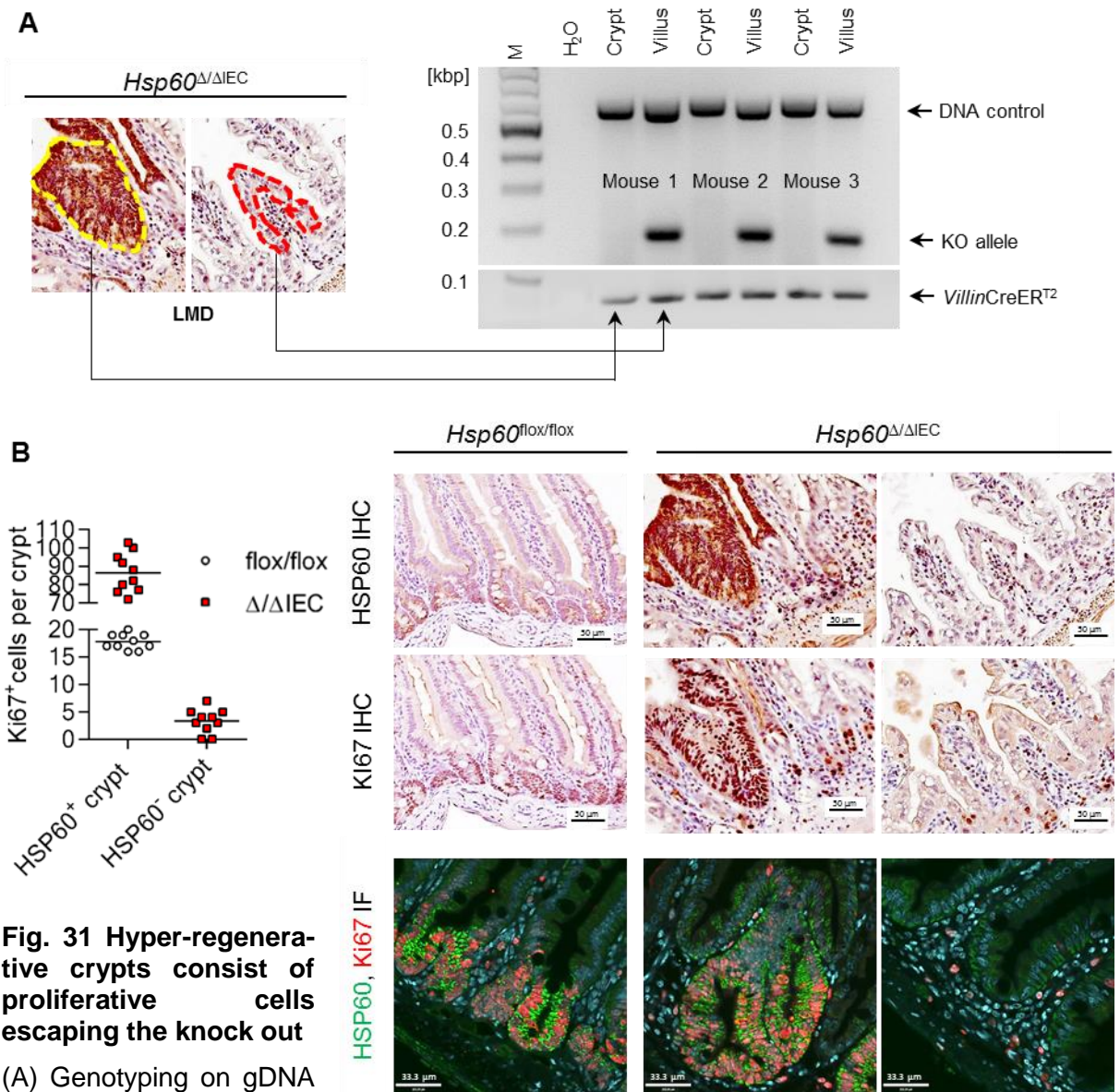


Fig. 31 Hyper-regenerative crypts consist of proliferative cells escaping the knock out
(A) Genotyping on gDNA from villi and hyper-regenerative crypts isolated by LMD (n=3). (B) HSP60 and Ki67 IHC of representative consecutive sections (250x). Left panel: Quantification of Ki67⁺ cells per crypt based on the IHC stainings (n=5; mean of 2 regions each). Additional IF to show co-expression (600x).

To investigate from which cell type the hyperproliferative crypts originate, an immunofluorescence analysis for the stem cell marker OLFM4 was performed. At d_0 , right after the end of tamoxifen treatment, only rare single cells remained HSP60 positive (and escaped the knock out). These cells were expressing the stem cell marker OLFM4. Two days later (d_2) a hyperproliferative crypt of OLFM4 positive cells has proliferated out of these single escapers (Fig. 32).

Figure 32

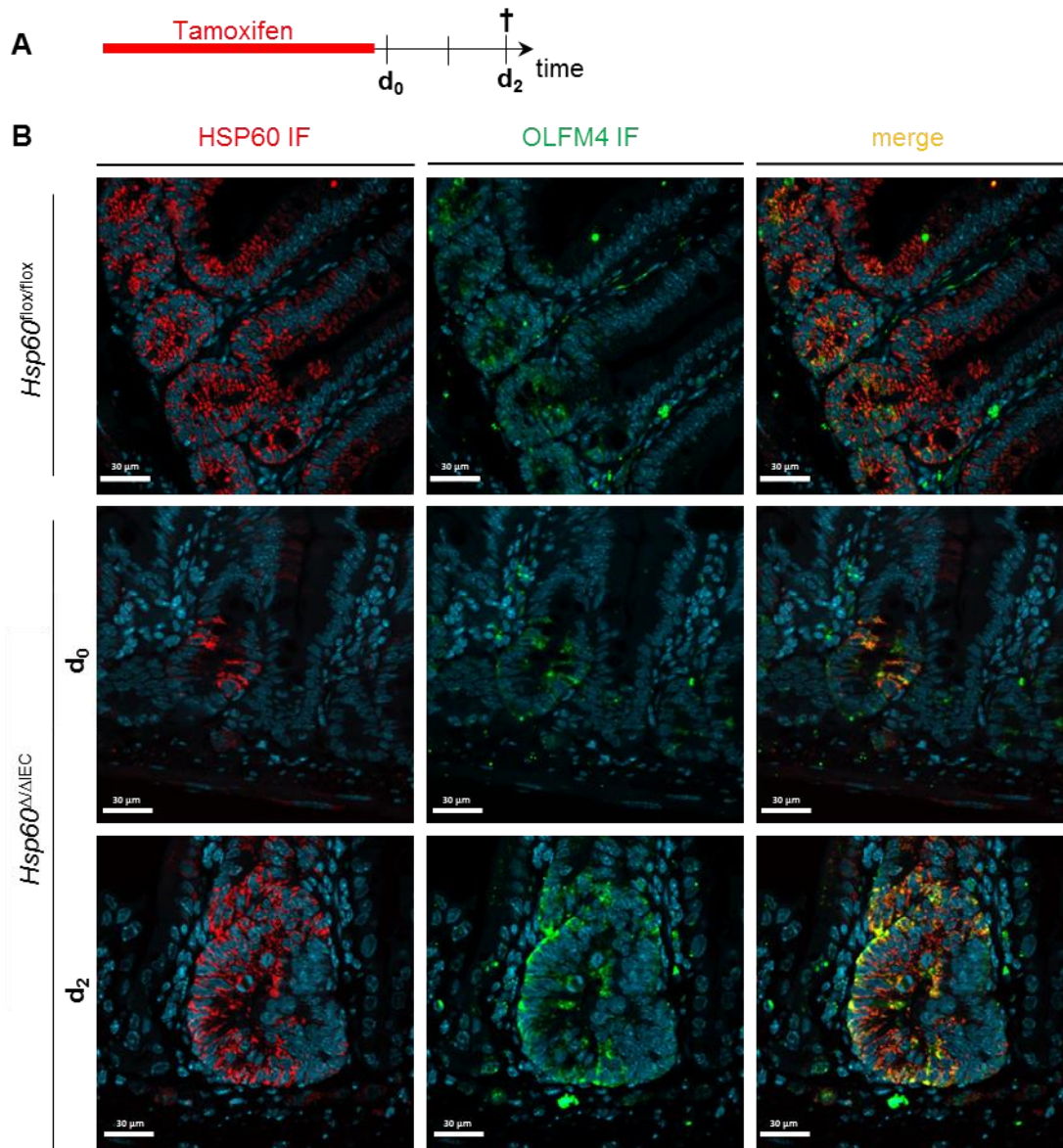


Fig. 32 Hyper-regenerative crypts originate from single escaping stem cells

(A) Time line of the experiment. (B) IF for HSP60, OLFM4 and the merge of both (representative pictures from $n=5$; 600x) to show co-expression at two different time points (d_0 and d_2) on control and *Hsp60*^{ΔIEC} jejunal sections. Nuclear staining (dapi) in cyan.

RESULTS

While *in situ* hybridization of jejunal tissue sections from control mice shows that almost every crypt bears at least one *Olfm4*⁺ stem cell (mostly ~8 cells per crypt), the number of *Olfm4*⁺ crypts in the *Hsp60*^{Δ/ΔIEC} mice at d₂ is markedly reduced. The number of residual *Olfm4*⁺ crypts (ca. 30%) fits to the number of hyperproliferative crypts in these mice (Fig. 23B) meaning that HSP60 deficiency causes a loss of stem cells on the one hand and a hyperproliferation of escaping stem cells on the other hand (Fig. 33A). qPCR analysis of isolated IEC from the jejunal crypt bottom (mixed population of HSP60⁺ and HSP60⁻ cells) for *Olfm4* and *Lgr5* confirmed the overall loss of stem cells (Fig. 33B). The Wnt-target genes *c-Myc* and *CyclinD1* (*Ccnd1*) showed clear induction whereas the Jak/Stat target gene *Socs9* was only induced by trend. Ki67 was - in sum - not altered in this mixed fraction of HSP60⁺ and HSP60⁻ crypts (Fig. 33B).

Figure 33

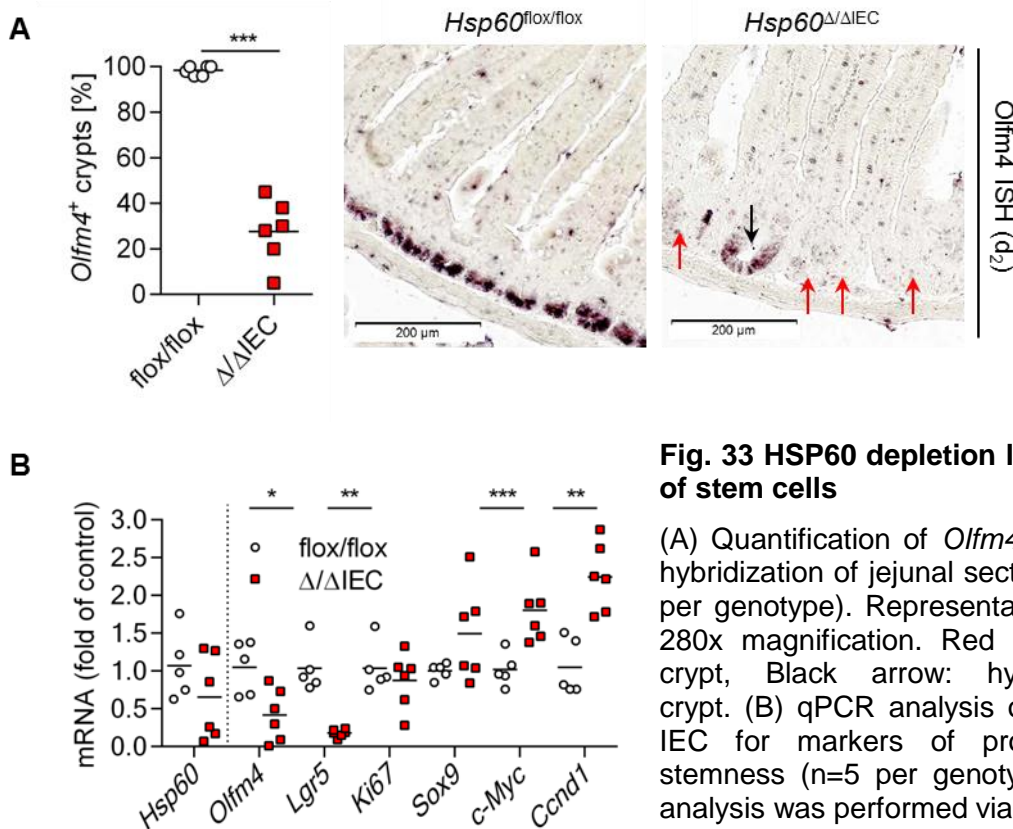


Fig. 33 HSP60 depletion leads to a loss of stem cells

(A) Quantification of *Olfm4* mRNA *in situ* hybridization of jejunal sections at d₂ (n=6 per genotype). Representative pictures in 280x magnification. Red arrows: *Olfm4* crypt, Black arrow: hyperproliferative crypt. (B) qPCR analysis of crypt bottom IEC for markers of proliferation and stemness (n=5 per genotype). Statistical analysis was performed via t-test.

To identify the signals that stimulate a proliferative response in escaping stem cells, growth factors were measured in the crypt fraction of the isolated epithelium. These factors are supposed to be secreted by Paneth cells, surrounding the stem cells. *Rspo1*, a Wnt signal enhancer, was substantially elevated in the crypt epithelium of *Hsp60* mice, whereas *Wnt3* itself was not regulated in this compartment. A staining for lysozyme, a typical marker for Paneth cells revealed an extension of this cell type in the proliferative crypts at d₂, pointing to elevated Paneth cell signaling surrounding the stem cells (Fig. 34A).

Additionally, levels of the pro-proliferative cytokine *Il-6* were elevated in the jejunal mucosa of *Hsp60^{Δ/ΔIEC}* mice. This upregulation could be confirmed in the isolated villus tip IEC (mainly HSP60⁻) and the crypt bottom (mixed HSP60⁻ and HSP60⁺; Fig. 34B). IL-6 dependent activation in terms of STAT3 phosphorylation could be observed in rare single crypt base cells at d₀ but not at d₂.

Figure 34

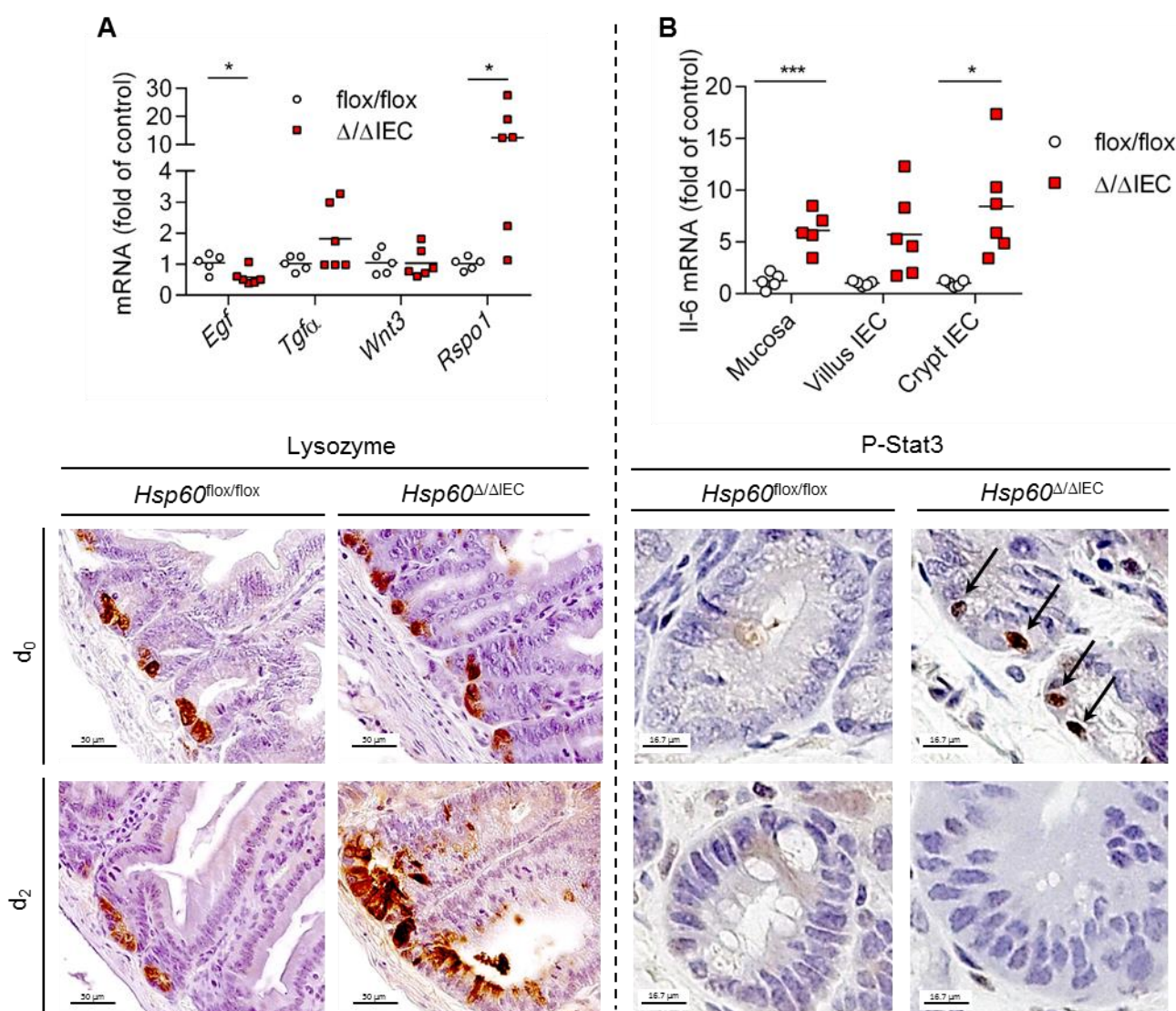


Fig. 34 Growth factor and cytokine signals trigger stem cell proliferation

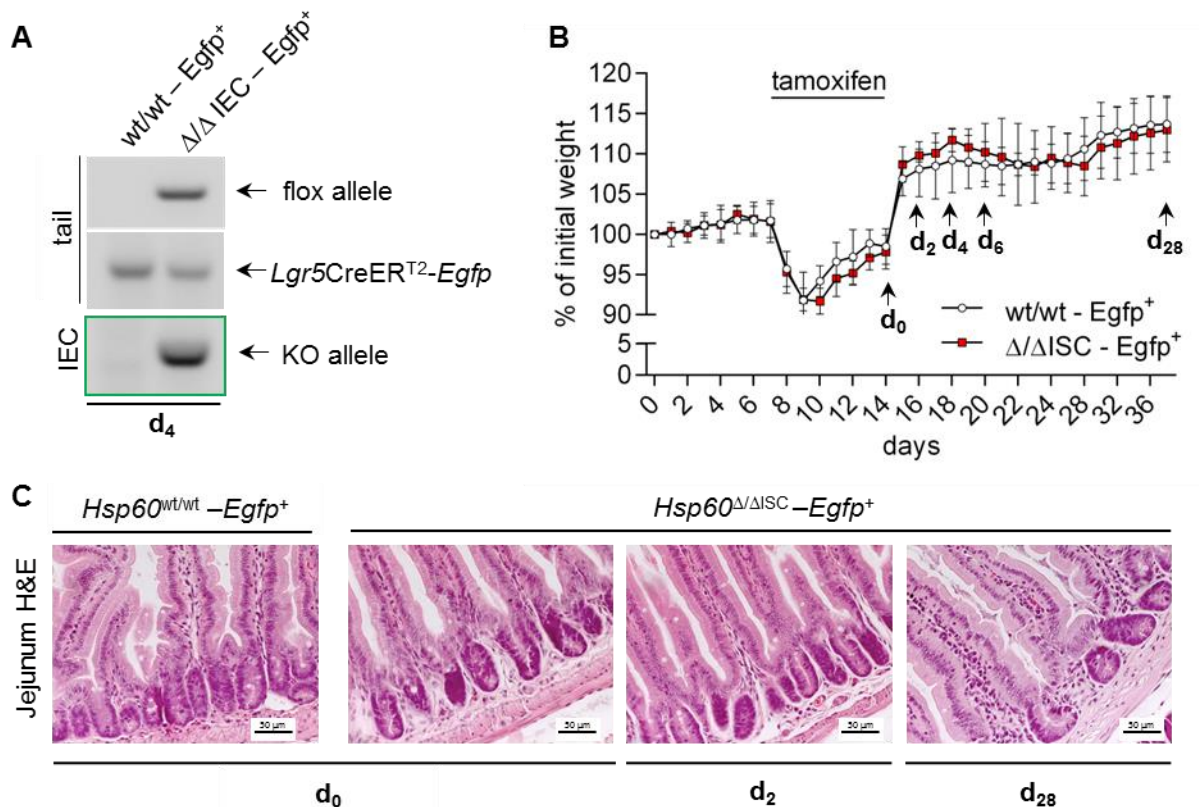
(A) qPCR analysis of known growth factors secreted by Paneth cells to stimulate stem cells. Lysozyme IHC staining (representative pictures from n=5; 250) at d₀ and d₂ showing extension of Paneth cells in the crypt. (B) qPCR analysis of *Il-6* in the whole jejunal mucosa, in isolated villus tip and crypt IEC. Statistical analysis was performed via t-test comparing genotypes. P-STAT3 IHC (750x) showing activated Jak/Stat signaling in single crypt bottom cells.

4.7 Characterization of a stem cell specific Hsp60 depletion in *Hsp60*^{ΔISC} mice

As indicated in Fig. 33, the epithelial specific deletion of HSP60 diminishes the number of stem cells at d₂. To pursue this phenomenon, *Hsp60*^{flx/flx} mice, were crossed with *Lgr5*CreER^{T2}-Ires-*Egfp*⁺ mice, which express CreER^{T2} and the reporter protein EGFP in parallel under the control of the stem cell specific *Lgr5* promoter. Despite the fact, that the knock out allele could be detected in IEC of stem cell specific knockout mice (*Hsp60*^{ΔISC} – *Egfp*⁺), they show neither obvious symptoms like weight loss nor any mucosal alterations at short (d₂) and long term (d₂₈; Fig. 35 B+C) in contrast to *Hsp60*^{ΔIEC} mice (Fig. 35 A).

EGFP as an indirect marker for *Lgr5*⁺ stem cells in this reporter model was stained at d₀, d₂, d₄, d₆ and d₂₈. The number of EGFP⁺ crypts, meaning the number of stem cells, declines after tamoxifen administration reaching a minimum at d₄. Thereafter, the number rises rapidly within 2 days reaching normal levels till d₂₈ latest (Fig. 35 D). Corresponding IHC stainings for HSP60 at d₄ revealed no HSP60 deficient crypt-villus units meaning that the IEC specific detetion of HSP60 did not pass through to the transit amplifying progenitor cells and their derivatives.

Figure 35



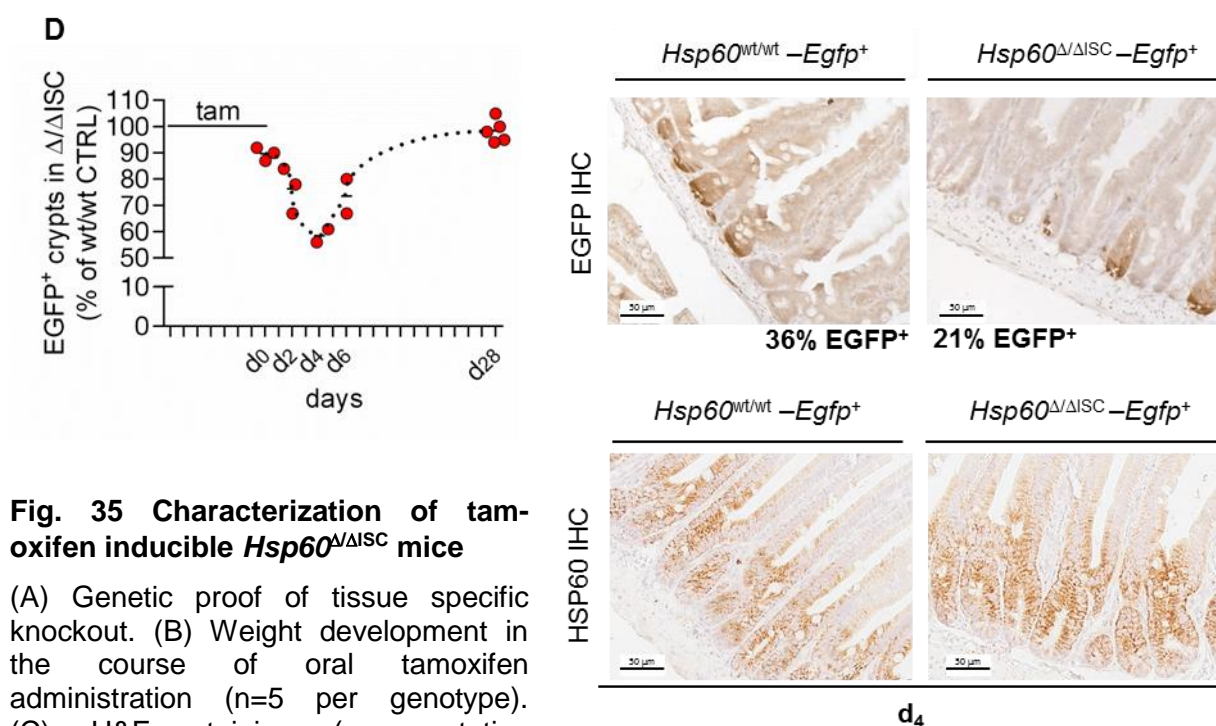


Fig. 35 Characterization of tamoxifen inducible *Hsp60* ^{$\Delta\Delta\text{ISC}$} mice

(A) Genetic proof of tissue specific knockout. (B) Weight development in the course of oral tamoxifen administration (n=5 per genotype). (C) H&E staining (representative pictures; 250x) of jejunal tissue sections at d₀, d₂ and d₂₈.

(D) Quantification of GFP IHC on tissue sections from various time points (n=2-5 per genotype). The dot plot shows percentage of EGFP⁺ crypts in $\Delta\Delta\text{ISC}$ -*Egfp*⁺ relative to percentage in wt/wt-*Egfp*⁺. Representative GFP IHC and corresponding HSP60 IHC pictures (250x) at d₄.

5 DISCUSSION

In previous studies, we and others have demonstrated the existence and relevance of activated ER UPR pathways in IEC [78] for the pathogenesis of chronic intestinal inflammation and other pathologies like colorectal cancer [85]. More recently, we shifted the focus to the mitochondrial UPR in IEC and found that ER and MT UPR are closely interrelated [68]. We have shown that the ER chaperone GRP78 and the MT chaperone HSP60 are induced in IEC of several mouse models of colitis and human IBD [68]. To answer the question, of whether activated UPR are just a consequence of inflammation which is accompanied by a high demand of energy and functional secretory proteins, or whether they contribute to the disease initiation, the use of mouse models are a valuable tool. The latter assumption is supported by the observation that *Xbp1*^{ΔIEC} deficient mice develop spontaneous enteritis and that the chemical chaperones TUDCA and PBA ameliorate signs of inflammation and ER stress in IEC. The purpose of the present study was to gain insight into the role of activated UPR on intestinal epithelial homeostasis by the use of IEC specific genetically modified mouse models. With the *Hsp60* deficient mouse, we developed a model of mitochondrial chaperone deficiency. This approach provides the possibility to elucidate the functional role of this protein in IEC, to provoke disturbances in the epithelial homeostasis and analyze respective effects. One of the key finding of the present study was the fact that an IEC-specific deletion of *Hsp60* (*Hsp60*^{ΔIEC}) caused a disruption of epithelial cell homeostasis in both the pre- and postnatal gut, independent of epithelial destruction and an inflammation-associated pathology.

5.1 *Hsp60*^{ΔIEC} mice – the paradox of embryolethality

The first attempt to generate an IEC specific homozygous *hsp60* knockout was the crossing of *Hsp60*^{flox/flox} mice with *Villin*Cre mice which express the Cre recombinase under the control of a 9 kb fragment of the endogenous *Villin* promoter [224]. *Hsp60*^{ΔIEC} mice showed a severe retardation of the overall embryonic development which keeps them retained between stage E10.5 and 11.5. By the use of β-galactosidase expressing reporter mice, Marjou *et al.* showed that Villin driven Cre recombination is already present at embryonic developmental stage E10.5 strongly in the extraembryonic visceral endoderm and moderately in the enterocyte precursors of the developing gut [224]. This is in accordance with the theory about the development of the intestine. At E10.5 the intestinal endoderm is seen as a compact pseudostratified epithelium without villi. Over the next 3 days of development the tube lengthens and widens. Villus formation initiates in a cranial to caudal wave at approximately E14.5, as clusters of mesenchymal cells form below the epithelium and extend toward the center of the lumen, creating villi [240]. The retaining of *Hsp60*^{ΔIEC} embryos between stage E10.5 and 11.5 indicates that right after onset of Cre expression, the HSP60

deficiency develops rapidly and the consequences of this deficiency compromise the overall embryonic development severely. Since it is not obviously evident that a chaperone deficiency restricted to a tissue expendable for the survival of the embryo at this early stage, causes such dramatic systemic defects, the visceral endoderm moved into the focus. Together with the visceral mesoderm, the visceral endoderm forms the visceral yolk sac which delivers yolk to the early embryo before placental supply begins and functions as a developmental circulatory system before internal circulation develops [240]. Interestingly, IHC staining on visceral yolk sac tissue revealed no reduction in HSP60 levels and H&E stainings provided no evidence of tissue impairment. Instead, the knockout allele could be detected in abdominal samples of the retarded embryos supporting the theory that indeed an impaired intestinal development affected the entire embryonic organism. Of note, intensive literature search revealed no published example of a *Villin*Cre driven gene knockout that affected embryo development at such an early stage. Only few examples are reported of *Villin*Cre mediated embryolethality at all. For example, IEC specific deletion of *c-Flip*, an inhibitor of caspase 8, resulted in perinatal lethality as a result of the enhanced apoptosis and programmed necrosis of IEC [241]. Besides apoptosis related factors also developmental gene knockouts display a peri-natal lethality. An IEC restricted knock out of CR6-interacting factor 1 (*Crif1*) e.g. which is a transcriptional co-activator of intestinal development, led to peri-natal death with severe alterations of tissue architecture in the small intestine, including poor microvillus formation and abnormal differentiation of absorptive enterocytes [242]. Finally, mice homozygous for *Villin*Cre-mediated *Lrp5* and *Lrp6* deficiency, both co-receptors of WNT ligands, died within one day after birth. Analysis of embryonic intestinal epithelium showed a progressive loss of cells, an absence of proliferation and a premature differentiation of crypt stem/precursor cells [243]. In summary, IEC residing HSP60 seems to be uniquely important for the embryonic development, since not even anti-apoptotic and development-related genes influence embryonic vitality as fundamentally as HSP60 does.

5.2 *Hsp60*^{ΔIEC} mice – the complexity of a fatal phenotype

This significance is emphasized by the fact that even the IEC specific knock out induced by administration of tamoxifen in adult animals caused a severe wasting phenotype in these mice necessitating the culling already two days after the end of tamoxifen treatment. Despite the explicit phenotype, the reasons for this are not that obvious and still a matter of discussion. From the macroscopic perspective, mice show a drop in feed and water consumption, a severe body weight loss with massive reduction of epididymal fat pads and thymus mass – a clear indicator of wasting. On the other hand, only 33% of the mice show intestinal symptoms. These are rather mild in the form of sticky stool and not comparably

severe to bloody diarrhea occurring during DSS colitis. Nevertheless, the affected mice show a tensely blown up caecum filled with water and thin mucus. One can hypothesize that the enlarged caecum causes abdominal pain leading to the refusal of food and water uptake. However, this appears rather unlikely, since all mice of the *Hsp60^{ΔIEC}* group show this behavior but only 33% are affected by a drastically enlarged caecum. In addition to the mild intestinal symptoms, there are other arguments that contribute to the unaccountability of the wasting phenotype. First, the excreted feces of *Hsp60^{ΔIEC}* mice showed only a marginal increase in energy content of about 0.5 MJ/kg. For comparison, PepT1 knockout mice which are unable to assimilate di- and tripeptides display an increase in fecal energy of 1.5 MJ/kg. This difference is still considered as subtle and has no pathological impact under steady-state conditions [244]. In addition, analysis of radioactively labelled glucose uptake by corresponding transporters expressed on small intestinal IEC didn't either provide evidence for a pronounced nutrient malabsorption. The measured reduction of PepT1 activity by half can explain the increased energy in feces but not the wasting phenotype.

Looking at the histological level, the colonic epithelium of HSP60 deficient mice shows no pathologic alterations including an appropriate mucus production. In contrast, the changes in small intestinal epithelial morphology are clearly visible due to the presence of hyper-regenerative crypt foci. Like in the colon, the line of IEC which build the epithelial barrier is intact in the small intestine as well without obvious gaps. These would enable invasion of intestinal bacteria and cause a massive immune response like it is reported for irradiation mediated epithelial destruction [245] and for the IEC specific E-cadherin deficient mouse. In this model, the epithelial architecture is severely disturbed due to apoptosis of IEC, defective adherence junctions and a loss of differentiated cells [246]. In *Hsp60^{ΔIEC}* mice, a TUNEL assay detecting DNA fragmentation did not provide evidence for an apoptotic process in the small intestinal epithelium. This is of note, since *in vitro* knock down of *Hsp60* by small interfering RNA has shown to have a pro-apoptotic phenotype on tumor cell lines and primary tumors, whereas it is well tolerated and does not cause apoptosis in normal cells. Conceptually, it has been suggested that acute ablation of *Hsp60* in tumor cells destabilizes the mitochondrial pool of survivin, induces mitochondrial dysfunction and activates caspase-dependent apoptosis. In addition, it disrupts HSP60-p53 complexes, which results in p53 stabilization, increased expression of pro-apoptotic Bax, and Bax-dependent apoptosis. Stabilization of mitochondrial survivin and restraining of p53 function are processes selectively exploited in cancer [152].

In accordance with the intact line of epithelial cells in *Hsp60^{ΔIEC}* mice, only a subtle mucosal immune response in the form of leukocyte infiltration could be observed along the intestinal tract. Infiltration of macrophages and dendritic cells displays a mild early innate host response. Chemokines for the recruitment of APC, neutrophils and T cells (via IP-10) are

expressed but infiltration of adaptive immune cells is not (yet) established, probably due to the short timespan between induction of the knockout and culling.

In summary, deletion of *Hsp60* in IEC leads a detrimental phenotype both pre- and postnatally, but the exact causes for this are still unknown. The data do not support the hypothesis of a causative relation between an activated UPR and the onset of an intestinal inflammation. However, one has to admit that the timeframe in which such an inflammation could develop is relatively short. It cannot be excluded that on the long term the activation of UPR leads to the development of intestinal inflammation. The transgenic CHOP and nATF6 mice may be a better model to study this hypothesis.

5.3 The impact of HSP60 deficiency on mitochondria in IEC

When targeting a mitochondrial chaperone by a knockout, changes in mitochondrial morphology and functionality are expectable. Surprisingly, the amount and diameter of mitochondria did not change in colonic nor in jejunal IEC. Accordingly, *Pgc1 α* , an inducer of mitochondrial biogenesis was inversely regulated in IEC isolated from colon and villus tips allowing no correlation with HSP60 deficiency. Nevertheless, the presence of dark and bright deposits within the mitochondrial matrix was apparent. Dark vesicles would be observed in the control mice as well, but the bright spheres are unique to the *Hsp60* ^{Δ IEC} mice. The identity of the spheres is a matter of speculation, since this phenomenon is not described in reliable literature reports. Due to the fact that these mice lack a chaperone, deposition of un- and misfolded proteins would be plausible. However, the bright appearance under the electron microscope is rather untypical for electron dense protein aggregates and may point to lipid droplets as described in the cytoplasm of adipocytes for instance [247]. Although it was not possible yet to assess mitochondrial functionality in terms of respiration in living IEC, one can draw conclusions from mRNA expression in isolated IEC as well. The abolishment of the mitochondrial encoded respiratory chain complex IV (cytochrome c oxidase) subunit I (*mtCoxI*) on mRNA level is striking in colonic and jejunal IEC profile. Of note, this subunit bears the catalytic center with a heme group and two copper ions - potential catalyzers for ROS production. This underlines the concept that HSP60 protects such enzymes from oxidative damage to avoid release of aggravating metal ions (see 5.4) and supports a previous report that a knockdown of *Hsp60* results in a decrease in complex IV activity [248]. Microarray analysis of colonic IEC mRNA showed metabolic processes to be the most regulated GO-term. Most of the genes enveloped by this GO-term were upregulated comprising nucleobase-, amino acid-, protein- and lipid metabolism reflecting a high degree of metabolic activity in HSP60 deficient colonocytes. Interestingly, among the most downregulated genes are *Otc* and *Cps1* catalyzing the only MT matrix located steps of the urea cycle. OTC was shown to be explicitly dependent on a functional *Hsp60/Hsp10*

chaperone system to form an enzymatically active trimer [249]. In the absence of HSP60, colonocytes may downregulate the expression of such genes to avoid MT stress in the form of accumulating protein aggregates and to protect mitochondrial integrity.

5.4 *Hsp60*^{ΔIEC} mice – a model for activated MT UPR and oxidative stress in IEC

The specific purpose of the IEC specific HSP60 deficient mouse model was to provoke an activated MT UPR in IEC and to study its impact on epithelial homeostasis. We could confirm that a deletion of *Hsp60* in the intestinal epithelium triggers the MT UPR with low interference with ER UPR and found a distinct response to oxidative stress in addition. *Hsp10*, *ClpP*, *Grp75* and *Tid1* known to typical markers of MT UPR from *in vitro* experiments [105] were upregulated in IEC isolated from colon and jejunal villus tips. Among the genes attributed to ER UPR only *Chop* and *Gadd34* were induced in colonocytes. CHOP is also an important transcription factor of the MT UPR, since it drives *Hsp60* expression. *Gadd34* is described to be directly transcriptionally induced by CHOP [250]. In IEC isolated from jejunal villus tips a broad ER UPR covering several key factors cannot be detected either despite the fact that *Grp78*, the hallmark of ER UPR, is induced on mRNA level. This induction may be the result of cross-signaling via JNK/AP1 which has been described to activate *Grp78* under certain conditions [251], rather than of classical ER pathways. Interestingly, the expression pattern of ER UPR genes in jejunal crypt IEC differs substantially from that of the villus tip, indicating that the proliferating cells overwrite the expression pattern of HSP60 deficient cells.

Since mitochondria are a major source of ROS, it is not surprising that oxidative stress responsive genes are regulated in *Hsp60*^{ΔIEC} IEC as well. Yeast studies revealed that under oxidative-stress conditions, HSP60 deficiency resulted in reduced cell viability as a consequence of elevated cell peroxide levels. HSP60 protects Fe/S-cluster and heme containing enzymes from oxidative inactivation and release of iron which itself acts as a catalyzer for free radical production [252, 253]. Accordingly, *Hif1α* and *Ho-1* are induced in HSP60 deficient colonocytes, jejunal villus tip and crypt IEC. Interestingly, levels of Catalase and *Sod2* were diminished in all three compartments, despite their ROS antagonizing function. This may be due to the fact that these enzymes bear iron and manganese in their catalytic center, therefore being potential sources for ROS themselves if not protected by HSP60. In line, studies in a rat small IEC line overexpressing HSP60 showed that cell viability after H₂O₂ treatment was significantly increased compared to control cells [254].

Chop is induced by several types of stress in a highly redundant manner. Inhibition of the respiratory chain by rotenone and antimycin A leads to ROS dependent p38 phosphorylation and *Chop* activation in an ATF2 dependent manner [255]. Amino acid starvation recruits ATF4 (and ATF2) to bind so called amino acid response elements (AARE) [256]. Upon ER stress, *Chop* is classically induced by ATF4 and ATF6 binding the C/EBP-ATF composite site

and ERSE respectively [53]. Mitochondrial UPR and oxidative stress have been shown to induce *Chop* via AP-1 binding to its promoter [257]. CHOP itself plays an ambiguous role in cellular signaling. On the one hand, it is part of a compensatory response towards cellular stress. On the other hand, it is able to induce cell cycle arrest [258] and apoptosis [259]. Some of its transcriptional responsive genes comprise *Gadd34*, the *Chop* repressors *Atf3* [54] and *Trib3* [260, 261], the ER disulfide bound oxidase *Ero1l* [262] and the anti-apoptotic factor *Bcl2* which is transcriptionally suppressed by CHOP action [263]. *Bcl2* levels were not altered in *Hsp60*^{ΔIEC} colonocytes meaning that CHOP does not promote apoptosis in this context. However, *Bcl2* was downregulated in IEC from villus tips - possibly priming the cells for rapid apoptosis upon a second hit. Of note, *Trib3* which is highly upregulated in colon as well as jejunum (villus and crypt) is discussed as a CHOP-dependent pro-apoptotic TF. The pure presence of *Trib3* is not sufficient to elicit apoptosis, only in combination with a noxious event (second hit) [264]. In addition, TRIB3 may serve as a negative feedback regulator to control *Chop* transcript levels. The ambiguous role of CHOP, together with the remarkable observation that its level is reduced under conditions of chronic inflammation (unpublished data; not shown) evoked the decision to generate a *Chop* transgenic mouse model, which overexpresses this factor specifically in the epithelium. The transcription factor nATF6 was chosen for the generation of a second IEC specific transgenic mouse, mainly due to its involvement in the ER-MT UPR network. We identified several putative ATF6 binding sites in the promoters of mitochondria residing enzymes namely *Gpr75*, *Tid1*, *ClpP* and *mtCk*. ChIP experiments revealed binding of ATF6 to these promoters upon ER stress. Moreover, nATF6 overexpression *in vitro* sensitized the cells towards additional ER stress signals. A response of the mitochondrial protease *Lon* to ER stress has been described before [113]. Like CHOP, ATF6 has also been implicated in cell proliferation [76] beyond its involvement in UPR. The functional analysis of both transgenic mouse models is covered by autonomous PhD projects and still ongoing.

The postulated relevance of UPR related transcription factors in proliferative control bridges back to *Hsp60*^{ΔIEC} mice.

5.5 *Hsp60*^{ΔIEC} mice – a model for stem cell loss and epithelial regeneration?

In this model, an activated UPR in IEC is accompanied by an impaired proliferative response and a loss of stemness. Jejunal HSP60 deficient crypts show an abolished expression of the global proliferation marker KI67 which is normally present in the Lgr5⁺ pluripotent stem cells and the transit amplifying (TA) cell zone. These represent the precursors of all absorptive and secretory IEC cell types [20]. Since the epithelium faces a turnover of three (small) to five (large intestine) days [265], this lack of proliferation deprives the intestinal epithelium from fresh supply derived from the crypts therefore severely impacting its renewal capacity.

Unfortunately, *Hsp60*^{ΔIEC} mice do not live long enough to explore the consequences of this impairment.

The anti-proliferative effect of an HSP60 deficiency has been reported *in vitro* before [266]. The mechanisms behind are not resolved, but HSP60 has been shown to modulate WNT signaling on various levels. First, the cytoplasmic form of the chaperone interacts directly with the WNT dependent TF β -catenin through the apical domain, whereby increasing its stability and enhancing its transcriptional activity *in vitro* and *in vivo* [267]. Inversely, it is reasonable to expect that HSP60 deficiency antagonizes β -catenin activity by the lack of its stabilization. Second, TF CHOP which is highly induced in HSP60 deficient IEC has been shown to inhibit WNT signaling by binding the TCF/ β -catenin complex and preventing its binding to the promoter of WNT target genes thereby prohibiting cell proliferation [268].

As mentioned above, the abolishment of KI67 in *Hsp60*^{ΔIEC} mice comprises transit amplifying cells and stem cells. Strikingly, also the levels of the typical stem cell markers *Olfm4* and *Lgr5* are diminished in the jejunal crypts on mRNA level and, in case of OLFM4, also at the level of protein expression. Moreover, *Lgr5* mediated deletion of *Hsp60*, leads to a transient drop in EGFP⁺ stem cells. Finally, a transit of the *Hsp60* deletion from the ISC to the progenitor cells and their derivatives which would provide the whole epithelium with the knockout could not be observed. Together, these results provide evidence that an HSP60 deficiency antagonizes the presence of pluripotent cycling *Lgr5*⁺ intestinal stem (so called crypt base columnar stem cells (CBC)). This is of note, since the same phenomenon has been reported for the IEC and ISC specific deletion of the ER chaperone *Grp78*. In this study, induction of ER stress caused loss of stemness in a PERK-eIF2 α -dependent manner. The authors conclude that the UPR plays an important role in the regulation of intestinal epithelial stem cell differentiation [269]. Since an HSP60 deficiency has the same outcome and CHOP is the TF that integrates combines ER dependent PERK-eIF2 α and MT dependent AP1 signaling, it appears plausible that CHOP is the TF that antagonizes stemness upon organelle stress. It can be speculated, whether these findings could end up in a cancer treatment strategy. A targeted induction of UPR (ER or MT) by the deletion of *Grp78* using protease subtilase (subA) has been successfully used to antagonize cancer growth *in vitro* and in respective mouse models [270-272] already.

The tamoxifen induced knockout of *Hsp60* in the *VillinCreER*^{T2} driven model is not complete. Besides HSP60 negative regions, there are abnormally enlarged HSP60⁺ crypt foci descending in number from the small to the large intestine. These hyper-proliferative crypt foci are characterized by an accumulation of KI67⁺ and OLFM4⁺ cells and have obviously escaped the knockout since they show no recombination at genomic level. Since OLFM4 is a robust marker for murine cycling CBC in the small (but not in the large) intestine [273], this process can be considered as stem cell hyper-proliferation. These aberrant crypts grow

within two days from single HSP60⁺ stem cells which have escaped the tamoxifen induced knock out. Several reasons for the occurrence of escaper cells are plausible. First, Madison *et al.* report that a 12.4 kb region of the Villin promoter is necessary for full activity along the intestinal tract and especially all along the villus-crypt axis. Truncated fragments show reduced activity in the crypt bottom [274]. For the generation of *Villin*CreER^{T2} mice, a 9kb fragment of the *Villin* promoter fused to the CreER^{T2} coding sequence was randomly integrated into the murine genome [224]. Four of five founders carrying this fragment showed stochastic silencing of the transgene in some crypts, so called “chromosomal position effect variegation” [275]. Although founders with low frequency of this event were chosen for further breeding, stochastic silencing could still occur. Second, epigenetic modification in the form of methylation at loxP sites has been reported to cause impaired Cre mediated recombination [276]. Third, spontaneous internal recombination within a loxP sequence if placed in a repetitive sequence locus can be a reason for defective genomic recombination [277].

Apparently, literature reports attribute stem cell hyper-proliferation to two distinct circumstances. First, aberrant growth signaling in the stem cells themselves leads to uncontrolled proliferation like e.g. in the APC^{min} mouse model. Here, abnormal stabilization of β -catenin in the crypt IEC leads to a constitutive activation of the WNT pathway and therefore to epithelial adenoma formation [278]. Transgenic expression of the WNT agonist R-spondin 1 (RSPD1) results in massive hyper-proliferation of intestinal crypts as well [279]. The second condition that stimulates crypts to proliferate is the necessity of epithelial renewal upon damage like after irradiation-mediated villus eradication. Few surviving CBC build up new crypts by proliferative expansion before differentiation limits stem cells back to the crypt bottom [280]. The knockout of essential epithelial genes is a comparable condition, since the escaper cells are surrounded by compromised cells which provides the escapers a proliferative advantage. Examples for this phenomenon are the IEC specific deletion of the proto-oncogene *c-Myc* [281] and the stem cell marker *Ascl-2* [282]. Strikingly, mice deficient in the β -catenin binding partner TCF4 completely reflect the phenotype of the *Hsp60* ^{Δ IEC} mice with a loss of stem- and TA cells on the one hand and focal hyper-proliferation on the other hand [283]. The fact, that HSP60 stabilizes β -catenin and therefore promotes WNT mediated signaling has been mentioned before. Interestingly, *c-Myc*, a target gene of WNT signaling, has been reported to transcriptionally activate *Hsp60* by binding its promoter in a positive feedback loop promoting neoplastic transformation [284]. Unfortunately, the question of whether the hyper-proliferative crypts in *Hsp60* ^{Δ IEC} mice differentiate into a normal villus-crypt structure or whether they transform into malignant tumors cannot be addressed due to the limited lifespan of these mice. However, if the lack of HSP60 and the resulting disappearance of proliferating stem- and TA cells were considered as an epithelial damage, the HSP60⁺ crypt foci could also be defined as hyper-regenerative crypts.

Nevertheless, unrevealing the signals that stimulate escaping ISC in *Hsp60*^{ΔIEC} mice to proliferate could add important information to the understanding of epithelial regeneration and hyper-proliferation. Among the growth factors that are supposed to be secreted by Paneth cells (*Egf*, *Tgfα*, *Wnt3*, *Rspd1* [285, 286]), only the WNT enhancer *Rspd1* was elevated on transcriptional level (Fig. 34A). An additional signal that could be responsible for stem cell proliferation is the cytokine IL-6 which was elevated in jejunal but not in colonic mucosa. Interestingly, IL-6 mRNA levels were induced in the isolated villus tip IEC (HSP60⁻) as well as in the crypt bottom IEC (HSP60⁻/HSP60⁺). Of note, CHOP has been shown to directly induce IL-6 in a human melanoma cell line [287]. If this is also the case in IEC, needs to be investigated. Nevertheless, single STAT3⁺ cells could be detected in the crypt bottom of *Hsp60*^{ΔIEC} mice at d₀ preceding hyper-proliferative crypt formation. In summary, proliferative signals originating either from the HSP60 deficient IEC or from the surrounding mesenchyme stimulate HSP60⁺ escaper stem cell to proliferate which results in the formation of hyper-regenerative crypt foci in *Hsp60*^{ΔIEC} (Fig. 36).

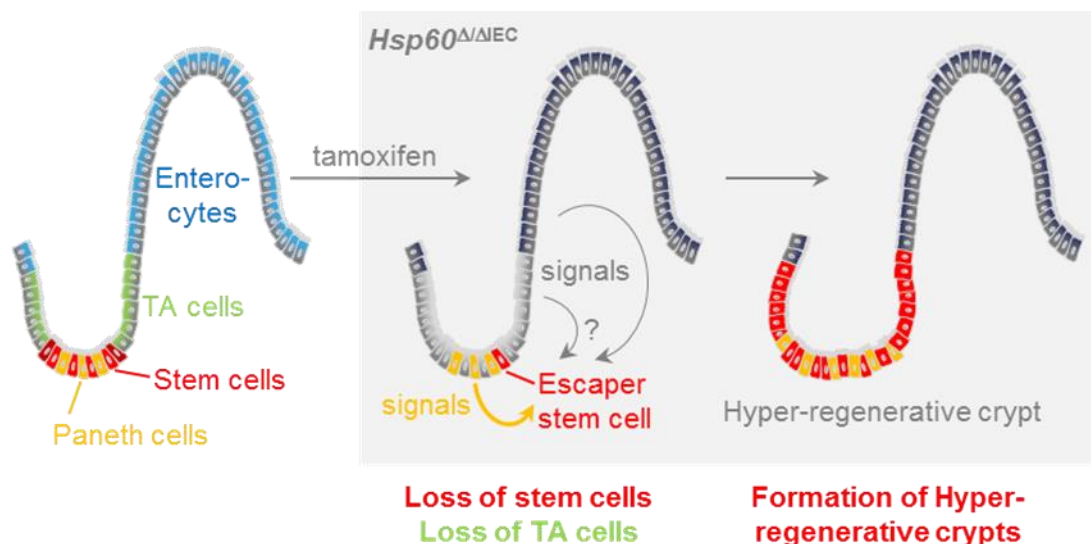


Fig. 36 Schematic model of hyper-regenerative crypt formation in *Hsp60*^{ΔIEC} mice

Proliferative signals originating either from the HSP60 deficient IEC or from the surrounding mesenchyme stimulate HSP60⁺ escaper stem cell to proliferate which results in the formation of hyper-regenerative crypt foci in *Hsp60*^{ΔIEC}.

5.6 The compensatory potential of HSP60 in haplodeficient *Hsp60*^{+/-} mice

It became apparent that a deletion of *Hsp60* has a severe impact on the affected organism. Conditional *Hsp60*^{ΔIEC} knockout mice undergo embryo lethality and inducible *Hsp60*^{ΔIEC} mice suffer from a detrimental wasting phenotype. In accordance with literature reports, a constitutive homozygous *Hsp60* knockout (*Hsp60*^{-/-}) is embryonically lethal as well.

Christensen *et al.* showed in a knock-in model of Hsp60 deficiency that *Hsp60*^{-/-} embryos died shortly after implantation (day 6.5 to 7.5 of gestation) [138], suggesting an important role for HSP60 in early embryonic development. Correspondingly, a homozygous constitutive knockout of the ER chaperone *Grp78* is embryonically lethal as well. From day 3.5 of gestation on - meaning before implantation - the inner cell mass of the blastocyst harboring the embryonic stem cells stops to proliferate and undergoes apoptosis. To address the compensatory potential of the mitochondrial chaperone HSP60, we investigated the appearance of *Hsp60*^{+/-} mice under steady-state conditions and under inflammatory challenges. *Hsp60*^{+/-} mice had no obvious phenotype, neither in the intestine nor in any of the other inspected organs. The lack of any disease-related phenotype was obviously not due to compensation from the remaining allele neither on mRNA nor on protein level. qPCR and Western Blot analysis of different intestinal compartments showed uniformly 50% expression level. In contrast, an equalization of GRP78 protein levels is reported for *Grp78*^{+/-} mice, since *Grp78* is tightly regulated on translational level [288]. Therefore, despite reduced mRNA levels, the knockout can hardly be detected on protein level in isolated IEC in this model [289]. However, IEC handle a haplodeficiency of *Hsp60* without obvious equalization and without the onset of UPR.

To further elucidate the compensatory potential, we challenged the epithelium *Hsp60*^{+/-} mice by oral administration of the colitogenic agent DSS, affecting mostly the distal colon. Applying this inflammatory trigger revealed a trend towards a more pronounced DSS induced colitis in *Hsp60*^{+/-} compared to WT mice, reflected by higher body weight loss, higher histopathological score and disease activity index. As an additional control *Grp78*^{+/-} and respective WT mice were treated with DSS as well. There, no difference in any of the measures taken could be observed; though one has to consider that *Grp78*^{+/-} mice are on the more susceptible genetic background Bl/6J, which may overwrite marginal differences due to the *Grp78* haplodeficiency. A different kind of challenge to the epithelium is the genetically driven intestinal inflammation in the *Tnf*^{ΔARE/WT} mouse model – mimicking a Crohn's disease phenotype. Inflammation is formed in the distal ileum, the proximal colon and the caecum tip in this model. Intercrossing of conventionally housed *Hsp60*^{+/-} with *Tnf*^{ΔARE/WT} mice revealed that at 18 weeks of age the ileal inflammation was not altered compared to *Tnf*^{ΔARE/WT} controls. At this time point, the inflammation is maximally developed so that a reduction of HSP60 by half could neither further deteriorate nor ameliorate the ileal inflammation. In contrast, inflammation in the proximal colon is rather mild and still shapeable. Here, the degree of leukocyte infiltration in the mucosa and submucosa as well as the degree of crypt loss was elevated in *ΔARE/Hsp60*^{+/-} mice compared to *ΔARE* controls. Although the exact mechanism of pathology in the *ΔARE* model is still unknown, an activated ER UPR in IEC and a leakiness of the intestinal barrier have been observed [95, 290]. An additional HSP60

deficiency may further sensitize IEC and compromise a proper barrier function. This aggravation of inflammation cannot be observed in $\Delta ARE/Grp78^{+/-}$ mice, probably due to the compensatory adjustment of GRP78 levels by translational regulation [289]. Since the development of ileal inflammation develops time dependently [291], an earlier time point of investigation, e.g. 8 – 12 weeks, may be better shapeable by mild alterations like Hsp60 or *Grp78* haplodeficiency. In summary, a 50% reduction in HSP60 represents a stable condition for IEC and for the whole organism pointing to an enormous resilience of the mitochondrial chaperone system to maintain cellular and tissue homeostasis. A further reduction of HSP60 whereas shifts the system towards UPR induction and impacts on cellular processes.

6 CONCLUSION AND PERSPECTIVE

Unfolded protein response pathways especially the well characterized ER UPR have been implicated in various chronic disorders like diabetes [66], neoplasia [292] and IBD [85]. In parallel, progress in the integrative approach of systems-biology deepens the understanding that single pathways cannot be regarded separately but are tightly interrelated. The intestinal epithelium is a prime example for this perception. At this cell layer signals from the lumen and the host converge and are processed into an adaptation of the epithelial function. Therefore, various cellular processes such as protein folding, secretion, organelle biosynthesis, bacteria and nutrient sensing, autophagy and apoptosis have to be dynamically interconnected to hold the epithelial functions. Impressively, the mitochondria center in this tightly interrelated network and the MT and ER UPR pathways form important connecting lines between these processes [35]. In the present study, we pursued the question whether intrinsically activated UPR pathways impact epithelial homeostasis and may favor the development of chronic intestinal inflammation.

Analysis of an IEC-specific mouse model deficient for the mitochondrial chaperone *Hsp60* (*Hsp60*^{ΔIEC}) revealed a disrupted epithelial cell homeostasis in both the pre- and postnatal gut, independent of epithelial destruction and an inflammation-associated pathology. We could not provide evidence of a causal relation between the presences of UPR and the development of intestinal inflammation. However, *Hsp60* deletion in the intestinal epithelium triggers MT UPR associated with alterations in morphology, mitochondrial function and most strikingly with an impaired proliferative response and a loss of stemness.

For a deeper investigation of mitochondrial function in HSP60 deficient IEC, respiration measurements will be performed on cultivated organoids isolated from small intestinal crypts. To further dissect UPR- and inflammation-related signaling pathways underlying the anti-proliferative effects as well as the stem cell hyperproliferation, intercrossings of *Hsp60*^{ΔIEC} mice with *Chop*^{-/-}, *TnfR*^{-/-} and *Il-6*^{-/-} mice will be performed. A further approach to revert the MT UPR driven loss of proliferative and stem cells could be the administration of the chemical chaperones TUDCA and PBA which have been proven to be effective in enhancing the folding capacity of the ER in IEC [83] thereby supporting the reconstitution of epithelial homeostasis [80]. Finally, the *Hsp60*^{ΔIEC} model could contribute to a better understanding of epithelial regeneration mechanisms as well as of epithelial cell neoplasia. The characterization of IEC specific *nAtf6* and *Chop* transgenic mice which is currently ongoing will probably add further insights into these processes. Finally, the knockout as well as the transgenic approach can be specifically transferred to other metabolically relevant organs. Liver-specific *Hsp60*^{Δhep} mice are already under investigation in close collaboration. Corresponding efforts on the adipose tissue and the pancreas will follow by and by.

7 APPENDIX

7.1 Sequence of HA-nATF6 and nAFT6-HA

Mus musculus activating transcription factor 6 (Atf6), mRNA (NM_001081304.1) CDS

```

1  gttactcacc catccgagtt gtgagggaga ggtgtctgtt tcggggaagc cggcttgtgt
61  tgccggcgcc ATGgagtcgc cttttagtcc ggttcttcc catggaccag atgaagactg
121 ggagtcgacg ttgtttgctg aacttggcta ttccacagac actgatgatg tgcactttga
181 tgcagcacat gaggcttatg aaaataattt tgatcatctt aattttgatt tggatttgat
241 gccttgggag tcagacctat ggagccccgg cagccacttc tgctcagaca tgaaggcaga
301 gccccagcct ctttctccgg ctctctccag ttgtctccatc tcctctcctc ggtccacaga
361 ctctgtgtct tcaactcagc acgttctctga ggagttggat ttgtttgtcta gttctcagtc
421 ccccttttcc ttatatggcg acagctgtaa tagccctcc tctgtagagc cactgaagga
481 agagaagcct gtcactggtc ctggaacaaa aacagaacat ggactgactc caaagaaaaa
541 aattcagatg agttcaaaac cttcagttca gcccaagcct ttattacttc cagcagcgcc
601 caagactcaa accaatgcc a gtgtcccagc aaaagccatc atcattcaga cactaccagc
661 ccttatgcc a ctggcaaagc agcagtcgat tatcagcata cagcctgcgc ccaccaaaagg
721 ccagactggt ttgtctcttc agccgactgt ggttcaactt cagagccctg cggttctgtc
781 gtctgtctcag ccggttcttg cagtcactgg gggagccgca cagctaccta accatgtggt
841 gaatgtgctg ccagcccctg tggtagcag cccggtgaat ggaaaacttt ccgtgactaa
901 acctgttcta caaagtgcc a ccagaagtat gggttcggat atcgctgtgc tgaggagaca
961 gcagcggatg ataaagaacc gagagtctgc ttgtcagtcg cgcaagaaga agaaagagta
1021 tatgctagga ctggaggcca ggctcaaggc tgccctctca gagaatgagc agctgaagaa
1081 ggagaatggc tccctgaagc gacagctgga cgaggtggtg tcagagaacc agaggctcaa
1141 agtcccaagt ccaaagcgaa gagctgtctg tgtgatgata gtattagcat ttataatgct
1201 gaactatggg cccatgagca tgctggagca agaatcccga agagtgaaac ctagtgtgag
1261 ccttgccaat cagaggaggg atctcttgga attttcagca aaagaagtta aagacacatc
1321 agatggtgac aaccagaaag acagttacag ctatgatcac tctgtgtcca atgacaaagc
1381 tttaatggtg ctaagtgaag agccattgct ttatatgcct ccacctccat gtcaaccctt
1441 gattaacaca acagagtctc tcaggttgaa ccatgaactt cgaggctggg ttcatagaca
1501 tgaagtggaa aggaccaa at ctagaagaat gacaaatagc caacagaaag cccgcattct
1561 ccaggggtgct ctggaacagg gctctaattc tcagctgatg gctgtccagt acacagaaac
1621 cactagcatc agtaggaatt ctgggagtg a gctgcaagtg tattacgcct cccctggaag
1681 ttaccaaggc ttctttgacg ccatccgcag gaggggagat acgttttacg ttgtctcatt
1741 tcgaagggat catctgctat taccagctac caccacaaac aagaccacaa gaccaaaaat
1801 gtcaattgta ttaccagcaa taaacataaa tgataatgtg atcaatgggc aggactatga
1861 agtaatgatg cagattgact gtcaggtgat ggacaccagg atcctccaca tcaaaagctc
1921 ctcggttccc ccttatctcc gggatcatca gcggaaccaa accagcacct tctttggttc
1981 cctccaaca accacagaga cgacccatgt ggtcagcacc atcctgagtc cgttgagcTA
2041 Gtgccccgagc ...

```

(Nested primer underlined; nAtf6 CDS in red; Atf6 ER-sensor domain in black; Start and Stop codon in bold and capitalized; Atf6 untranslated region in grey)

HA-nATF6

... acc**ATG**taccatacgatgttccagattacgct**gcggccgct**atggag ... **ccaagtTAG** ...

nATF6-HA

... acc**ATG**gag ... ccaagt**gcggccgct**ta**ccatacga**tgttccagattacgct**TAG** ...

(Kozak consensus sequence underlined; HA-tag sequence in green; linker sequence in blue; nAtf6 CDS in red)

Mus musculus activating transcription factor 6 (Atf6), protein sequence (NP_001074773.1)

```

1  MESPFSPVLP HGPDEDWEST LFAELGYFTD TDDVHFDAAH EAYENNFDHL NFDLDLMPWE
61  SDLWSPGSHF CSDMKAEPQP LSPASSSCSI SSPRSTDSCS STQHVPEELD LLSSSQSPLS
121 LYGDSCNSPS SVEPLKEEKP VTGPGNKTEH GLTPKKKIQM SSKPSVQPKP LLLPAAPKTQ
181 TNASVPAKAI IIQTLPALMP LAKQQSIISI QPAPTKGQTV LLSQPTVVQL QSPAVLSSAQ
241 PVLAVTGGAQ QLPNHVVNVL PAPVVSSPVN GKLSVTKPVL QSATRSMGSD IAVLRRQQRM
301 IKNRESACQS RKKKKKEYMLG LEARLKAALS ENEQLKKENG SLKRQLDEVV SENQRLKVPS
361 PKRRAVCVMI VLAFIMLNYG PMSMLEQESR RVKPSVSPAN QRRHLLEFSA KEVKDTS DGD
421 NQKDSYSYDH SVSNDKALMV LSEEPLLYMP PPQCPLINT TESLRLNHEL RGWVHRHEVE
481 RTKSRRMTNS QQKARILQGA LEQGSNSQLM AVQYTETTSI SRNSGSELQV YYASPGSYQG
541 FFDAIRRRGD TFYVVSFRRD HLLLPATTHN KTTRPKMSIV LPAININDNV INGQDYEVM
601 QIDCQVMDTR ILHIKSSSVP PYLRDHQRNQ TSTFFGSPPT TTETTHVVST IPESLQ

```

(nATF6 in red; ATF6 ER-sensor domain in black; nuclear localization sequence marked in yellow; internal start transfer sequence/ transmembrane sequence in orange; S1/2P cleavage site underlined)

HA-nATF6

Met-Tyr-Pro-Tyr-Asp-Val-Pro-Asp-Tyr-Ala-Ala-Ala-Ala-**Met**-Glu - -Pro-Ser-**STOP**

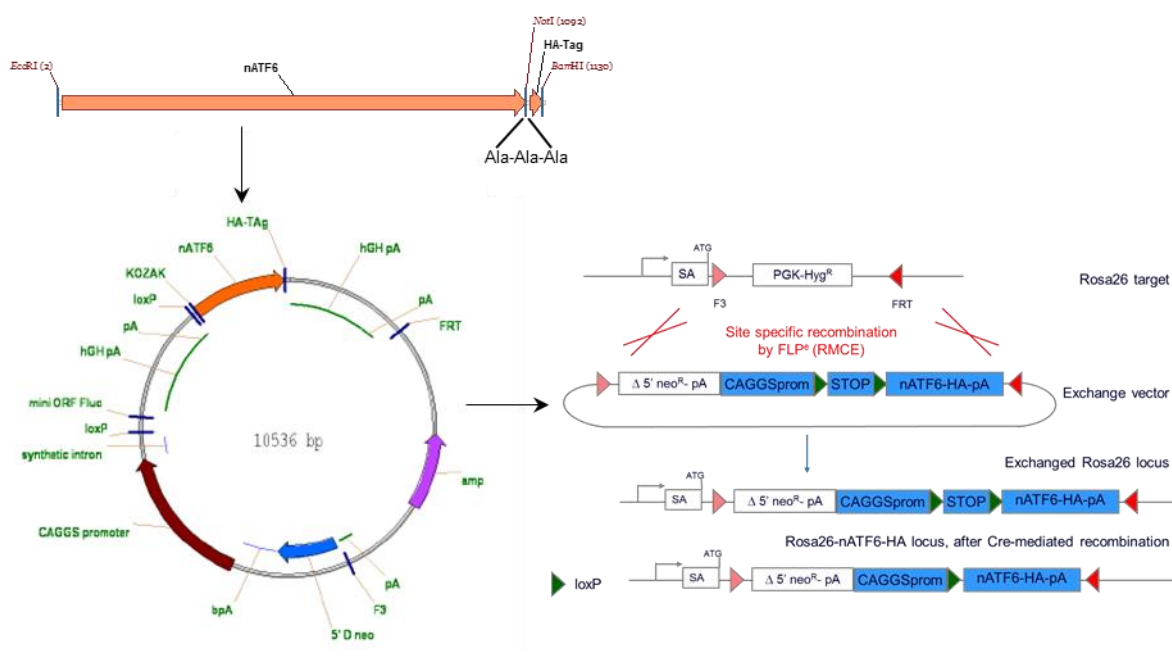
nATF6-HA

Met-Glu- -Pro-Ser-Ala-Ala-Ala-Tyr-Pro-Tyr-Asp-Val-Pro-Asp-Tyr-Ala-**STOP**

(nATF6 in red; HA-Tag in green; linker in blue; Start/STOP bold)

7.2 Generation of the *nAtf6-HA* conditional transgenic mouse

Table 27


Project TUM0002: <i>nAtf6-HA</i> conditional transgenic mouse	
Milestone 1 Cloning and targeting strategy; Performed by TUM / Taconic-Artemis	
 <p>The diagram illustrates the cloning and targeting strategy for the <i>nAtf6-HA</i> conditional transgenic mouse. It shows the <i>nAtf6</i> gene structure, the construction of a circular plasmid vector (10536 bp) containing the <i>nAtf6-HA</i> construct, and the targeting strategy using recombination-mediated cassette exchange (RMCE) to insert the construct into the <i>Rosa26</i> locus. The final result is the <i>Rosa26-nAtf6-HA</i> locus after Cre-mediated recombination.</p>	
<ul style="list-style-type: none"> • The CDS of <i>nAtf6</i> was fused to a HA-tag sequence via a <i>NotI</i> restriction site coding for an 3xAla linker sequence. • Targeting strategy allows generation of <i>Rosa26-nAtf6-HA</i> knock in allele. • A construct containing the CAGGS promoter, a loxP-flanked STOP cassette, and the <i>nAtf6-HA</i> ORF was inserted into the <i>Rosa26</i> locus using recombination-mediated cassette exchange (RMCE). • The STOP cassette was made of a FLuc mini ORF and a polyadenylation site to stop transcription from the CAGGS promoter. • The strong CAGGS promoter will drive expression of the <i>nAtf6-HA</i> open reading frame, after Cre-mediated removal of the STOP cassette. • Termination of <i>ROSA</i> transcript by Neo cassette. 	

(Table continued on next page)

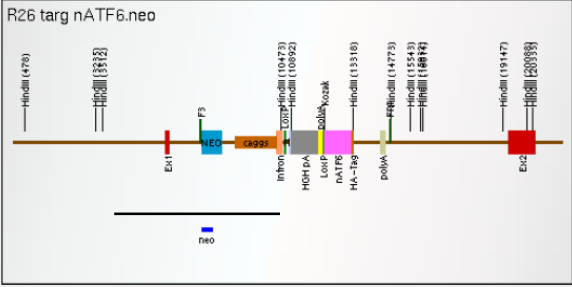
Milestone 2 Transfection and selection of ES cells; Performed by Taconic-Artemis

After lipofection of ES cells with the targeting vector and subsequent antibiotic selection, six ES cell clones were analysed for single integration into the ROSA26 locus. The picture shows one of six southern blot analyses.

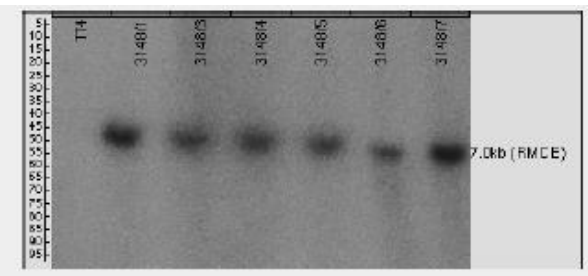
R26 targ pTT4.neo



R26 targ nATF6.neo



Genomic DNA was digested with *HindIII* (upper scheme WT mouse; lower scheme Tg mouse) and a *neo* probe was hybridized to the 7 kb DNA fragments. The agarose gel shows correct insertion of the target vector by RMCE at 5' site and single integration in all 6 ES cell clones (TT4 as untransfected CTRL).



Milestone 3 Production of chimeric mice; Performed by Taconic-Artemis

ES cell clones were transferred to Balb/c blastocysts to generate chimeras. Chimera breeding (ChB) with C57 Bl/6NTac WT mice was performed to check for germ line transmission of chimerism.

ESC Clone	nATF6 3148 7	nATF6 3148 5
Karyotype 40, XY	n/a	n/a
Transferred blastocysts	48	96
Transfers	3	6
Litters	2	3
Pups born	10	9
Chimeric Pups	7	6
> 50% chimeric male pups	5	3

42% genotyped *nAtf6-HA*^{Tg flox/WT}

48% genotyped *nATF6-HA*^{Tg WT/WT}

Chimeras for clone nATF6 3148 7					
Id	DoB	Sex	% Chimerism	Status	Used in ChB
130444	13.06.2009	m	50 - 75	sacrificed	9755
130445	13.06.2009	m	50 - 75	sacrificed	9756
130446	13.06.2009	m	50 - 75	sacrificed	9757
130447	13.06.2009	m	50 - 75	sacrificed	10052
130448	13.06.2009	m	50 - 75	sacrificed	
130449	13.06.2009	m	25 - 50	sacrificed	
130450	13.06.2009	m	25 - 50	sacrificed	

100% of pubs Bl/6NTac (germ line transmission)

Tab. 27 Overview of the generation of *nAtf6-HA*^{Tg flox/flox} mice

114

7.3 Sequence of HA-CHOP and CHOP-HA

Mus musculus DNA-damage inducible transcript 3 (Ddit3), mRNA (NM_007837.3) CDS

```

1  ggtcagttat cttgagccta acacgtcgat tatatcatgt tgaagatgag cgggtggcag
61  cgacagagcc agaataacag ccggaacctg aggagagagt gttccagaag gaagtgcac
121  ttcatacacc accacacctg aaagcagaac ctggtccacg tgcagtcATG gcagctgagt
181  ccctgccttt caccttgagg acggtgtcca gctgggagct ggaagcctgg tatgaggatc
241  tgcaggaggt cctgtcctca gatgaaattg ggggcaccta tatctcatcc ccaggaaacg
301  aagaggaaga atcaaaaacc ttcactactc ttgaccctgc gtccctagct tggctgacag
361  aggagccagg gccaacagag gtcacacgca catcccaaag ccctcgctct ccagattcca
421  gtcagagttc tatggcccag gaggaagagg aggaagagca aggaagaact aggaaacgga
481  aacagagtgg tcagtgccca gcccggcctg ggaagcaacg catgaaggag aaggagcagg
541  agaacgagcg gaaagtggca cagctagctg aagagaacga gcggctcaag caggaaatcg
601  agcgctgac cagggaggtg gagaccacac ggcgggctct gatcgaccgc atggtcagcc
661  tgcaccaagc aTGAacagtg ggcacacact cctgtctgtc tctccggaag tgtaccagc
721  accatcgcg cagcgccaag catgtgaccc tgcactgcac tgcacatgct gaggagggga
781  ctgagggtag accaggagag ggctcggcct gcacatagac ggtacattgt ttattactgt
841  ccatgtccag taaagtgact ttgtgtcaac aaaaaaaaaa

```

(Nested primer underlined; Chop CDS in red; Start and Stop codon bold and capitalized; Chop untranslated region in grey)

HA-Chop

... acc**ATG**tacccatacgatgttccagattacgctgcggccgctatggca ... caagca**TAG** ...

Chop-HA

... acc**ATG**gca ... caagcagcggccgctta**acc**catacgatgttccagattacgct**TAG** ...

(Kozak consensus sequence underlined; HA-tag sequence in green; linker sequence in blue; Chop CDS in red)

DNA-damage inducible transcript 3 (Ddit3), protein sequence (NP_031863.3)

```

1  MAAESLPFTL ETVSSWELEA WYEDLQEVLS SDEIGGTYIS SPGNEEEESK TFTTLDPASL
61  AWLTEEPGPT EVTRTSQSPR SPDSSQSSMA QEEEEEEQGR TRKRKQSGQC PARPGKQRMK
121  EKEQENERKV AQLAEENERL KQEIERLTRE VETTRRALID RMVSLHQA

```

(CHOP in red; nuclear localization sequence marked in yellow)

HA-Chop

Met-Tyr-Pro-Tyr-Asp-Val-Pro-Asp-Tyr-Ala-Ala-Ala-Ala-Met-Ala - -Gln-Ala-**STOP**

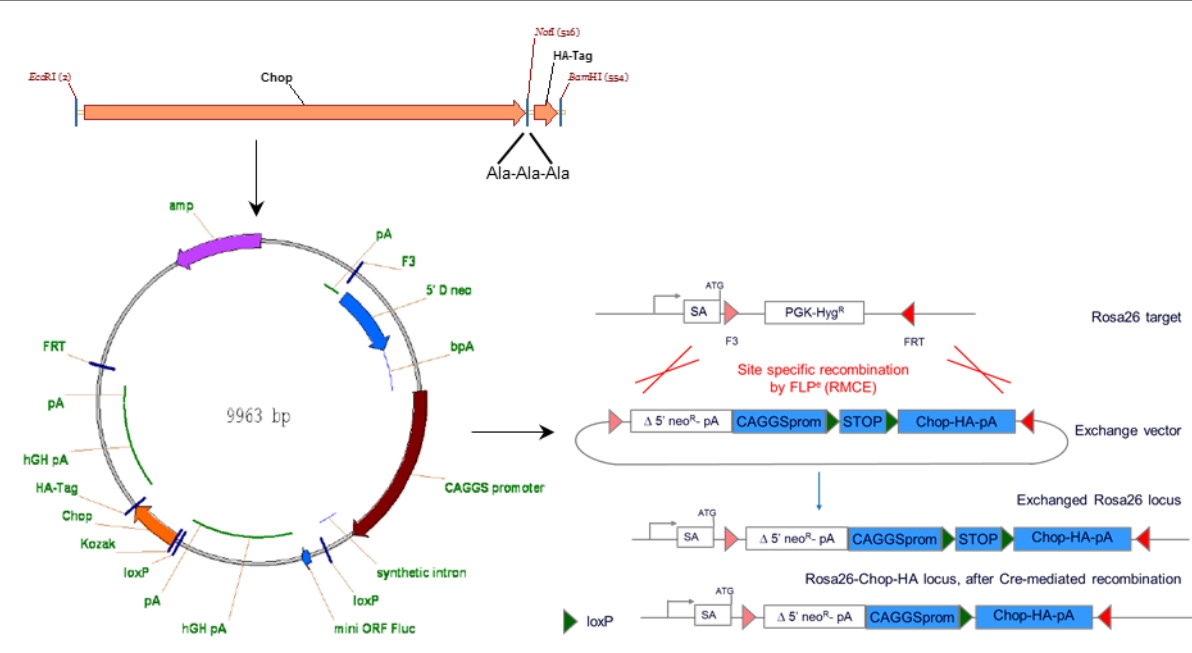
Chop-HA

Met-Ala- -Gln-Ala-Ala-Ala-Ala-Tyr-Pro-Tyr-Asp-Val-Pro-Asp-Tyr-Ala-**STOP**

(CHOP in red; HA-Tag in green; linker in blue; Start/STOP bold)

7.4 Generation of the *Chop-HA* conditional transgenic mouse

Table 28

Project TUM0003: <i>Chop-HA</i> conditional transgenic mouse	
Milestone 1 Cloning and targeting strategy; Performed by TUM / Taconic-Artemis	
 <p>The diagram illustrates the cloning and targeting strategy for the <i>Chop-HA</i> conditional transgenic mouse. It shows the <i>Chop</i> gene structure, the construction of a circular plasmid (9963 bp) containing various elements like <i>amp</i>, <i>pA</i>, <i>F3</i>, <i>5' D neo</i>, <i>bpA</i>, <i>CAGGS promoter</i>, <i>synthetic intron</i>, <i>loxP</i>, <i>mini ORF Fluc</i>, <i>hGH pA</i>, <i>HA-Tag</i>, <i>Chop</i>, <i>Kozak</i>, and <i>pA</i>. The targeting strategy involves the Rosa26 target locus, which is targeted by the Exchange vector (containing Δ 5' neo^R, pA, CAGGSprom, STOP, and Chop-HA-pA) via site-specific recombination by FLP (RMCE). The resulting Exchange vector is then recombined into the Rosa26 locus, creating the Rosa26-Chop-HA locus, after Cre-mediated recombination.</p>	
<ul style="list-style-type: none"> • The CDS of <i>Chop</i> was fused to a HA-tag sequence via a <i>NotI</i> restriction site coding for an 3xAla linker sequence. • Targeting strategy allows generation of Rosa26-<i>Chop-HA</i> knock in allele. • A construct containing the CAGGS promoter, a loxP-flanked STOP cassette, and the <i>Chop-HA</i> ORF was inserted into the ROSA26 locus using recombination-mediated cassette exchange (RMCE). • The STOP cassette was made of a FLuc mini ORF and a polyadenylation site to stop transcription from the CAGGS promoter. • The strong CAGGS promoter will drive expression of the <i>Chop-HA</i> open reading frame, after Cre-mediated removal of the STOP cassette. • Termination of ROSA transcript by Neo cassette. 	

(Table continued on next page)

R26 targ pTT4.neo

Diagram illustrating the R26 targeting strategy. The targeting vector (pTT4.neo) is integrated into the R26 locus via homologous recombination. The R26 locus contains Exon 1, Exon 2, and Exon 3. The targeting vector contains LacZ, Neo, and a polyA signal. The resulting R26 targeting strategy shows the LacZ gene expressed from the R26 promoter, and the Neo gene flanked by LoxP sites, allowing for its removal by Cre recombinase.

R26 targ nATF6.neo

Diagram illustrating the R26 targeting strategy for nATF6. The targeting vector (pTT4.neo) is integrated into the R26 locus via homologous recombination. The R26 locus contains Exon 1, Exon 2, and Exon 3. The targeting vector contains nATF6, Neo, and a polyA signal. The resulting R26 targeting strategy shows the nATF6 gene expressed from the R26 promoter, and the Neo gene flanked by LoxP sites, allowing for its removal by Cre recombinase.

Milestone 3 Production of chimeric mice; Performed by Taconic-Artemis

ESC Clone	Chop 3085 8	Chop 3085 4
Karyotype 40, XY	n/a	n/a
Transferred blastocysts	48	48
Transfers	3	3
Litters	3	2
Pups born	14	5
Chimeric Pups	12	4
> 50% chimeric male pups	4	0

Chimeras for clone Chop 3085 8					
Id	DoB	Sex	% Chimerism	Status	Used in ChE
130401	04.06.2009	m	> 75	sacrificed	9716
130402	04.06.2009	m	50 - 75	sacrificed	9717
130403	04.06.2009	m	50 - 75	Breeding	9718
130404	04.06.2009	m	50 - 75	sacrificed	
130405	04.06.2009	m	25 - 50	sacrificed	
130406	04.06.2009	m	25 - 50	sacrificed	
130407	04.06.2009	m	25 - 50	sacrificed	
130408	04.06.2009	m	25 - 50	sacrificed	
130409	04.06.2009	m	25 - 50	sacrificed	

40% genotyped *Chop-HA*^{Tg flox/WT}
60% genotyped *Chop-HA*^{Tg WT/WT}

92% of pubs BI/6NTac
(germ line transmission)

Tab. 28 Overview of the generation of *Chop-HA*^{Tg flox/flox} mice.

7.5 Sequence of HSP60 and truncated HSP60

Hspd1 heat shock protein 1 (chaperonin) genomic sequence (Gene ID: 15510)

... intron 3 ...

```
3661 accaggctag ttagcttcaa actcagagat ctgcctgctt cttctgcctt cagagtgcta
3721 ggattaaagg tgggcactac cacacccaga ccaagaccct gtactcttaa cctttaagct
3781 atctctgcag ccaagaatga gtaggtctta gccttccctg gcatgggtgc ctgtataaat
3841 acatgctggt ctcaaat tttt tagccattct gtcttagtct ttagtcttag tcagggtactg
3901 ggattacagg tgtgagccac cacacaacat ctaggtcaag ttttcaaaat gttgttggtt
```

... intron 8 ...

```
7141 ggtacacagg tattggatta aggtcatggt tctaacttgc tgagcctggc gtgagaatgg
7201 acatagttaa acattcttct caaaacttta agtgattttg ttctgggtata ccagtgggtct
7261 tgacatctca aagaaaaaca gcatttcttt ttctggatat ttttaagcttt atgtatatgg
7321 atgttttgtc tgctgtttg tatgggtgat gcataccaga aggcgtccat ccagtcccat
7381 aggactgcag tttatagaca gttgcaagct gccatgttgc aacttgaact caggacacct
```

...

(sites of sequence insertion via homologous recombination in bold and capitalized)

After homologous recombination with targeting vector and FLP mediated recombination

... intron 3 ...

```
gttctctgta gaccaggcta gttagcttca aactcagaga tctgcctgct tcttctgcct
tcagagtgct aggattaaag gtgggcacta ccacaccag accaagaccc tgtactctta
acctttaagc tatctctgtc gagcctagga taacttctgta taatgtatgc tatacgaagt
tatggtaacc catttaaagt aagttcctat tccgaagtgc ctattcttca aatagtatag
gaacatttaa atagttacgc tagggataac agggtaaata gttaatggcg cgccgcagcc
aagaatgagt aggtcttagc cttccctggc atgggtgcct gtataaatac atgctgggtct
caaattttta gccattctgt cttagtcttt agtcttagtc aggtactggg attacagggtg
tgagccacca cacaacatct aggtcaagtt ttcaaaatgt tgttggtttt ...
```

... intron 8 ...

```
gtacacagggt attggattaa ggtcatgttt ctaacttgct gagcctggcg tgagaatgga
catagttaaa cattcttctc aaaactttaa gtgattggcc ggcctcgaca taacttctgta
taatgtatgc tatacgaagt tataagctta aggaattgag gcctgagggt gttctggtat
accagtgggc ttgacatctc aaagaaaaac agcatttctt tttctggata ttttaagctt
tatgtatatg gatgttttgt ctgcctgttt gtatggtgta tgcataccag aaggcgtcca
tccagtccca taggactgca ...
```

After Cre mediated recombination

... intron 3 ...

```
gttctctgta gaccaggcta gttagcttca aactcagaga tctgcctgct tcttctgcct
tcagagtgct aggattaaag gtgggcacta ccacaccag accaagaccc tgtactctta
acctttaagc tatctctgtc gagcctagga taacttctgta taatgtatgc tatacgaagt
tataagctta aggaattgag gcctgagggt gttctggtat accagtgggc ttgacatctc
aaagaaaaac agcatttctt tttctggata ttttaagctt tatgtatatg gatgttttgt
ctgcctgttt gtatggtgta tgcataccag aaggcgtcca tccagtccca taggactgca
```

... intron 8 ...

(endogenous *Hsp60* sequence in black, inserted sequence in grey; flox allele primer sequence in green; knockout allele primer sequence in dark blue; loxP sites underlined, F3 site dashed underlined)

Hspd1 heat shock protein 1 (chaperonin), protein sequence

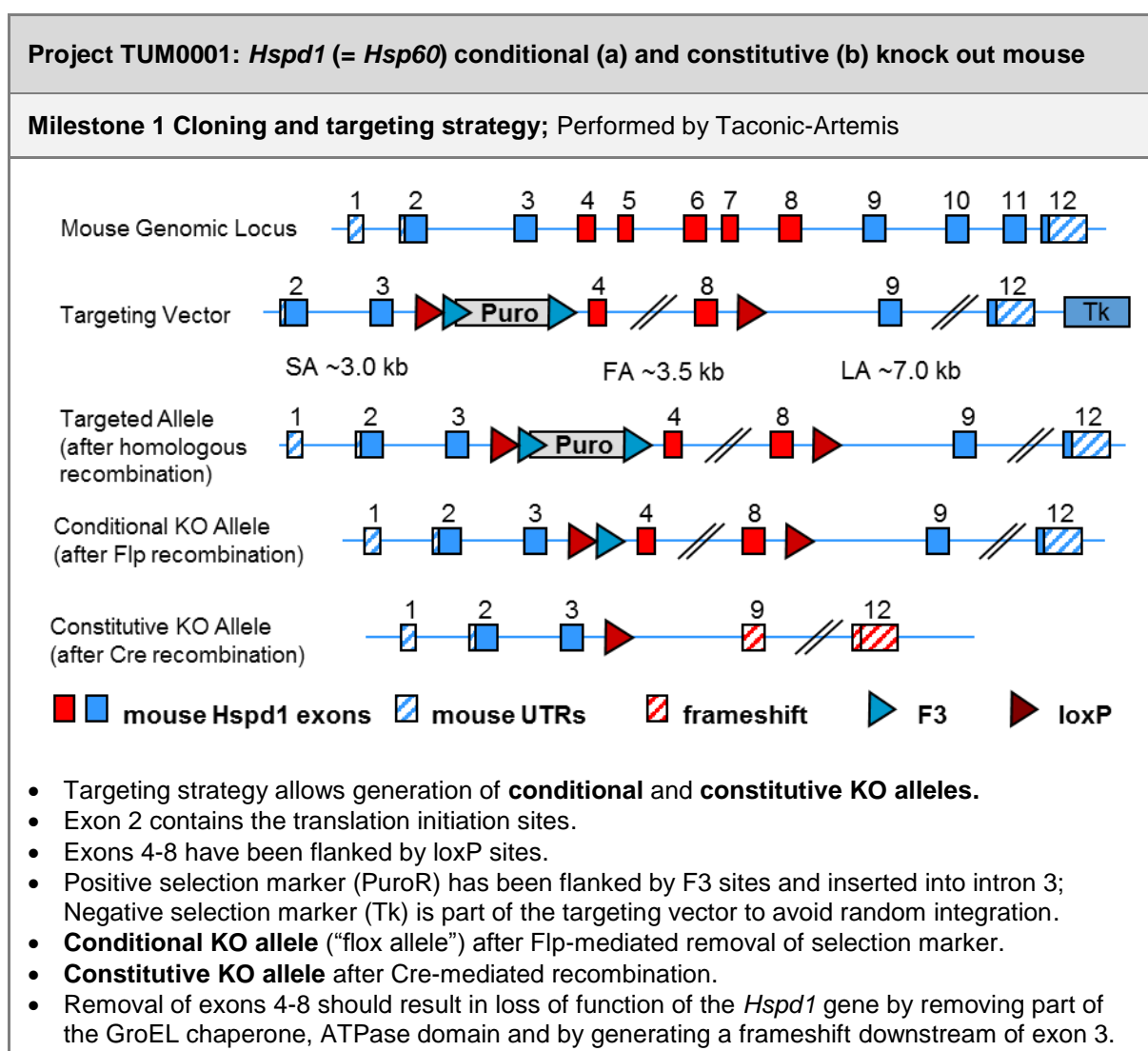
```

1  MLRLPTVLRQ MRPVSRALAP HLTRAYAKDV KFGADARALM LQGVDLLADA VAVTMGPKGR
61 TVIIEQSWGS PKVTKDGVTV AKSIDLKDKY KNIGAKLVQD VANNTNEEAG DGTTTATVLA
121 RSIAGEGFKEK ISKGANPVEI RRGVMLAVDA VIAELKKQSK PVTTPPEIAQ VATISANGDK
181 DIGNIISDAM KKVGRKGVIT VKDGKTLNDE LEIIEGMKFD RGYISPYFIN TSKGQKCEFQ
241 DAYVLLSEKK ISSVQSIVPA LEIANAHKRP LVIIAEDVDG EALSTLVVLR LKVGGLQVVAV
301 KAPGFGDNRK NQLKDMAIAT GGAVFGEEGL NLNLEDVQAH DLGKVGEVIV TKDDAMLLKG
361 KGDKAHIEKR IQEITEQLDI TTSEYEKEKL NERLAKLSDG VAVLKVGGTS DVEVNEKKDR
421 VTDALNATRA AVEEGIVLGG GCALLRCIPA LDSLKPANED QKIGIEIIKR ALKIPAMTIA
481 KNAGVEGSLI VEKILQSSSE VGYDAMLGDF VNMVEKGIID PTKVVVRTALL DAAGVASLLT
541 TAEAVVTEIP KEEKDPGMGA MGGMGGGMGG GMF

```

(Truncated HSP60 in red; deleted HSP60 sequence in black; frameshift mutated sequence in grey)

7.6 Generation of the *Hsp60* constitutive and conditional knock out mouse model



Milestone 3b Production of chimeric mice; Performed by Taconic-Artemis

ES cell clones were transferred to balb/c blastocysts to generate chimeras. Chimera breeding (ChB) with Cre-deleter mice (C57 Bl/6NTac) was performed to establish the constitutive KO and check for germ line transmission of chimerism.

ESC Clone	Hspd1 2817 A-B5	Hspd1 2817 C-B12	Chimeras for clone Hspd1 2817 C-B12			
Karyotype 40, XY	n/a	n/a	Id	DoB	Sex	% Chimerism
Transferred blastocysts	52	48	127780	20.02.2009	m	> 75
Transfers	3	3	127781	20.02.2009	m	50 - 75
Litters	3	2	127782	20.02.2009	m	50 - 75
Pups born	6	10	127783	20.02.2009	m	50 - 75
Chimeric Pups	6	9	127784	20.02.2009	m	25 - 50
> 50% chimeric male pups	5	6	127785	20.02.2009	m	25 - 50
			127786	20.02.2009	f	50 - 75
			127787	20.02.2009	f	50 - 75
			127788	20.02.2009	f	25 - 50
						Status
						Used in ChB
						9163
						9159

24% genotyped *Hsp60*^{+/-}
76% genotyped *Hsp60*^{+/+}

98% of pups Bl/6NTac
(germ line transmission)

Tab. 29 Overview of *Hsp60*^{flx/flx} and *Hsp60*^{+/-} mice generation

LIST OF FIGURES

Fig. 1 Current model for the pathogenesis of IBD	16
Fig. 2 Graphical overview of the different types of IEC in the intestinal mucosa	18
Fig. 3 Principle scheme of UPR.....	20
Fig. 4 The three branches of the ER UPR – an overview	22
Fig. 5 The mitochondrial unfolded protein response	27
Fig. 6 Mitochondria in the center of cellular signaling	28
Fig. 7 Structure of HSP60 from bacterial origin (GroEL)	29
Fig. 8 Vector map of pBluescript-CAG-lox-CAT-lox	47
Fig. 9 Crosslink between ER and MT UPR via TF ATF6 and CHOP	64
Fig. 10 Vector maps for the overexpression of HA-tagged CHOP and nATF6.....	65
Fig. 11 Validation of TF overexpression <i>in vitro</i>	65
Fig. 12 Validation of the functionality of nATF6-HA and Chop-HA overexpressing plasmids.....	66
Fig. 13 Genotyping of <i>Hsp60</i> ^{+/-} mice	67
Fig. 14 H&E stainings of selected organ sections from old <i>Hsp60</i> ^{+/-} mice	68
Fig. 15 Histopathological evaluation of different gut compartments of <i>Hsp60</i> ^{+/-} mice.....	69
Fig. 16 <i>Hsp60</i> mRNA and protein expression in IEC of <i>Hsp60</i> ^{+/-} mice	70
Fig. 17 Integrity of the colonic mucosal barrier in <i>Hsp60</i> ^{+/-} mice.....	71
Fig. 18 DSS colitis in <i>Grp78</i> ^{+/-} and <i>Hsp60</i> ^{+/-} mice.....	73
Fig. 19 Chronic ileitis in <i>Grp78</i> ^{+/-} and <i>Hsp60</i> ^{+/-} mice.....	75
Fig. 20 Genotyping of <i>Hsp60</i> ^{fllox/fllox} mice	76
Fig. 21 Embryonic lethality of <i>Hsp60</i> ^{ΔIEC} mice	77
Fig. 22 Characterization of the phenotypic, metabolic and morphologic appearance of tamoxifen inducible <i>Hsp60</i> ^{ΔIEC} mice	79
Fig. 23 Histologic characterization of the GI tract in tamoxifen inducible <i>Hsp60</i> ^{ΔIEC} mice	80
Fig. 24 Characterization of mucosal inflammation in tamoxifen inducible <i>Hsp60</i> ^{ΔIEC} mice	82
Fig. 25 Epithelial apoptosis in tamoxifen inducible <i>Hsp60</i> ^{ΔIEC} mice	82
Fig. 26 Functionality of the ileal epithelium of tamoxifen inducible <i>Hsp60</i> ^{ΔIEC} mice.....	83
Fig. 27 mRNA expression profiling of colonocytes from <i>Hsp60</i> ^{ΔIEC} mice	85
Fig. 28 mRNA expression profiling of colonocytes from <i>Hsp60</i> ^{ΔIEC} mice	86
Fig. 29 Differential (villus vs. crypt) UPR profiling of jejunal epithelium in <i>Hsp60</i> ^{ΔIEC} mice.....	88
Fig. 30 Mitochondrial morphology and functionality in IEC of <i>Hsp60</i> ^{ΔIEC} mice.....	89
Fig. 31 Hyper-regenerative crypts consist of proliferative cells escaping the knock out.....	90
Fig. 32 Hyper-regenerative crypts originate from single escaping stem cells	91
Fig. 33 HSP60 depletion leads to a loss of stem cells	92
Fig. 34 Growth factor and cytokine signals trigger stem cell proliferation	93
Fig. 35 Characterization of tam-oxifen inducible <i>Hsp60</i> ^{ΔISC} mice.....	95
Fig. 36 Schematic model of hyper-regenerative crypt formation in <i>Hsp60</i> ^{ΔIEC} mice	105

LIST OF TABLES

Tab. 1 Examples for IBD susceptibility genes with verified impact on epithelial function in human IBD and experimental intestinal inflammation (adapted from [2])	16
Tab. 2 Examples for mouse models of intestinal inflammation with primary defects of the epithelium function (adapted from [19])	19
Tab. 3 Summary of available UPR related mouse models for IBD (adapted from [85])	24
Tab. 4 Involvement of HSP60 in human diseases	31
Tab. 5 Expression levels of HSP60 in selected tumor types (adapted from [217])	33
Tab. 6 Companies purchasing experimental material used for the thesis.	37
Tab. 7 Cre expressing mouse stains and their properties.....	39
Tab. 8 Primer pairs used for genotyping of mouse strains.....	40
Tab. 9 Dehydration and paraffin embedding of formalin fixed tissue.....	42
Tab. 10 Deparaffination, rehydration and H&E staining of tissue sections	42
Tab. 11 Alcian blue staining of acetic mucus	43
Tab. 12 Primary and secondary antibodies used for IHC and IF	44
Tab. 13 Plasmids and their properties.....	47
Tab. 14 Nested primers and their properties used for amplification of coding sequences	48
Tab. 15 PCR-conditions for CDS amplification from cDNA.....	49
Tab. 16 PCR conditions for addition of restriction sites on CDS.....	49
Tab. 17 Primers and their properties used for introduction of restriction sites.....	50
Tab. 18 N- and C-terminal HA-tag sequences	51
Tab. 19 Primers and their properties used for amplification of tagged CDS.....	52
Tab. 20 PCR conditions for colony PCR	54
Tab. 21 Primers used for amplification of ChIP gained promoter fragments	56
Tab. 22 Reaction conditions for probe based qPCR	57
Tab. 23 Primers and probes used for qPCR	58
Tab. 24 Primary and secondary antibodies used for Western Blot visualization	60
Tab. 25 Bioinformatical promoter analysis of UPR responsive genes	63
Tab. 26 Embryo lethality of <i>Hsp60</i> ^{-/-} offspring	68
Tab. 27 Overview of the generation of <i>nAtf6</i> -HA ^{Tg flox/flox} mice	114
Tab. 28 Overview of the generation of <i>Chop</i> -HA ^{Tg flox/flox} mice.	117
Tab. 29 Overview of <i>Hsp60</i> ^{flox/flox} and <i>Hsp60</i> ^{+/-} mice generation.....	121

LIST OF ABBREVIATIONS

Abbreviation	Full Term	Abbreviation	Full Term
AARE	Amino acid starvation response element	IL	interleukin
AP	activator protein	ISC	Intestinal stem cell(s)
APC	Antigen presenting cell(s)	ISH	In situ hybridisation
ARE	Antioxidant response element	KO	knockout
ATF	activating transcription factor	LPL	Lamina propria lymphocytes
ATP	adenosine triphosphate	MALT	Mucosa associated lymphoid tissue
CD	Crohn's disease	MAPK	mitogen-activated protein kinase
CD	cluster of differentiation	MEK	MAPK/ERK kinase
CD	Colon distal	MHC	major histocompatibility complex
ChIP	chromatin immuno-precipitation	MT	mitochondrial
Chop	CCAAT/enhancer-binding protein homologous protein	NaF	Sodium fluorescein
ClpP	caseinolytic peptidase protease	nATF6	Nuclear ATF6
CP	Colon proximal	NK (cells)	Natural killer (cells)
CRE	cAMP response element	OTC	ornithine transcarbamylase
DAI	disease activity index	OXPHOS	Oxidative phosphorylation
DARE	deletion of AU-rich element	RAG	recombination activating gene
DC	dendritic cell(s)	ROS	Reactive oxygen species
DSS	dextran sodium sulfate	PBA	Phenylbutyric acid
eIF	eukaryotic translation initiation factor	PERK	PKR-like ER kinase
ER	endoplasmic reticulum	PKR	double-stranded RNA-activated protein kinase
ERAD	ER associated degradation	SAPK/JNK	stress-activated phospho-kinases/ c-Jun N-terminal kinase
ERSE	ER stress response element	SDS-PAGE	sodium dodecyl sulfate polyacrylamide gel electrophoresis
ER ^{T2}	Estrogen receptor (tamoxifen binding variant 2)	TA (cells)	Transit amplifying (cells)
flox	flanked by loxP	TER	transepithelial electrical resistance
GRP	glucose-regulated protein	TEM	Transmission electron microscopy
GO	gene ontology	Tg	transgenic
GWAS	genome wide association study	TLR	Toll-like receptor
H&E	hematoxylin and eosin	Tm	tunicamycin
HSP	heat shock protein	TUDCA	tauro-ursodeoxycholic acid
IBD	inflammatory bowel disease	TUNEL	TdT-mediated dUTP-biotin nick end labeling
ID	Ileum distal	UC	ulcerative colitis
IEC	intestinal epithelial cell(s)	UPR	unfolded protein response
IEL	intraepithelial lymphocytes	UPRE	UPR response element
IF	immunofluorescence	VE	Visceral endoderm
Ig	immunoglobulin	VM	visceral mesoderm
IHC	immunohistochemistry	VY	Visceral yolk sac

LIST OF REFERENCES

1. Loftus, E.V., Jr., *Clinical epidemiology of inflammatory bowel disease: Incidence, prevalence, and environmental influences*. Gastroenterology, 2004. **126**(6): p. 1504-17.
2. Sartor, R.B., *Mechanisms of disease: pathogenesis of Crohn's disease and ulcerative colitis*. Nat Clin Pract Gastroenterol Hepatol, 2006. **3**(7): p. 390-407.
3. Henderson, P., et al., *Function of the intestinal epithelium and its dysregulation in inflammatory bowel disease*. Inflamm Bowel Dis, 2011. **17**(1): p. 382-95.
4. Halfvarson, J., et al., *Inflammatory bowel disease in a Swedish twin cohort: a long-term follow-up of concordance and clinical characteristics*. Gastroenterology, 2003. **124**(7): p. 1767-73.
5. Jostins, L., et al., *Host-microbe interactions have shaped the genetic architecture of inflammatory bowel disease*. Nature, 2012. **491**(7422): p. 119-24.
6. Hugot, J.P., et al., *Association of NOD2 leucine-rich repeat variants with susceptibility to Crohn's disease*. Nature, 2001. **411**(6837): p. 599-603.
7. Ogura, Y., et al., *A frameshift mutation in NOD2 associated with susceptibility to Crohn's disease*. Nature, 2001. **411**(6837): p. 603-6.
8. Peltekova, V.D., et al., *Functional variants of OCTN cation transporter genes are associated with Crohn disease*. Nat Genet, 2004. **36**(5): p. 471-5.
9. Stoll, M., et al., *Genetic variation in DLG5 is associated with inflammatory bowel disease*. Nat Genet, 2004. **36**(5): p. 476-80.
10. Sugawara, K., et al., *Linkage to peroxisome proliferator-activated receptor-gamma in SAMP1/YitFc mice and in human Crohn's disease*. Gastroenterology, 2005. **128**(2): p. 351-60.
11. Rioux, J.D., et al., *Genome-wide association study identifies new susceptibility loci for Crohn disease and implicates autophagy in disease pathogenesis*. Nat Genet, 2007. **39**(5): p. 596-604.
12. Hampe, J., et al., *A genome-wide association scan of nonsynonymous SNPs identifies a susceptibility variant for Crohn disease in ATG16L1*. Nat Genet, 2007. **39**(2): p. 207-11.
13. Kaser, A., et al., *XBP1 links ER stress to intestinal inflammation and confers genetic risk for human inflammatory bowel disease*. Cell, 2008. **134**(5): p. 743-56.
14. Ho, G.T., et al., *Allelic variations of the multidrug resistance gene determine susceptibility and disease behavior in ulcerative colitis*. Gastroenterology, 2005. **128**(2): p. 288-96.
15. Brant, S.R., et al., *MDR1 Ala893 polymorphism is associated with inflammatory bowel disease*. Am J Hum Genet, 2003. **73**(6): p. 1282-92.
16. Kyo, K., et al., *Association of ulcerative colitis with rare VNTR alleles of the human intestinal mucin gene, MUC3*. Hum Mol Genet, 1999. **8**(2): p. 307-11.
17. Kyo, K., et al., *Associations of distinct variants of the intestinal mucin gene MUC3A with ulcerative colitis and Crohn's disease*. J Hum Genet, 2001. **46**(1): p. 5-20.
18. Rivas, M.A., et al., *Deep resequencing of GWAS loci identifies independent rare variants associated with inflammatory bowel disease*. Nat Genet, 2011. **43**(11): p. 1066-73.
19. Pastorelli, L., et al., *Central Role of the Gut Epithelial Barrier in the Pathogenesis of Chronic Intestinal Inflammation: Lessons Learned from Animal Models and Human Genetics*. Front Immunol, 2013. **4**: p. 280.
20. van der Flier, L.G. and H. Clevers, *Stem cells, self-renewal, and differentiation in the intestinal epithelium*. Annu Rev Physiol, 2009. **71**: p. 241-60.
21. Simon-Assmann, P., et al., *In vitro models of intestinal epithelial cell differentiation*. Cell Biol Toxicol, 2007. **23**(4): p. 241-56.
22. Ramasundara, M., et al., *Defensins and inflammation: the role of defensins in inflammatory bowel disease*. J Gastroenterol Hepatol, 2009. **24**(2): p. 202-8.
23. Snoeck, V., B. Goddeeris, and E. Cox, *The role of enterocytes in the intestinal barrier function and antigen uptake*. Microbes Infect, 2005. **7**(7-8): p. 997-1004.
24. Cerutti, A. and M. Rescigno, *The biology of intestinal immunoglobulin A responses*. Immunity, 2008. **28**(6): p. 740-50.
25. Mostov, K.E. and D.L. Deitcher, *Polymeric immunoglobulin receptor expressed in MDCK cells transcytoses IgA*. Cell, 1986. **46**(4): p. 613-21.
26. Stadnyk, A.W., *Intestinal epithelial cells as a source of inflammatory cytokines and chemokines*. Can J Gastroenterol, 2002. **16**(4): p. 241-6.
27. Panja, A., et al., *The regulation and functional consequence of proinflammatory cytokine binding on human intestinal epithelial cells*. J Immunol, 1998. **161**(7): p. 3675-84.
28. O'Connor, W., Jr., L.A. Zenewicz, and R.A. Flavell, *The dual nature of T(H)17 cells: shifting the focus to function*. Nat Immunol, 2010. **11**(6): p. 471-6.

29. Ruiz, P.A., et al., *IL-10 gene-deficient mice lack TGF-beta/Smad-mediated TLR2 degradation and fail to inhibit proinflammatory gene expression in intestinal epithelial cells under conditions of chronic inflammation*. Ann N Y Acad Sci, 2006. **1072**: p. 389-94.
30. Okayasu, I., et al., *A novel method in the induction of reliable experimental acute and chronic ulcerative colitis in mice*. Gastroenterology, 1990. **98**(3): p. 694-702.
31. Hermiston, M.L. and J.I. Gordon, *Inflammatory bowel disease and adenomas in mice expressing a dominant negative N-cadherin*. Science, 1995. **270**(5239): p. 1203-7.
32. Nenci, A., et al., *Epithelial NEMO links innate immunity to chronic intestinal inflammation*. Nature, 2007. **446**(7135): p. 557-61.
33. Heazlewood, C.K., et al., *Aberrant mucin assembly in mice causes endoplasmic reticulum stress and spontaneous inflammation resembling ulcerative colitis*. PLoS Med, 2008. **5**(3): p. e54.
34. Sundberg, J.P., et al., *Spontaneous, heritable colitis in a new substrain of C3H/HeJ mice*. Gastroenterology, 1994. **107**(6): p. 1726-35.
35. Rath, E. and D. Haller, *Mitochondria at the interface between danger signaling and metabolism: role of unfolded protein responses in chronic inflammation*. Inflamm Bowel Dis, 2012. **18**(7): p. 1364-77.
36. Ron, D. and P. Walter, *Signal integration in the endoplasmic reticulum unfolded protein response*. Nat Rev Mol Cell Biol, 2007. **8**(7): p. 519-29.
37. Ryan, M.T. and N.J. Hoogenraad, *Mitochondrial-nuclear communications*. Annu Rev Biochem, 2007. **76**: p. 701-22.
38. Bukau, B., J. Weissman, and A. Horwich, *Molecular chaperones and protein quality control*. Cell, 2006. **125**(3): p. 443-51.
39. Yoshida, H., *ER stress response, peroxisome proliferation, mitochondrial unfolded protein response and Golgi stress response*. IUBMB Life, 2009. **61**(9): p. 871-9.
40. Rutkowski, D.T. and R.J. Kaufman, *That which does not kill me makes me stronger: adapting to chronic ER stress*. Trends Biochem Sci, 2007. **32**(10): p. 469-76.
41. Yoshida, H., et al., *A time-dependent phase shift in the mammalian unfolded protein response*. Dev Cell, 2003. **4**(2): p. 265-71.
42. Calton, M., et al., *IRE1 couples endoplasmic reticulum load to secretory capacity by processing the XBP-1 mRNA*. Nature, 2002. **415**(6867): p. 92-6.
43. Lee, A.H., N.N. Iwakoshi, and L.H. Glimcher, *XBP-1 regulates a subset of endoplasmic reticulum resident chaperone genes in the unfolded protein response*. Mol Cell Biol, 2003. **23**(21): p. 7448-59.
44. Sriburi, R., et al., *XBP1: a link between the unfolded protein response, lipid biosynthesis, and biogenesis of the endoplasmic reticulum*. J Cell Biol, 2004. **167**(1): p. 35-41.
45. Nishitoh, H., et al., *ASK1 is essential for endoplasmic reticulum stress-induced neuronal cell death triggered by expanded polyglutamine repeats*. Genes Dev, 2002. **16**(11): p. 1345-55.
46. Urano, F., et al., *Coupling of stress in the ER to activation of JNK protein kinases by transmembrane protein kinase IRE1*. Science, 2000. **287**(5453): p. 664-6.
47. Harding, H.P., Y. Zhang, and D. Ron, *Protein translation and folding are coupled by an endoplasmic-reticulum-resident kinase*. Nature, 1999. **397**(6716): p. 271-4.
48. Harding, H.P., et al., *Perk is essential for translational regulation and cell survival during the unfolded protein response*. Mol Cell, 2000. **5**(5): p. 897-904.
49. Vattem, K.M. and R.C. Wek, *Reinitiation involving upstream ORFs regulates ATF4 mRNA translation in mammalian cells*. Proc Natl Acad Sci U S A, 2004. **101**(31): p. 11269-11274.
50. Lu, P.D., H.P. Harding, and D. Ron, *Translation reinitiation at alternative open reading frames regulates gene expression in an integrated stress response*. J Cell Biol, 2004. **167**(1): p. 27-33.
51. Luo, S., et al., *Induction of Grp78/BiP by translational block: activation of the Grp78 promoter by ATF4 through and upstream ATF/CRE site independent of the endoplasmic reticulum stress elements*. J Biol Chem, 2003. **278**(39): p. 37375-85.
52. Ma, Y. and L.M. Hendershot, *Delineation of a negative feedback regulatory loop that controls protein translation during endoplasmic reticulum stress*. J Biol Chem, 2003. **278**(37): p. 34864-73.
53. Ma, Y., et al., *Two distinct stress signaling pathways converge upon the CHOP promoter during the mammalian unfolded protein response*. J Mol Biol, 2002. **318**(5): p. 1351-65.
54. Fawcett, T.W., et al., *Complexes containing activating transcription factor (ATF)/cAMP-responsive-element-binding protein (CREB) interact with the CCAAT/enhancer-binding protein (C/EBP)-ATF composite site to regulate Gadd153 expression during the stress response*. Biochem J, 1999. **339** (Pt 1): p. 135-41.

55. Cullinan, S.B. and J.A. Diehl, *Coordination of ER and oxidative stress signaling: the PERK/Nrf2 signaling pathway*. Int J Biochem Cell Biol, 2006. **38**(3): p. 317-32.
56. Cullinan, S.B., et al., *Nrf2 is a direct PERK substrate and effector of PERK-dependent cell survival*. Mol Cell Biol, 2003. **23**(20): p. 7198-209.
57. Chen, X., J. Shen, and R. Prywes, *The luminal domain of ATF6 senses endoplasmic reticulum (ER) stress and causes translocation of ATF6 from the ER to the Golgi*. J Biol Chem, 2002. **277**(15): p. 13045-52.
58. Haze, K., et al., *Mammalian transcription factor ATF6 is synthesized as a transmembrane protein and activated by proteolysis in response to endoplasmic reticulum stress*. Mol Biol Cell, 1999. **10**(11): p. 3787-99.
59. Yoshida, H., et al., *Identification of the cis-acting endoplasmic reticulum stress response element responsible for transcriptional induction of mammalian glucose-regulated proteins. Involvement of basic leucine zipper transcription factors*. J Biol Chem, 1998. **273**(50): p. 33741-9.
60. Yoshida, H., et al., *XBP1 mRNA is induced by ATF6 and spliced by IRE1 in response to ER stress to produce a highly active transcription factor*. Cell, 2001. **107**(7): p. 881-91.
61. Yamamoto, K., et al., *Transcriptional induction of mammalian ER quality control proteins is mediated by single or combined action of ATF6alpha and XBP1*. Dev Cell, 2007. **13**(3): p. 365-76.
62. Sano, R. and J.C. Reed, *ER stress-induced cell death mechanisms*. Biochim Biophys Acta, 2013.
63. Kaufman, R.J., *Orchestrating the unfolded protein response in health and disease*. J Clin Invest, 2002. **110**(10): p. 1389-98.
64. Doyle, K.M., et al., *Unfolded proteins and endoplasmic reticulum stress in neurodegenerative disorders*. J Cell Mol Med, 2011. **15**(10): p. 2025-39.
65. Ozcan, U., et al., *Chemical chaperones reduce ER stress and restore glucose homeostasis in a mouse model of type 2 diabetes*. Science, 2006. **313**(5790): p. 1137-40.
66. Ozcan, U., et al., *Endoplasmic reticulum stress links obesity, insulin action, and type 2 diabetes*. Science, 2004. **306**(5695): p. 457-61.
67. Nakamura, T., et al., *Double-stranded RNA-dependent protein kinase links pathogen sensing with stress and metabolic homeostasis*. Cell, 2010. **140**(3): p. 338-48.
68. Rath, E., et al., *Induction of dsRNA-activated protein kinase links mitochondrial unfolded protein response to the pathogenesis of intestinal inflammation*. Gut, 2012. **61**(9): p. 1269-78.
69. Huang, C.J., et al., *Induction of endoplasmic reticulum stress-induced beta-cell apoptosis and accumulation of polyubiquitinated proteins by human islet amyloid polypeptide*. Am J Physiol Endocrinol Metab, 2007. **293**(6): p. E1656-62.
70. Kharroubi, I., et al., *Free fatty acids and cytokines induce pancreatic beta-cell apoptosis by different mechanisms: role of nuclear factor-kappaB and endoplasmic reticulum stress*. Endocrinology, 2004. **145**(11): p. 5087-96.
71. Harding, H.P., et al., *Diabetes mellitus and exocrine pancreatic dysfunction in perk-/- mice reveals a role for translational control in secretory cell survival*. Mol Cell, 2001. **7**(6): p. 1153-63.
72. Delepine, M., et al., *EIF2AK3, encoding translation initiation factor 2-alpha kinase 3, is mutated in patients with Wolcott-Rallison syndrome*. Nat Genet, 2000. **25**(4): p. 406-9.
73. Koumenis, C., et al., *Regulation of protein synthesis by hypoxia via activation of the endoplasmic reticulum kinase PERK and phosphorylation of the translation initiation factor eIF2alpha*. Mol Cell Biol, 2002. **22**(21): p. 7405-16.
74. Blais, J.D., et al., *Activating transcription factor 4 is translationally regulated by hypoxic stress*. Mol Cell Biol, 2004. **24**(17): p. 7469-82.
75. Romero-Ramirez, L., et al., *XBP1 is essential for survival under hypoxic conditions and is required for tumor growth*. Cancer Res, 2004. **64**(17): p. 5943-7.
76. Schewe, D.M. and J.A. Aguirre-Ghiso, *ATF6alpha-Rheb-mTOR signaling promotes survival of dormant tumor cells in vivo*. Proc Natl Acad Sci U S A, 2008. **105**(30): p. 10519-24.
77. Lee, A.S., *GRP78 induction in cancer: therapeutic and prognostic implications*. Cancer Res, 2007. **67**(8): p. 3496-9.
78. Shkoda, A., et al., *Interleukin-10 blocked endoplasmic reticulum stress in intestinal epithelial cells: impact on chronic inflammation*. Gastroenterology, 2007. **132**(1): p. 190-207.
79. Bertolotti, A., et al., *Increased sensitivity to dextran sodium sulfate colitis in IRE1beta-deficient mice*. J Clin Invest, 2001. **107**(5): p. 585-93.
80. Cao, S.S., et al., *The unfolded protein response and chemical chaperones reduce protein misfolding and colitis in mice*. Gastroenterology, 2013. **144**(5): p. 989-1000 e6.

81. Brandl, K., et al., *Enhanced sensitivity to DSS colitis caused by a hypomorphic Mbtsp1 mutation disrupting the ATF6-driven unfolded protein response*. Proc Natl Acad Sci U S A, 2009. **106**(9): p. 3300-3305.
82. Namba, T., et al., *Positive role of CCAAT/enhancer-binding protein homologous protein, a transcription factor involved in the endoplasmic reticulum stress response in the development of colitis*. Am J Pathol, 2009. **174**(5): p. 1786-98.
83. Berger, E. and D. Haller, *Structure-function analysis of the tertiary bile acid TUDCA for the resolution of endoplasmic reticulum stress in intestinal epithelial cells*. Biochem Biophys Res Commun, 2011. **409**(4): p. 610-5.
84. Park, S.W., et al., *The protein disulfide isomerase AGR2 is essential for production of intestinal mucus*. Proc Natl Acad Sci U S A, 2009. **106**(17): p. 6950-5.
85. Kaser, A., T.E. Adolph, and R.S. Blumberg, *The unfolded protein response and gastrointestinal disease*. Semin Immunopathol, 2013. **35**(3): p. 307-19.
86. Rath, E. and D. Haller, *Inflammation and cellular stress: a mechanistic link between immune-mediated and metabolically driven pathologies*. Eur J Nutr, 2011. **50**(4): p. 219-33.
87. Martinon, F., et al., *TLR activation of the transcription factor XBP1 regulates innate immune responses in macrophages*. Nat Immunol, 2010. **11**(5): p. 411-8.
88. Woo, C.W., et al., *Adaptive suppression of the ATF4-CHOP branch of the unfolded protein response by toll-like receptor signalling*. Nat Cell Biol, 2009. **11**(12): p. 1473-80.
89. Messlik, A., et al., *Loss of Toll-like receptor 2 and 4 leads to differential induction of endoplasmic reticulum stress and proapoptotic responses in the intestinal epithelium under conditions of chronic inflammation*. J Proteome Res, 2009. **8**(10): p. 4406-17.
90. Ogata, M., et al., *Autophagy is activated for cell survival after endoplasmic reticulum stress*. Mol Cell Biol, 2006. **26**(24): p. 9220-31.
91. Jo, E.K., et al., *Roles of autophagy in elimination of intracellular bacterial pathogens*. Front Immunol, 2013. **4**: p. 97.
92. Shanahan, M.T., et al., *Mouse Paneth cell antimicrobial function is independent of Nod2*. Gut, 2013.
93. Bevins, C.L., E.F. Stange, and J. Wehkamp, *Decreased Paneth cell defensin expression in ileal Crohn's disease is independent of inflammation, but linked to the NOD2 1007fs genotype*. Gut, 2009. **58**(6): p. 882-3; discussion 883-4.
94. Cadwell, K., et al., *A key role for autophagy and the autophagy gene Atg16l1 in mouse and human intestinal Paneth cells*. Nature, 2008. **456**(7219): p. 259-63.
95. Werner, T., et al., *Intestinal epithelial cell proteome from wild-type and TNFDeltaARE/WT mice: effect of iron on the development of chronic ileitis*. J Proteome Res, 2009. **8**(7): p. 3252-64.
96. Clavel, T. and D. Haller, *Bacteria- and host-derived mechanisms to control intestinal epithelial cell homeostasis: implications for chronic inflammation*. Inflamm Bowel Dis, 2007. **13**(9): p. 1153-64.
97. Frey, T.G. and C.A. Mannella, *The internal structure of mitochondria*. Trends Biochem Sci, 2000. **25**(7): p. 319-24.
98. Arco, A.D. and J. Satrustegui, *New mitochondrial carriers: an overview*. Cell Mol Life Sci, 2005. **62**(19-20): p. 2204-27.
99. Ryan, M.T. and N. Pfanner, *Hsp70 proteins in protein translocation*. Adv Protein Chem, 2001. **59**: p. 223-42.
100. Wiedemann, N., A.E. Frazier, and N. Pfanner, *The protein import machinery of mitochondria*. J Biol Chem, 2004. **279**(15): p. 14473-6.
101. Hoogenraad, N.J., L.A. Ward, and M.T. Ryan, *Import and assembly of proteins into mitochondria of mammalian cells*. Biochim Biophys Acta, 2002. **1592**(1): p. 97-105.
102. Voos, W. and K. Rottgers, *Molecular chaperones as essential mediators of mitochondrial biogenesis*. Biochim Biophys Acta, 2002. **1592**(1): p. 51-62.
103. Broadley, S.A. and F.U. Hartl, *Mitochondrial stress signaling: a pathway unfolds*. Trends Cell Biol, 2008. **18**(1): p. 1-4.
104. Zhao, Q., et al., *A mitochondrial specific stress response in mammalian cells*. Embo J, 2002. **21**(17): p. 4411-9.
105. Aldridge, J.E., T. Horibe, and N.J. Hoogenraad, *Discovery of genes activated by the mitochondrial unfolded protein response (mtUPR) and cognate promoter elements*. PLoS One, 2007. **2**(9): p. e874.
106. Horibe, T. and N.J. Hoogenraad, *The chop gene contains an element for the positive regulation of the mitochondrial unfolded protein response*. PLoS One, 2007. **2**(9): p. e835.

107. Haynes, C.M. and D. Ron, *The mitochondrial UPR - protecting organelle protein homeostasis*. J Cell Sci, 2010. **123**(Pt 22): p. 3849-55.
108. Pizzo, P. and T. Pozzan, *Mitochondria-endoplasmic reticulum choreography: structure and signaling dynamics*. Trends Cell Biol, 2007. **17**(10): p. 511-7.
109. Gething, M.J., *Role and regulation of the ER chaperone BiP*. Semin Cell Dev Biol, 1999. **10**(5): p. 465-72.
110. Griffiths, E.J. and G.A. Rutter, *Mitochondrial calcium as a key regulator of mitochondrial ATP production in mammalian cells*. Biochim Biophys Acta, 2009. **1787**(11): p. 1324-33.
111. Tu, B.P. and J.S. Weissman, *The FAD- and O₂-dependent reaction cycle of Ero1-mediated oxidative protein folding in the endoplasmic reticulum*. Mol Cell, 2002. **10**(5): p. 983-994.
112. Simmen, T., et al., *Oxidative protein folding in the endoplasmic reticulum: tight links to the mitochondria-associated membrane (MAM)*. Biochim Biophys Acta, 2010. **1798**(8): p. 1465-73.
113. Hori, O., et al., *Transmission of cell stress from endoplasmic reticulum to mitochondria: enhanced expression of Lon protease*. J Cell Biol, 2002. **157**(7): p. 1151-60.
114. Bouman, L., et al., *Parkin is transcriptionally regulated by ATF4: evidence for an interconnection between mitochondrial stress and ER stress*. Cell Death Differ, 2011. **18**(5): p. 769-82.
115. Vannuvel, K., et al., *Functional and morphological impact of ER stress on mitochondria*. J Cell Physiol, 2013. **228**(9): p. 1802-18.
116. Haga, N., et al., *Mitochondria regulate the unfolded protein response leading to cancer cell survival under glucose deprivation conditions*. Cancer Sci, 2010. **101**(5): p. 1125-32.
117. Lim, J.H., et al., *Coupling mitochondrial dysfunction to endoplasmic reticulum stress response: a molecular mechanism leading to hepatic insulin resistance*. Cell Signal, 2009. **21**(1): p. 169-77.
118. Santos, C.X., et al., *Mechanisms and implications of reactive oxygen species generation during the unfolded protein response: roles of endoplasmic reticulum oxidoreductases, mitochondrial electron transport, and NADPH oxidase*. Antioxid Redox Signal, 2009. **11**(10): p. 2409-27.
119. Fukushima, K. and C. Fiocchi, *Paradoxical decrease of mitochondrial DNA deletions in epithelial cells of active ulcerative colitis patients*. American Journal of Physiology-Gastrointestinal and Liver Physiology, 2004. **286**(5): p. G804-G813.
120. Beltran, B., et al., *Mitochondrial dysfunction, persistent oxidative damage, and catalase inhibition in immune cells of naive and treated Crohn's disease*. Inflamm Bowel Dis, 2010. **16**(1): p. 76-86.
121. Barrett, J.C., et al., *Genome-wide association defines more than 30 distinct susceptibility loci for Crohn's disease*. Nat Genet, 2008. **40**(8): p. 955-62.
122. Rinaldo, P., D. Matern, and M.J. Bennett, *Fatty acid oxidation disorders*. Annu Rev Physiol, 2002. **64**: p. 477-502.
123. Shekhawat, P.S., et al., *Spontaneous development of intestinal and colonic atrophy and inflammation in the carnitine-deficient jvs (OCTN2(-/-)) mice*. Mol Genet Metab, 2007. **92**(4): p. 315-24.
124. Roediger, W.E. and S. Nance, *Metabolic induction of experimental ulcerative colitis by inhibition of fatty acid oxidation*. Br J Exp Pathol, 1986. **67**(6): p. 773-82.
125. Kaser, A., S. Zeissig, and R.S. Blumberg, *Inflammatory bowel disease*. Annu Rev Immunol, 2010. **28**: p. 573-621.
126. He, D., et al., *Clostridium difficile toxin A triggers human colonocyte IL-8 release via mitochondrial oxygen radical generation*. Gastroenterology, 2002. **122**(4): p. 1048-57.
127. Kamizato, M., et al., *Interleukin 10 inhibits interferon gamma- and tumor necrosis factor alpha-stimulated activation of NADPH oxidase 1 in human colonic epithelial cells and the mouse colon*. J Gastroenterol, 2009. **44**(12): p. 1172-84.
128. Nazli, A., et al., *Epithelia under metabolic stress perceive commensal bacteria as a threat*. Am J Pathol, 2004. **164**(3): p. 947-57.
129. Schurmann, G., et al., *Transepithelial transport processes at the intestinal mucosa in inflammatory bowel disease*. Int J Colorectal Dis, 1999. **14**(1): p. 41-6.
130. Soderholm, J.D., et al., *Augmented increase in tight junction permeability by luminal stimuli in the non-inflamed ileum of Crohn's disease*. Gut, 2002. **50**(3): p. 307-13.
131. Levy-Rimler, G., et al., *Type I chaperonins: not all are created equal*. FEBS Lett, 2002. **529**(1): p. 1-5.
132. Cheng, M.Y., et al., *Mitochondrial heat-shock protein hsp60 is essential for assembly of proteins imported into yeast mitochondria*. Nature, 1989. **337**(6208): p. 620-5.

133. Ostermann, J., et al., *Protein folding in mitochondria requires complex formation with hsp60 and ATP hydrolysis*. *Nature*, 1989. **341**(6238): p. 125-30.
134. Koll, H., et al., *Antifolding activity of hsp60 couples protein import into the mitochondrial matrix with export to the intermembrane space*. *Cell*, 1992. **68**(6): p. 1163-75.
135. Martin, J., A.L. Horwich, and F.U. Hartl, *Prevention of protein denaturation under heat stress by the chaperonin Hsp60*. *Science*, 1992. **258**(5084): p. 995-8.
136. Kaufman, B.A., et al., *A function for the mitochondrial chaperonin Hsp60 in the structure and transmission of mitochondrial DNA nucleoids in Saccharomyces cerevisiae*. *J Cell Biol*, 2003. **163**(3): p. 457-61.
137. Hallberg, E.M., Y. Shu, and R.L. Hallberg, *Loss of mitochondrial hsp60 function: nonequivalent effects on matrix-targeted and intermembrane-targeted proteins*. *Mol Cell Biol*, 1993. **13**(5): p. 3050-7.
138. Christensen, J.H., et al., *Inactivation of the hereditary spastic paraplegia-associated Hspd1 gene encoding the Hsp60 chaperone results in early embryonic lethality in mice*. *Cell Stress Chaperones*, 2010. **15**(6): p. 851-63.
139. Magen, D., et al., *Mitochondrial hsp60 chaperonopathy causes an autosomal-recessive neurodegenerative disorder linked to brain hypomyelination and leukodystrophy*. *Am J Hum Genet*, 2008. **83**(1): p. 30-42.
140. Hansen, J.J., et al., *Hereditary spastic paraplegia SPG13 is associated with a mutation in the gene encoding the mitochondrial chaperonin Hsp60*. *Am J Hum Genet*, 2002. **70**(5): p. 1328-1332.
141. Hansen, J., et al., *A novel mutation in the HSPD1 gene in a patient with hereditary spastic paraplegia*. *J Neurol*, 2007. **254**(7): p. 897-900.
142. Braig, K., et al., *The crystal structure of the bacterial chaperonin GroEL at 2.8 Å*. *Nature*, 1994. **371**(6498): p. 578-86.
143. Chen, S., et al., *Location of a folding protein and shape changes in GroEL-GroES complexes imaged by cryo-electron microscopy*. *Nature*, 1994. **371**(6494): p. 261-4.
144. Hunt, J.F., et al., *The crystal structure of the GroES co-chaperonin at 2.8 Å resolution*. *Nature*, 1996. **379**(6560): p. 37-45.
145. Mande, S.C., et al., *Structure of the heat shock protein chaperonin-10 of Mycobacterium leprae*. *Science*, 1996. **271**(5246): p. 203-7.
146. Parnas, A., et al., *Identification of elements that dictate the specificity of mitochondrial Hsp60 for its co-chaperonin*. *PLoS One*, 2012. **7**(12): p. e50318.
147. Hartl, F.U., *Molecular chaperones in cellular protein folding*. *Nature*, 1996. **381**(6583): p. 571-9.
148. Horwich, A.L., G.W. Farr, and W.A. Fenton, *GroEL-GroES-mediated protein folding*. *Chem Rev*, 2006. **106**(5): p. 1917-30.
149. Horovitz, A., *Structural aspects of GroEL function*. *Curr Opin Struct Biol*, 1998. **8**(1): p. 93-100.
150. Levy-Rimler, G., et al., *The effect of nucleotides and mitochondrial chaperonin 10 on the structure and chaperone activity of mitochondrial chaperonin 60*. *Eur J Biochem*, 2001. **268**(12): p. 3465-72.
151. Hansen, J.J., et al., *Genomic structure of the human mitochondrial chaperonin genes: HSP60 and HSP10 are localised head to head on chromosome 2 separated by a bidirectional promoter*. *Hum Genet*, 2003. **112**(1): p. 71-7.
152. Ghosh, J.C., et al., *Hsp60 regulation of tumor cell apoptosis*. *J Biol Chem*, 2008. **283**(8): p. 5188-94.
153. Deocaris, C.C., S.C. Kaul, and R. Wadhwa, *On the brotherhood of the mitochondrial chaperones mortalin and heat shock protein 60*. *Cell Stress Chaperones*, 2006. **11**(2): p. 116-28.
154. Kirchhoff, S.R., S. Gupta, and A.A. Knowlton, *Cytosolic heat shock protein 60, apoptosis, and myocardial injury*. *Circulation*, 2002. **105**(24): p. 2899-904.
155. Gupta, S. and A.A. Knowlton, *Cytosolic heat shock protein 60, hypoxia, and apoptosis*. *Circulation*, 2002. **106**(21): p. 2727-33.
156. Chun, J.N., et al., *Cytosolic Hsp60 is involved in the NF-kappaB-dependent survival of cancer cells via IKK regulation*. *PLoS One*, 2010. **5**(3): p. e9422.
157. Chandra, D., G. Choy, and D.G. Tang, *Cytosolic accumulation of HSP60 during apoptosis with or without apparent mitochondrial release: evidence that its pro-apoptotic or pro-survival functions involve differential interactions with caspase-3*. *J Biol Chem*, 2007. **282**(43): p. 31289-301.
158. Itoh, H., et al., *Mammalian HSP60 is quickly sorted into the mitochondria under conditions of dehydration*. *Eur J Biochem*, 2002. **269**(23): p. 5931-8.

159. Soltys, B.J. and R.S. Gupta, *Cell surface localization of the 60 kDa heat shock chaperonin protein (hsp60) in mammalian cells*. Cell Biol Int, 1997. **21**(5): p. 315-20.
160. Piselli, P., et al., *Different expression of CD44, ICAM-1, and HSP60 on primary tumor and metastases of a human pancreatic carcinoma growing in scid mice*. Anticancer Res, 2000. **20**(2A): p. 825-31.
161. Feng, H., et al., *Stressed apoptotic tumor cells stimulate dendritic cells and induce specific cytotoxic T cells*. Blood, 2002. **100**(12): p. 4108-15.
162. Shin, B.K., et al., *Global profiling of the cell surface proteome of cancer cells uncovers an abundance of proteins with chaperone function*. J Biol Chem, 2003. **278**(9): p. 7607-16.
163. Belles, C., et al., *Plasma membrane expression of heat shock protein 60 in vivo in response to infection*. Infect Immun, 1999. **67**(8): p. 4191-200.
164. Torok, Z., et al., *Evidence for a lipochaperonin: association of active protein-folding GroESL oligomers with lipids can stabilize membranes under heat shock conditions*. Proc Natl Acad Sci U S A, 1997. **94**(6): p. 2192-7.
165. Osterloh, A., et al., *Lipopolysaccharide-free heat shock protein 60 activates T cells*. J Biol Chem, 2004. **279**(46): p. 47906-11.
166. Campanella, C., et al., *The odyssey of Hsp60 from tumor cells to other destinations includes plasma membrane-associated stages and Golgi and exosomal protein-trafficking modalities*. PLoS One, 2012. **7**(7): p. e42008.
167. Merendino, A.M., et al., *Hsp60 is actively secreted by human tumor cells*. PLoS One, 2010. **5**(2): p. e9247.
168. Hayoun, D., et al., *HSP60 is transported through the secretory pathway of 3-MCA-induced fibrosarcoma tumour cells and undergoes N-glycosylation*. FEBS J, 2012. **279**(12): p. 2083-95.
169. Bassan, M., et al., *The identification of secreted heat shock 60 -like protein from rat glial cells and a human neuroblastoma cell line*. Neurosci Lett, 1998. **250**(1): p. 37-40.
170. Pockley, A.G., et al., *Identification of human heat shock protein 60 (Hsp60) and anti-Hsp60 antibodies in the peripheral circulation of normal individuals*. Cell Stress Chaperones, 1999. **4**(1): p. 29-35.
171. Lewthwaite, J., et al., *Circulating human heat shock protein 60 in the plasma of British civil servants: relationship to physiological and psychosocial stress*. Circulation, 2002. **106**(2): p. 196-201.
172. Shamaei-Tousi, A., et al., *Differential regulation of circulating levels of molecular chaperones in patients undergoing treatment for periodontal disease*. PLoS One, 2007. **2**(11): p. e1198.
173. Rizzo, M., et al., *Heat-shock protein 60 kDa and atherogenic dyslipidemia in patients with untreated mild periodontitis: a pilot study*. Cell Stress Chaperones, 2012. **17**(3): p. 399-407.
174. Gao, Y. and Z.P. Guo, *[Expression of HSP60, TLR4 and NF-kappaBp65 in the peripheral blood of patients with atopic dermatitis]*. Sichuan Da Xue Xue Bao Yi Xue Ban, 2009. **40**(4): p. 655-7.
175. Marino Gammazza, A., et al., *Elevated blood Hsp60, its structural similarities and cross-reactivity with thyroid molecules, and its presence on the plasma membrane of oncocytes point to the chaperonin as an immunopathogenic factor in Hashimoto's thyroiditis*. Cell Stress Chaperones, 2013.
176. Anraku, I., et al., *Circulating heat shock protein 60 levels are elevated in HIV patients and are reduced by anti-retroviral therapy*. PLoS One, 2012. **7**(9): p. e45291.
177. Marker, T., et al., *Heat shock protein 60 as a mediator of adipose tissue inflammation and insulin resistance*. Diabetes, 2012. **61**(3): p. 615-25.
178. Xu, Q., et al., *Serum soluble heat shock protein 60 is elevated in subjects with atherosclerosis in a general population*. Circulation, 2000. **102**(1): p. 14-20.
179. Pockley, A.G., et al., *Circulating heat shock protein 60 is associated with early cardiovascular disease*. Hypertension, 2000. **36**(2): p. 303-7.
180. Shamaei-Tousi, A., et al., *Plasma heat shock protein 60 and cardiovascular disease risk: the role of psychosocial, genetic, and biological factors*. Cell Stress Chaperones, 2007. **12**(4): p. 384-92.
181. Chen, W., et al., *Human 60-kDa heat-shock protein: a danger signal to the innate immune system*. J Immunol, 1999. **162**(6): p. 3212-9.
182. Flohe, S.B., et al., *Human heat shock protein 60 induces maturation of dendritic cells versus a Th1-promoting phenotype*. J Immunol, 2003. **170**(5): p. 2340-8.
183. Kol, A., et al., *Chlamydial and human heat shock protein 60s activate human vascular endothelium, smooth muscle cells, and macrophages*. J Clin Invest, 1999. **103**(4): p. 571-7.

184. Gobert, A.P., et al., *Helicobacter pylori* heat shock protein 60 mediates interleukin-6 production by macrophages via a toll-like receptor (TLR)-2-, TLR-4-, and myeloid differentiation factor 88-independent mechanism. *J Biol Chem*, 2004. **279**(1): p. 245-50.
185. Vabulas, R.M., et al., *Endocytosed HSP60s use toll-like receptor 2 (TLR2) and TLR4 to activate the toll/interleukin-1 receptor signaling pathway in innate immune cells*. *J Biol Chem*, 2001. **276**(33): p. 31332-9.
186. Tian, J., et al., *Extracellular HSP60 induces inflammation through activating and up-regulating TLRs in cardiomyocytes*. *Cardiovasc Res*, 2013. **98**(3): p. 391-401.
187. Habich, C. and V. Burkart, *Heat shock protein 60: regulatory role on innate immune cells*. *Cell Mol Life Sci*, 2007. **64**(6): p. 742-51.
188. Marker, T., et al., *Heat shock protein 60 and adipocytes: characterization of a ligand-receptor interaction*. *Biochem Biophys Res Commun*, 2010. **391**(4): p. 1634-40.
189. Peetermans, W.E., et al., *Mycobacterial 65-kilodalton heat shock protein induces tumor necrosis factor alpha and interleukin 6, reactive nitrogen intermediates, and toxoplasma activity in murine peritoneal macrophages*. *Infect Immun*, 1995. **63**(9): p. 3454-8.
190. Chopra, U., et al., *TH1 pattern of cytokine secretion by splenic cells from pyelonephritic mice after in-vitro stimulation with hsp-65 of Escherichia coli*. *J Med Microbiol*, 1997. **46**(2): p. 139-44.
191. Sharma, S.A., et al., *T-cell, antibody, and cytokine responses to homologs of the 60-kilodalton heat shock protein in Helicobacter pylori infection*. *Clin Diagn Lab Immunol*, 1997. **4**(4): p. 440-6.
192. Hinode, D., et al., *The GroEL-like protein from Campylobacter rectus: immunological characterization and interleukin-6 and -8 induction in human gingival fibroblast*. *FEMS Microbiol Lett*, 1998. **167**(1): p. 1-6.
193. de Graeff-Meeder, E.R., et al., *Antibodies to human HSP60 in patients with juvenile chronic arthritis, diabetes mellitus, and cystic fibrosis*. *Pediatr Res*, 1993. **34**(4): p. 424-8.
194. de Graeff-Meeder, E.R., et al., *Juvenile chronic arthritis: T cell reactivity to human HSP60 in patients with a favorable course of arthritis*. *J Clin Invest*, 1995. **95**(3): p. 934-40.
195. Grundtman, C. and G. Wick, *The autoimmune concept of atherosclerosis*. *Curr Opin Lipidol*, 2011. **22**(5): p. 327-34.
196. Johnson, B.J., et al., *Heat shock protein 10 inhibits lipopolysaccharide-induced inflammatory mediator production*. *J Biol Chem*, 2005. **280**(6): p. 4037-47.
197. Morton, H., *Early pregnancy factor: an extracellular chaperonin 10 homologue*. *Immunol Cell Biol*, 1998. **76**(6): p. 483-96.
198. Rodolico, V., et al., *Hsp60 and Hsp10 increase in colon mucosa of Crohn's disease and ulcerative colitis*. *Cell Stress Chaperones*, 2010. **15**(6): p. 877-84.
199. Puga Yung, G.L., et al., *Heat shock protein-derived T-cell epitopes contribute to autoimmune inflammation in pediatric Crohn's disease*. *PLoS One*, 2009. **4**(11): p. e7714.
200. Tomasello, G., et al., *Changes in immunohistochemical levels and subcellular localization after therapy and correlation and colocalization with CD68 suggest a pathogenetic role of Hsp60 in ulcerative colitis*. *Appl Immunohistochem Mol Morphol*, 2011. **19**(6): p. 552-61.
201. Di Felice, V., et al., *Senescence-associated HSP60 expression in normal human skin fibroblasts*. *Anat Rec A Discov Mol Cell Evol Biol*, 2005. **284**(1): p. 446-53.
202. Cappello, F. and G. Zummo, *HSP60 expression during carcinogenesis: a molecular "proteus" of carcinogenesis?* *Cell Stress Chaperones*, 2005. **10**(4): p. 263-4.
203. Cappello, F. and G. Zummo, *HSP60 expression during carcinogenesis: where is the pilot?* *Pathol Res Pract*, 2006. **202**(5): p. 401-2.
204. Wadhwa, R., et al., *Identification and characterization of molecular interactions between mortalin/mtHsp70 and HSP60*. *Biochem J*, 2005. **391**(Pt 2): p. 185-90.
205. Thomas, X., et al., *Expression of heat-shock proteins is associated with major adverse prognostic factors in acute myeloid leukemia*. *Leuk Res*, 2005. **29**(9): p. 1049-58.
206. Faried, A., et al., *Expression of heat-shock protein Hsp60 correlated with the apoptotic index and patient prognosis in human oesophageal squamous cell carcinoma*. *Eur J Cancer*, 2004. **40**(18): p. 2804-11.
207. Lebre, T., et al., *Heat shock proteins HSP27, HSP60, HSP70, and HSP90: expression in bladder carcinoma*. *Cancer*, 2003. **98**(5): p. 970-7.
208. Bajramovic, J.J., et al., *The stress kit: a new method based on competitive reverse transcriptase-polymerase chain reaction to quantify the expression of human alphaB-crystallin, Hsp27, and Hsp60*. *Cell Stress Chaperones*, 2000. **5**(1): p. 30-5.
209. Cappello, F., et al., *Immunopositivity of heat shock protein 60 as a biomarker of bronchial carcinogenesis*. *Lancet Oncol*, 2005. **6**(10): p. 816.

210. Yamasaki, R., et al., *Immune response in Helicobacter pylori-induced low-grade gastric-mucosa-associated lymphoid tissue (MALT) lymphoma*. J Med Microbiol, 2004. **53**(Pt 1): p. 21-9.
211. Cappello, F., et al., *60KDa chaperonin (HSP60) is over-expressed during colorectal carcinogenesis*. Eur J Histochem, 2003. **47**(2): p. 105-10.
212. Cappello, F., et al., *The expression of HSP60 and HSP10 in large bowel carcinomas with lymph node metastase*. BMC Cancer, 2005. **5**: p. 139.
213. He, Y., et al., *Proteomics-based identification of HSP60 as a tumor-associated antigen in colorectal cancer*. Proteomics Clin Appl, 2007. **1**(3): p. 336-42.
214. Kuramitsu, Y. and K. Nakamura, *Current progress in proteomic study of hepatitis C virus-related human hepatocellular carcinoma*. Expert Rev Proteomics, 2005. **2**(4): p. 589-601.
215. Cappello, F., et al., *Immunohistochemical evaluation of PCNA, p53, HSP60, HSP10 and MUC-2 presence and expression in prostate carcinogenesis*. Anticancer Res, 2003. **23**(2B): p. 1325-31.
216. Cappello, F., et al., *Expression of 60-kD heat shock protein increases during carcinogenesis in the uterine exocervix*. Pathobiology, 2002. **70**(2): p. 83-8.
217. Cappello, F., et al., *Hsp60 expression, new locations, functions and perspectives for cancer diagnosis and therapy*. Cancer Biol Ther, 2008. **7**(6): p. 801-9.
218. Luo, S., et al., *GRP78/BiP is required for cell proliferation and protecting the inner cell mass from apoptosis during early mouse embryonic development*. Mol Cell Biol, 2006. **26**(15): p. 5688-97.
219. Kontoyiannis, D., et al., *Interleukin-10 targets p38 MAPK to modulate ARE-dependent TNF mRNA translation and limit intestinal pathology*. EMBO J, 2001. **20**(14): p. 3760-70.
220. Sauer, B., *Functional expression of the cre-lox site-specific recombination system in the yeast Saccharomyces cerevisiae*. Mol Cell Biol, 1987. **7**(6): p. 2087-96.
221. Sauer, B. and N. Henderson, *Site-specific DNA recombination in mammalian cells by the Cre recombinase of bacteriophage P1*. Proc Natl Acad Sci U S A, 1988. **85**(14): p. 5166-70.
222. Feil, R., et al., *Ligand-activated site-specific recombination in mice*. Proc Natl Acad Sci U S A, 1996. **93**(20): p. 10887-90.
223. Indra, A.K., et al., *Temporally-controlled site-specific mutagenesis in the basal layer of the epidermis: comparison of the recombinase activity of the tamoxifen-inducible Cre-ER(T) and Cre-ER(T2) recombinases*. Nucleic Acids Res, 1999. **27**(22): p. 4324-7.
224. el Marjou, F., et al., *Tissue-specific and inducible Cre-mediated recombination in the gut epithelium*. Genesis, 2004. **39**(3): p. 186-93.
225. Barker, N., et al., *Identification of stem cells in small intestine and colon by marker gene Lgr5*. Nature, 2007. **449**(7165): p. 1003-7.
226. Schicho, R., et al., *Hydrogen sulfide is a novel prosecretory neuromodulator in the Guinea-pig and human colon*. Gastroenterology, 2006. **131**(5): p. 1542-52.
227. Moolenbeek, C. and E.J. Ruitenbergh, *The "Swiss roll": a simple technique for histological studies of the rodent intestine*. Lab Anim, 1981. **15**(1): p. 57-9.
228. Ferraris, R.P. and J. Diamond, *Crypt-villus site of glucose transporter induction by dietary carbohydrate in mouse intestine*. Am J Physiol, 1992. **262**(6 Pt 1): p. G1069-73.
229. Mariadason, J.M., et al., *Gene expression profiling of intestinal epithelial cell maturation along the crypt-villus axis*. Gastroenterology, 2005. **128**(4): p. 1081-8.
230. Vidal, K., et al., *Immortalization of mouse intestinal epithelial cells by the SV40-large T gene. Phenotypic and immune characterization of the MODE-K cell line*. J Immunol Methods, 1993. **166**(1): p. 63-73.
231. Bertani, G., *Studies on lysogenesis. I. The mode of phage liberation by lysogenic Escherichia coli*. J Bacteriol, 1951. **62**(3): p. 293-300.
232. de Almeida, S.F., et al., *Chemical chaperones reduce endoplasmic reticulum stress and prevent mutant HFE aggregate formation*. J Biol Chem, 2007. **282**(38): p. 27905-12.
233. Laemmli, U.K., *Cleavage of structural proteins during the assembly of the head of bacteriophage T4*. Nature, 1970. **227**(5259): p. 680-5.
234. Dai, M., et al., *Evolving gene/transcript definitions significantly alter the interpretation of GeneChip data*. Nucleic Acids Res, 2005. **33**(20): p. e175.
235. Bolstad, B.M., et al., *A comparison of normalization methods for high density oligonucleotide array data based on variance and bias*. Bioinformatics, 2003. **19**(2): p. 185-93.
236. Irizarry, R.A., et al., *Summaries of Affymetrix GeneChip probe level data*. Nucleic Acids Res, 2003. **31**(4): p. e15.

237. Sartor, M.A., et al., *Intensity-based hierarchical Bayes method improves testing for differentially expressed genes in microarray experiments*. BMC Bioinformatics, 2006. **7**: p. 538.
238. Storey, J.D. and R. Tibshirani, *Statistical significance for genomewide studies*. Proc Natl Acad Sci U S A, 2003. **100**(16): p. 9440-5.
239. Lin, K., et al., *MADMAX - Management and analysis database for multiple -omics experiments*. J Integr Bioinform, 2011. **8**(2): p. 160.
240. Noah, T.K., B. Donahue, and N.F. Shroyer, *Intestinal development and differentiation*. Exp Cell Res, 2011. **317**(19): p. 2702-10.
241. Piao, X., et al., *c-FLIP maintains tissue homeostasis by preventing apoptosis and programmed necrosis*. Sci Signal, 2012. **5**(255): p. ra93.
242. Kwon, M.C., et al., *Essential role of CR6-interacting factor 1 (Crif1) in E74-like factor 3 (ELF3)-mediated intestinal development*. J Biol Chem, 2009. **284**(48): p. 33634-41.
243. Zhong, Z., et al., *Lrp5 and Lrp6 play compensatory roles in mouse intestinal development*. J Cell Biochem, 2012. **113**(1): p. 31-8.
244. Kolodziejczak, D., et al., *Mice lacking the intestinal peptide transporter display reduced energy intake and a subtle maldigestion/malabsorption that protects them from diet-induced obesity*. Am J Physiol Gastrointest Liver Physiol, 2013. **304**(10): p. G897-907.
245. Crawford, P.A. and J.I. Gordon, *Microbial regulation of intestinal radiosensitivity*. Proc Natl Acad Sci U S A, 2005. **102**(37): p. 13254-9.
246. Schneider, M.R., et al., *A key role for E-cadherin in intestinal homeostasis and Paneth cell maturation*. PLoS One, 2010. **5**(12): p. e14325.
247. Blanchette-Mackie, E.J., et al., *Perilipin is located on the surface layer of intracellular lipid droplets in adipocytes*. J Lipid Res, 1995. **36**(6): p. 1211-26.
248. Kim, K.H., et al., *Rescue of PINK1 protein null-specific mitochondrial complex IV deficits by ginsenoside Re activation of nitric oxide signaling*. J Biol Chem, 2012. **287**(53): p. 44109-20.
249. Zheng, X., et al., *GroEL, GroES, and ATP-dependent folding and spontaneous assembly of ornithine transcarbamylase*. J Biol Chem, 1993. **268**(10): p. 7489-93.
250. Marciniak, S.J., et al., *CHOP induces death by promoting protein synthesis and oxidation in the stressed endoplasmic reticulum*. Genes Dev, 2004. **18**(24): p. 3066-77.
251. Shinkai, Y., C. Yamamoto, and T. Kaji, *Lead induces the expression of endoplasmic reticulum chaperones GRP78 and GRP94 in vascular endothelial cells via the JNK-AP-1 pathway*. Toxicol Sci, 2010. **114**(2): p. 378-86.
252. Cabisco, E., et al., *Mitochondrial Hsp60, resistance to oxidative stress, and the labile iron pool are closely connected in Saccharomyces cerevisiae*. J Biol Chem, 2002. **277**(46): p. 44531-8.
253. Gozzelino, R., V. Jeney, and M.P. Soares, *Mechanisms of cell protection by heme oxygenase-1*. Annu Rev Pharmacol Toxicol, 2010. **50**: p. 323-54.
254. Takada, M., et al., *Overexpression of a 60-kDa heat shock protein enhances cytoprotective function of small intestinal epithelial cells*. Life Sci, 2010. **86**(13-14): p. 499-504.
255. Ishikawa, F., et al., *Gene expression profiling identifies a role for CHOP during inhibition of the mitochondrial respiratory chain*. J Biochem, 2009. **146**(1): p. 123-32.
256. Bruhat, A., et al., *Amino acids control mammalian gene transcription: activating transcription factor 2 is essential for the amino acid responsiveness of the CHOP promoter*. Mol Cell Biol, 2000. **20**(19): p. 7192-204.
257. Guyton, K.Z., Q. Xu, and N.J. Holbrook, *Induction of the mammalian stress response gene GADD153 by oxidative stress: role of AP-1 element*. Biochem J, 1996. **314** (Pt 2): p. 547-54.
258. Barone, M.V., et al., *CHOP (GADD153) and its oncogenic variant, TLS-CHOP, have opposing effects on the induction of G1/S arrest*. Genes Dev, 1994. **8**(4): p. 453-64.
259. Maytin, E.V., et al., *Stress-inducible transcription factor CHOP/gadd153 induces apoptosis in mammalian cells via p38 kinase-dependent and -independent mechanisms*. Exp Cell Res, 2001. **267**(2): p. 193-204.
260. Jousse, C., et al., *TRB3 inhibits the transcriptional activation of stress-regulated genes by a negative feedback on the ATF4 pathway*. J Biol Chem, 2007. **282**(21): p. 15851-61.
261. Ohoka, N., et al., *TRB3, a novel ER stress-inducible gene, is induced via ATF4-CHOP pathway and is involved in cell death*. EMBO J, 2005. **24**(6): p. 1243-55.
262. Li, G., et al., *Role of ERO1- α -mediated stimulation of inositol 1,4,5-triphosphate receptor activity in endoplasmic reticulum stress-induced apoptosis*. J Cell Biol, 2009. **186**(6): p. 783-92.
263. McCullough, K.D., et al., *Gadd153 sensitizes cells to endoplasmic reticulum stress by down-regulating Bcl2 and perturbing the cellular redox state*. Mol Cell Biol, 2001. **21**(4): p. 1249-59.

264. Shimizu, K., et al., *Stress-inducible caspase substrate TRB3 promotes nuclear translocation of procaspase-3*. PLoS One, 2012. **7**(8): p. e42721.
265. Karam, S.M., *Lineage commitment and maturation of epithelial cells in the gut*. Front Biosci, 1999. **4**: p. D286-98.
266. Bie, A.S., et al., *A cell model to study different degrees of Hsp60 deficiency in HEK293 cells*. Cell Stress Chaperones, 2011. **16**(6): p. 633-40.
267. Tsai, Y.P., et al., *Interaction between HSP60 and beta-catenin promotes metastasis*. Carcinogenesis, 2009. **30**(6): p. 1049-57.
268. Horndasch, M., et al., *The C/EBP homologous protein CHOP (GADD153) is an inhibitor of Wnt/TCF signals*. Oncogene, 2006. **25**(24): p. 3397-407.
269. Heijmans, J., et al., *ER stress causes rapid loss of intestinal epithelial stemness through activation of the unfolded protein response*. Cell Rep, 2013. **3**(4): p. 1128-39.
270. Backer, M.V., J.M. Backer, and P. Chinnaiyan, *Targeting the unfolded protein response in cancer therapy*. Methods Enzymol, 2011. **491**: p. 37-56.
271. Prabhu, A., et al., *Targeting the unfolded protein response in glioblastoma cells with the fusion protein EGF-SubA*. PLoS One, 2012. **7**(12): p. e52265.
272. Firczuk, M., et al., *GRP78-targeting subtilase cytotoxin sensitizes cancer cells to photodynamic therapy*. Cell Death Dis, 2013. **4**: p. e741.
273. Dehmer, J.J., et al., *Expansion of intestinal epithelial stem cells during murine development*. PLoS One, 2011. **6**(11): p. e27070.
274. Madison, B.B., et al., *Cis elements of the villin gene control expression in restricted domains of the vertical (crypt) and horizontal (duodenum, cecum) axes of the intestine*. J Biol Chem, 2002. **277**(36): p. 33275-83.
275. Pinto, D., et al., *Regulatory sequences of the mouse villin gene that efficiently drive transgenic expression in immature and differentiated epithelial cells of small and large intestines*. J Biol Chem, 1999. **274**(10): p. 6476-82.
276. Rasoulpour, R.J. and K. Boekelheide, *The Sycp1-Cre transgenic mouse and male germ cell inhibition of NF-kappa b*. J Androl, 2006. **27**(6): p. 729-33.
277. Glaser, S.P., et al., *Anti-apoptotic Mcl-1 is essential for the development and sustained growth of acute myeloid leukemia*. Genes Dev, 2012. **26**(2): p. 120-5.
278. Moser, A.R., H.C. Pitot, and W.F. Dove, *A dominant mutation that predisposes to multiple intestinal neoplasia in the mouse*. Science, 1990. **247**(4940): p. 322-4.
279. Pinto, D., et al., *Canonical Wnt signals are essential for homeostasis of the intestinal epithelium*. Genes Dev, 2003. **17**(14): p. 1709-13.
280. Hua, G., et al., *Crypt base columnar stem cells in small intestines of mice are radioresistant*. Gastroenterology, 2012. **143**(5): p. 1266-76.
281. Muncan, V., et al., *Rapid loss of intestinal crypts upon conditional deletion of the Wnt/Tcf-4 target gene c-Myc*. Mol Cell Biol, 2006. **26**(22): p. 8418-26.
282. van der Flier, L.G., et al., *Transcription factor achaete scute-like 2 controls intestinal stem cell fate*. Cell, 2009. **136**(5): p. 903-12.
283. van Es, J.H., et al., *A critical role for the Wnt effector Tcf4 in adult intestinal homeostatic self-renewal*. Mol Cell Biol, 2012. **32**(10): p. 1918-27.
284. Tsai, Y.P., S.C. Teng, and K.J. Wu, *Direct regulation of HSP60 expression by c-MYC induces transformation*. FEBS Lett, 2008. **582**(29): p. 4083-8.
285. Zhao, J., et al., *R-spondin1, a novel intestinotrophic mitogen, ameliorates experimental colitis in mice*. Gastroenterology, 2007. **132**(4): p. 1331-43.
286. Sato, T., et al., *Paneth cells constitute the niche for Lgr5 stem cells in intestinal crypts*. Nature, 2011. **469**(7330): p. 415-8.
287. Hattori, T., et al., *C/EBP homologous protein (CHOP) up-regulates IL-6 transcription by trapping negative regulating NF-IL6 isoform*. FEBS Lett, 2003. **541**(1-3): p. 33-9.
288. Gulow, K., D. Bienert, and I.G. Haas, *BiP is feed-back regulated by control of protein translation efficiency*. J Cell Sci, 2002. **115**(Pt 11): p. 2443-52.
289. Chang, J.S., et al., *Endoplasmic reticulum stress response promotes cytotoxic phenotype of CD8alpha-beta+ intraepithelial lymphocytes in a mouse model for Crohn's disease-like ileitis*. J Immunol, 2012. **189**(3): p. 1510-20.
290. Steck, N., et al., *Bacterial proteases in IBD and IBS*. Gut, 2012. **61**(11): p. 1610-8.
291. Baur, P., et al., *Metabolic phenotyping of the Crohn's disease-like IBD etiopathology in the TNF(DeltaARE/WT) mouse model*. J Proteome Res, 2011. **10**(12): p. 5523-35.
292. Ma, Y. and L.M. Hendershot, *The role of the unfolded protein response in tumour development: friend or foe?* Nat Rev Cancer, 2004. **4**(12): p. 966-77.

ACKNOWLEDGEMENTS

First, I want to express my gratitude to Prof. Dirk Haller for offering me the possibility to explore the interesting and diversified tasks of performing basic science within the scope of a doctoral research study at his chair. These tasks comprised independent experimental design and conducting within an international research team, scientific publishing and presentation at national and international conferences as well as education of students. All this was enabled by Prof. Haller's financial and personal support, for which he deserves great acknowledgement.

Furthermore, I want to thank the numerous collaborators involved in my PhD project for their competent support: Prof. Mathias Heikenwälder, Detian Yuan, Nicole Simonavicius, PD Klaus-Peter Janssen, Prof. Markus Gerhard, Michael Allgäuer, Prof. Achim Weber, Prof. Michael Müller, Mark Boekschoten, Prof. Marco Prinz, Ori Staszewski, Prof. Jan Wehkamp, Maureen Ostaff, Prof. Martin Klingenspor, Theresa Schöttl, Christoph Hoffmann, Prof. Hannelore Daniel, Pia Röder, Veronika Müller and Prof. Michael Schemann.

I am deeply thankful for the help and support of the "UPR team" comprising Eva Rath, Nadine Waldschmitt and Elena Lobner, who accompanied me with their competent advice and experience over the years. Beyond planning and discussing experiments, they were always on the spot, when I needed a helping hand in the lab.

Besides them, all of my colleagues presently working at the chair of Nutrition and Immunology (formerly Biofunctionality) deserve acknowledgement for their kindness and cooperativeness: Thomas Clavel, Gabi Hörmannspurger, Sigrid Kisling, Tiago Nunes, Irina Sava-Piroddi, Ingrid Schmöller, Monika Bazanella, Jelena Calasan, Jana Hemmerling, Sarah Just, Amira Metwaly, Sören Ocvirk, Monika Schaubeck, Annemarie Schmidt, Valentina Schüppel, Hongsup Yoon, Nico Gebhardt, Silvia Pitariu, Melanie Klein, Simone Daxauer, Sandra Henning, Caroline Ziegler, Alexandra Buse, Brita Sturm and Sonja Böhm. Also my former colleagues Pedro A. Ruiz-Castro, Susan Chang, Micha Hoffmann, Anja Messlik, Tanja Werner, Lisa Gruber, Marie-Anne von Schillde, Pia Baur, Natalie Steck, Stephanie May, Job Mapesa, Stefan Wagner, Katharina Heller, Anna Zhenchuk, Katharina Rank, Benjamin Thiemann and Theresa Asen deserve my appreciation.

Many thanks to Sarah Lehmann, Julia Rieker and Julia Wiesner for their committed collaboration on my PhD project in the scope of their Bachelor Thesis and practical course, respectively.

Furthermore, I want to express my personal gratitude to my present and former office-mates Marie-Anne von Schillde, Natalie Steck, Lisa Gruber, Pia Lichti, Jana Hemmerling and Sören Ocvirk, who became good friends over the years. Many thanks for your kindness and best wishes for the future!

Finally, I want to thank my Mom and Dad as well as my brother Simon for accompanying my long years of studies and the present doctoral work with their kind all-round support and their great patience. They deserve my perfect appreciation.

CURRICULUM VITAE

Personal information

Name	Emanuel Clemens Berger
Date of birth	July 7 th 1983 in Munich, Germany
Citizenship	German
Address	Vöttinger Strasse 34, 85354 Freising, Germany
Email	emanuel.berger@tum.de, emanuelberger@gmx.net
Phone	+49-(0)8161-712377, +49-(0)172-1365876

Work experience

Since 05/2008 Postgraduate/ scientific employee at the chair of nutrition and immunology at the Technical University of Munich

Topic of the PhD thesis: "Impact of unfolded protein responses on intestinal epithelial homeostasis in genetically modified mouse models"

Studies and education

10/2006 – 04/2008	Molecular Biotechnology (Master degree course) at the Technical University of Munich Degree: Master of Science (MSc; passed with high distinction) Topic of the thesis: "Effect of chemical chaperones TUDCA and PBA on the regulation of endoplasmic reticulum stress responses in intestinal epithelial cells"
10/2003 – 09/2006	Molecular Biotechnology (Bachelor degree course) at the Technical University of Munich Degree: Bachelor of Science (BSc; passed with high distinction) Topic of the thesis: „Investigating the synergism between non-cellulosomal cellulases Cel48Y und Cel9I of <i>Clostridium thermocellum</i> for the degradation of microcrystalline cellulose“
09/1994 – 06/2003	High School Gymnasium Wolnzach, Germany Degree: General qualification for university entrance (Grade A)
09/1992 – 08/1994	Basic School Grundschule Rohrbach, Germany
09/1990 – 08/1992	Basic School Josef-Maria-Lutz-Grundschule, Pfaffenhofen a.d.Ilm, Germany

ERKLÄRUNG

Hiermit erkläre ich, dass ich die vorliegende Doktorarbeit selbstständig angefertigt habe. Es wurden nur die in der Arbeit genannten Quellen und Hilfsmittel benutzt. Wörtlich oder sinngemäß übernommenes Gedankengut habe ich als solches kenntlich gemacht.

Ort, Datum

Unterschrift